STIBINE AND PHOSPHITE MIXED LIGAND RHODIUM VASKA-TYPE COMPLEXES

by

CLARE ELIZABETH HENNION

DISSERTATION

Submitted in accordance with the
requirements for the degree

MASTER OF SCIENCE

in

FACULTY OF SCIENCE

in the

DEPARTMENT OF CHEMISTRY

at the

UNIVERSITY OF THE FREE STATE

SUPERVISOR: PROF. A. ROODT

NOVEMBER 2005

ACKNOWLEDGEMENTS

I would like to thank Prof. Roodt for his unwavering enthusiasm and support, and for always finding the light in any 'challenging' situation, chemistry related or not. It has been a privilege working for you, and learning under your guidance. I have been spoilt for all future bosses!

Thank you, also, to Prof. Roodt and Dr Ola Wendt for including me in the SIDA program. The experiences I had in Sweden were beyond any of my expectations, and I will be forever grateful for receiving the opportunity.

To the Inorganic Group boys: Inus, Leo, Reinout and Fanie, thank you for all the chemistry advice and for making my days in the office such an enjoyable challenge!

*I would like to thank the NRF, SIDA and DST Center of Excellence c*change program, for financial support.*

To my Mom, and Linda and Mike O'Brien, words don't express my gratitude for your love, your sacrifices and your guidance. Without your constant support, none of this would have been possible.

Lastly, Ray, thank you for your love and patience. Thank you for understanding all my needs and putting up with my chemistry highs and lows. I know that with you by my side we can achieve anything we dream.

TABLE OF CONTENTS

TABLE OF CONTENTS

TABLE OF CONTENTS

TABLE OF CONTENTS

ABBREVIATIONS AND SYMBOLS

Abbreviation / Symbol	Meaning
MeOH	Methanol
EtOH	Ethanol
DCM	Dichloromethane
atm	Atmospheres pressure
aq	Aqueous solution
π^*	Pi antibonding
σ	Sigma
n/iso	Linear to branched ratio
η	Hapto
NMR	Nuclear Magnetic Resonance
I	Spin
δ	Chemical shift
J	Coupling constant
s	Singlet
d	Doublet
m	Multiplet
dd	Doublet of doublets
dt	Doublet of triplets
UV-Vis	Ultra Violet – Visible
λ	Wavelength
IR	Infrared
υ	Stretching frequency
au	Absorbance units
e	Electrons
HOMO	Highest Occupied Molecular Orbital
LUMO	Lowest Unoccupied Molecular Orbital
HPLC	High Performance Liquid Chromatography
WGS	Water Gas Shift
O	Oxidise
Z	Number of molecules per unit cell
TMS	Tetramethyl silane
T	Temperature
F(*hkl*)	Structure factor
ρ	Electron density
K_{eq}	Equilibrium constant
k	Rate constant
k_{oa}	Oxidative addition rate constant
k_{obs}	Observed rate constant
$t_{1/2}$	Half-life
$X^{\dagger}$	Transition state complex
$\Delta G^{\dagger}$	Gibbs Free energy of activation
$\Delta H^{\dagger}$	Thermodynamic Enthalpy
$\Delta S^{\dagger}$	Thermodynamic Entropy

ABBREVIATIONS AND SYMBOLS

R	Gas constant
A	Frequency factor
E_a	Activation energy
k_B	Boltzman's constant
h	Planck's constant
2,4-TBPP	Tris(2,4-di-^{t}butylphenyl)phosphite
2,6-MPP	Tris(2,6-dimethylphenyl)phosphite
TPP	Triphenylphosphite
4-ClPP	Tris(4-chlorophenyl)phosphite
4-MPP	Tris(4-methylphenyl)phosphite
4-BPP	Tris(4-^{t}butylphenyl)phosphite

ABSTRACT

The aim of this study was to synthesise simple rhodium stibine complexes and to react them with a range of phosphite ligands in order to determine the rate constants and reaction mechanism for the substitution reactions. The phosphites were selected in order to provide a range of sterically demanding incoming ligand systems, as determined by their Tolman cone angles.

Spectroscopic investigation revealed there were two different reaction mechanisms evident for the reaction of the stibine system, *trans*-[Rh(Cl)(CO)($SbPh_3$)$_2$] with the larger and smaller cone angle phosphites. Low temperature ^{31}P NMR indicated that the reaction of *trans*-[Rh(Cl)(CO)($SbPh_3$)$_2$] with small cone angle phosphites resulted in a series of addition and elimination reactions to form a range of four and five coordinate mixed stibine and phosphite intermediate species. These reactions appeared to be in equilibrium and were terminated by the formation of a phosphite analogue of Wilkinson's catalyst, [Rh(Cl){$P(OR)_3$}$_3$]. The bulky phosphites, however, reacted by two consecutive substitution reactions to form firstly a *mono*-stibine *mono*-phosphite intermediate, *trans*-[Rh(Cl)(CO)($SbPh_3$){$P(OR)_3$}] followed by a *bis*-phosphite complex, *trans*-[Rh(Cl)(CO){$P(OR)_3$}$_2$].

While attempting to characterise the mixed stibine/phosphite complexes crystallographically, a single crystal was obtained. This was subsequently solved as the Rh(III) complex, *trans-mer*-[$Rh(Cl)_2(Ph)(SbPh_3)_3$].2CH_2Cl_2. This system appears to form through oxidative addition and phenyl migration of triphenylstibine onto rhodium(I). This Rh(III) complex was reacted with triphenylphosphine and single crystals of [$Rh(Cl)_2(Ph)(PPh_3)_2$] were collected.

The six coordinate stibine system crystallised from dichloromethane in the triclinic space group, $P\bar{1}$ with Z = 2, while the five coordinate phosphine complex crystallized in the

ABSTRACT

monoclinic space group, C2/c with Z = 4. Both complexes contain a rhodium center with two *trans* chloride atoms and a metal bound phenyl ring. The stibine system contains two *trans* triphenylstibine molecules, with a third stibine *trans* to the phenyl. The phosphine system contains two triphenylphosphine groups bound to the metal.

A kinetic study was conducted to investigate the reaction of *trans*-[Rh(Cl)(CO)($SbPh_3$)$_2$] with the bulky phosphite, tris(2,4-di-^{t}butylphenyl)phosphite (2,4-TBPP). Stopped-Flow spectrophotometry showed two consecutive reactions at 310nm, a fast first reaction followed by a slower second reaction. The kinetic investigation was conducted in two different solvents, namely, dichloromethane and ethyl acetate, to determine the effect of solvent polarity and donicity on the reaction rates. It soon became evident that the first reaction was too fast to follow under standard first order conditions and excess tripehenylstibine was added to the system to introduce the five coordinate *tris*-stibine complex, *trans*-[Rh(Cl)(CO)($SbPh_3$)$_3$]. This had the desired effect of slowing down the reaction and the kinetic data for the first reaction could be calculated from the derived rate law. The first order rate constants, k_{12}, for the reaction to form *trans*-[Rh(Cl)(CO)($SbPh_3$)(2,6-TBPP)] from *trans*-[Rh(Cl)(CO)($SbPh_3$)$_2$] are 5.2(1) $M^{-1}.s^{-1}$ and 4.2(3) $M^{-1}.s^{-1}$ for DCM and ethyl acetate, respectively. While the first order rate constants, k_{13}, forming *trans*-[Rh(Cl)(CO)($SbPh_3$)(2,6-TBPP)] from *trans*-[Rh(Cl)(CO)($SbPh_3$)$_3$] are 3.3(9) $M^{-1}.s^{-1}$ and 4(8) $M^{-1}.s^{-1}$ for DCM and ethyl acetate, respectively.

The second reaction step to form [Rh(Cl)(CO)(2,4-TBPP)$_2$] from [Rh(Cl)(CO)($SbPh_3$)(2,4-TBPP)] was investigated in order to determine the thermodynamic data for the reaction step. The first order rate constants, k_2 at 298 K, are 33.0(8) $M^{-1}.s^{-1}$ and 719(16) $M^{-1}.s^{-1}$ for the reaction in DCM and ethyl acetate respectively. The corresponding activation parameters are $\Delta H^{\dagger}$ = 22.6(6) $kJ.mol^{-1}$ and $\Delta S^{\dagger}$ = -214(2) $J.mol^{-1}.K^{-1}$ for DCM and $\Delta H^{\dagger}$ = 27.8(5) $kJ.mol^{-1}$ and $\Delta S^{\dagger}$ = -171(2) $J.mol^{-1}.K^{-1}$ for ethyl acetate. The significantly negative entropy calculated indicates an associative pathway forming the transition state, as has been found for many stibine systems that readily form five coordinate complexes. Scheme 1 gives the predicted reaction mechanism.

ABSTRACT

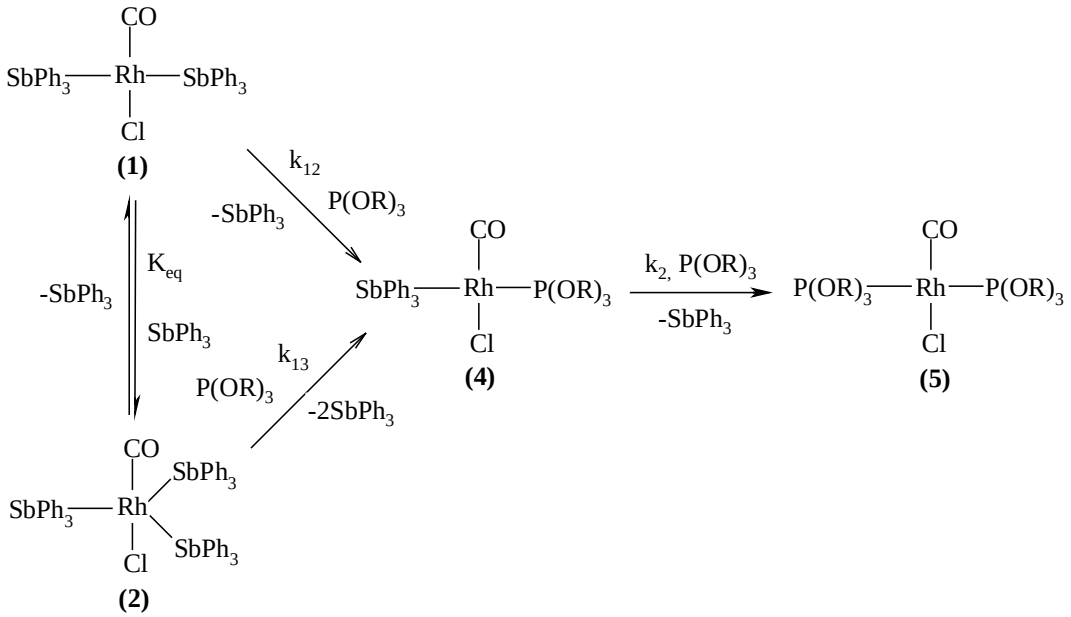

$P(OR)_3 = P(O\text{-}2,4\text{-}^tBuC_6H_3)_3$

Scheme 1: **Proposed reaction mechanism for the formation of *trans*-[Rh(Cl)(CO)(SbPh$_3$){P(O-2,4-^{t}Bu$_2$C$_6$H$_3$)$_3$}] and *trans*-[Rh(Cl)(CO){P(O-2,4-^{t}Bu$_2$C$_6$H$_3$)$_3$}$_2$]**

Key Terms: Rhodium systems
Stibine systems
Phosphite systems
Reaction kinetics
Crystal structure determination
Ligand substitution reactions
trans Effect and *trans* influence
Solvent effects
Phenyl migration

OPSOMMING

Die doel van die studie was die sintetisering van eenvoudige rhodium stibienkomplekse en ‘n kinetiese studie van die stibienkomplekse met ‘n reeks fosfiete ligande. Sodoende is die tempokonstantes en die reaksiemeganisme van die substitusiereaksies bepaal. Die fosfiet ligande is gekies om ‘n reeks inkomende ligande daar te stel met verskillende steriese invloede op die metaalsenter gebaseer op die Tolman konushoek.

n’ Spektroskopiese studie het getoon dat daar twee verskillende reaksiemeganismes gevolg word vir die reaksie van die stibiensisteem, *trans*-[Rh(Cl)(CO)($SbPh_3$)$_2$], met groot en klein konushoek fosfiete. Lae temperatuur ^{31}P KMR dui daarop dat reaksie met klein konushoek fosfiete lei tot ‘n reeks van addisie- en eliminasie-reaksies, en dus ‘n gemengde reeks van vier- en vyf-gekoödineerde stibien en fosfiet intermediëre spesies tot gevolg het. Die ewewig is getermineer met die vorming van Wilkinson se katalis se fosfiet analoog. Die meer steriese fosfiet ligande reageer in ‘n twee-stap substitusiereaksie en vorm eerstens ‘n *mono*-stibien *mono*-fosfiet intermediër, *trans*-[Rh(Cl)(CO)($SbPh_3$){$P(OR)_3$}], gevolg deur ‘n *bis*-fosfiet kompleks, *trans*-[Rh(Cl)(CO){$P(OR)_3$}$_2$].

Pogings om enkelkristalle van die gemengde stibien/fosfiet komplekse te isoleer het misluk. Enkelkristal data is afgeneem, maar op die Rh(III) kompleks, *trans-mer*-[$Rh(Cl)_2(Ph)(SbPh_3)_3$] met twee dichlorometaan oplosmiddel molekules is geisoleer. Die sisteem vorm blykbaar deur oksidatiewe addisie en fenielmigrasie vanaf trifenielstibien na die rhodium(I) senter. Die Rh(III) kompleks is gereageer met trifenielfosfien en enkelkristalle van [$Rh(Cl)_2(Ph)(PPh_3)_2$] is verkry.

Die sesgekoödineerde stibien sisteem kristalliseer vanuit CH_2Cl_2 in die trikliniese ruimtegroep $P\bar{1}$, met Z = 2, terwyl die vyfgekoödineerde fosfien kompleks kristalliseer in die monokliniese ruimtegroep C2/c, met Z = 4. Albei komplekse bevat ‘n rhodium senter met twee *trans* georienteerde chloried ligande en ‘n metaal gebonde fenielring. Die

stibien sisteem bevat twee *trans* trifenielstibien ligande, met ‘n derde stibien *trans* teenoor die fenielring. Die fosfien sisteem bevat twee trifenielfosfien ligande gebind aan die metal.

‘n Kinetiese studie is uitgevoer om die reaksie tussen *trans*-[Rh(Cl)(CO)($SbPh_3$)$_2$] en die meer steriese fosfiet, tris(2,4-di-^{t}butielfeniel)fosfiet (2,4-TBPP) te bestudeer. ‘n Tweestap reaksie is gevolg met behulp van die Stop-Vloei spektrofotometer by ‘n golflengte van 310 nm. Die kinetiese studie is uitgevoer in twee verskillende oplosmiddels, naamlik, dichlorometaan en etiel asetaat, om die effek van die oplosmiddel polariteit en donerings verskille op die reaksie tempo te bestudeer.

Daar was gevind dat die eerste reaksie stap te vinning is om gevolg te word onder standaard eerste orde reaksie kondisies. Dus is ‘n oormaat trifenielstibien bygevoeg om so die vyf gekoördineerde *tris*-stibien kompleks, *trans*-[Rh(Cl)(CO)($SbPh_3$)$_3$] te verkry, wat dan die reaksie vertraag. So kon die kinetiese data van die eerste reaksie stap bereken word vanaf die afgeleide tempowet. Die eerste orde tempo konstantes, k_{12}, vir die reaksie om *trans*-[Rh(Cl)(CO)($SbPh_3$)(2,6-TBPP)] te vorm vanaf *trans*-[Rh(Cl)(CO)($SbPh_3$)$_2$] is 5.2(1) $M^{-1}.s^{-1}$ en 4.2(3) $M^{-1}.s^{-1}$ vir CH_2Cl_2 en etiel asetaat onderskeidelik. Terwyl die eerste orde tempo konstantes, k_{13}, vir die vorming van *trans*-[Rh(Cl)(CO)($SbPh_3$)(2,6-TBPP)] vanaf *trans*-[Rh(Cl)(CO)($SbPh_3$)$_3$]: 3.3(9) $M^{-1}.s^{-1}$ en 4(8) $M^{-1}.s^{-1}$ vir CH_2Cl_2 en etiel asetaat, onderskeidelik is.

Die tweede reaksiestap, die vorming van *trans*-[Rh(Cl)(CO)(2,4-TBPP)$_2$], vanaf *trans*-[Rh(Cl)(CO)($SbPh_3$)(2,4-TBPP)] is gevolg en die termodinamiese data vir die spesifieke reaksiestap bepaal. By 298 K is die eerste-orde tempokonstantes, k_2, bepaal as 33.0(8) $M^{-1}.s^{-1}$ en 719(16) $M^{-1}.s^{-1}$ vir reagering in CH_2Cl_2 en etiel asetaat onderskeidelik. Ooreenkomstig is die aktiveringsparameters as volg bereken: $\Delta H^{\dagger}$ = 22.6(6) kJ.mol^{-1} en $\Delta S^{\dagger}$ = -214(2) J.mol^{-1}.K^{-1} (CH_2Cl_2), en $\Delta H^{\dagger}$ = 27.8(5) kJ.mol^{-1} en $\Delta S^{\dagger}$ = -171(2) J.mol^{-1}.K^{-1} (etiel asetaat).

OPSOMMING

Die negatiewe entropie dui op ‘n assosiatiewe pad vir die forming van die oorgangsstadium, soos voorheen gevind vir ander stibiensisteme waar die vyf gekoördineerde komplekse maklik vorm. Skema 1 gee die voorgestelde reaksie meganisme.

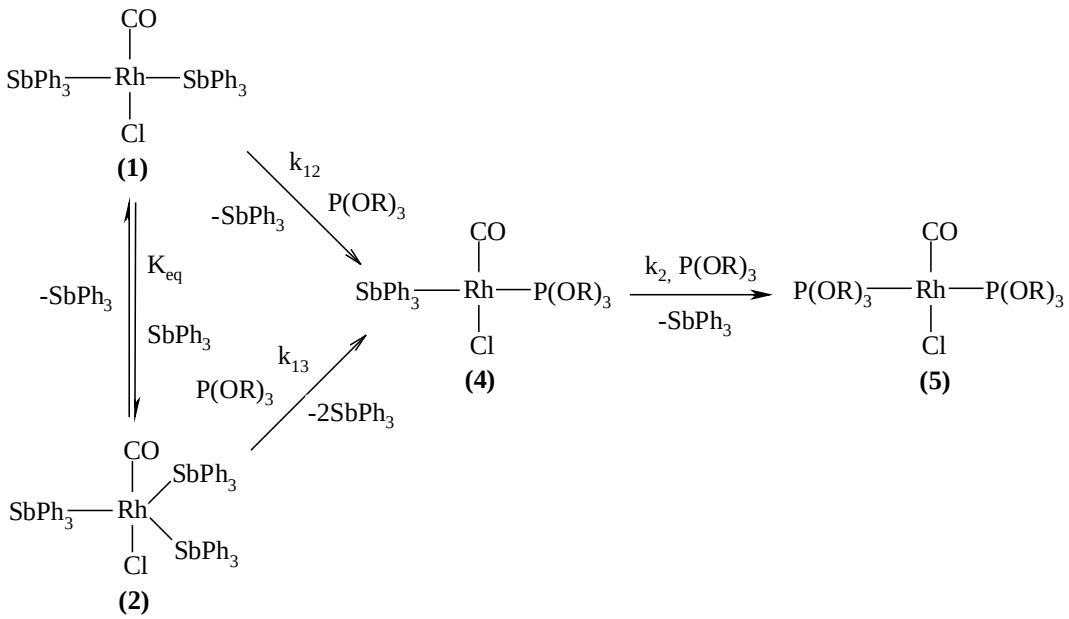

$P(OR)_3 = P(O\text{-}2,4\text{-}^tBuC_6H_3)_3$

Skema 1: Voorgestelde reaksiemeganisme vir die vorming van *trans*-[Rh(Cl)(CO)(SbPh$_3$){P(O-2,4-^{t}Bu$_2$C$_6$H$_3$)$_3$}] en *trans*-[Rh(Cl)(CO){P(O-2,4-^{t}Bu$_2$C$_6$H$_3$)$_3$}$_2$]

1. INTRODUCTION

1.1 GENERAL

Many important chemicals are produced commercially by reactions which are catalysed by organometallic compounds. This fact provides one of the motivating forces for studying organometallic chemistry. Most organic chemicals produced in bulk quantities are oxygenated compounds such as alcohols, ketones, and carboxylic acids, and hydrocarbons such as ethene, propene, and butadiene. These hydrocarbons may be polymerised to higher alkenes, including polyethene, polypropene, and rubbers. Many are used as starting materials for other syntheses.[1]

Catalytic reactions that are utilized on a worldwide scale include hydroformylation, the Monsanto acetic acid process and to a lesser extent, hydrogenation reactions. These procedures mostly use rhodium or cobalt as catalysts with a combination of various phosphorus and/or carbonyl ligand systems.

The catalyst systems utilized for industrial hydroformylation reactions have evolved over the past decades to facilitate increased yield and selectivity as well as optimal plant process conditions. The original catalyst system consisted of a simple unmodified cobalt precursor, $[Co_2(CO)_8]$, which operated at process conditions of 150 – 180 ˚C and syngas pressures exceeding 200 atm. This system produced predominantly branched chain aldehydes as opposed to the preferred linear molecules.[1]

The replacement of cobalt by modified rhodium catalysts allowed the development of processes which operate under much milder conditions (<100 ˚C and at only a few atmospheres pressure). The addition of phosphine ligands to rhodium carbonyl catalyst

[1] J.P. Collman, L.S. Hegedus, 'Principals and Applications of Organotransition Metal Chemistry', University Science Books, Calif., 1980

precursors produced highly active catalysts with excellent selectivity for the formation of the desired linear aldehydes. Optimal process parameters have been determined for the modified rhodium system based on $[HRh(CO)(PPh_3)_3]$.[2] Recently, however, phosphite ligand systems have been introduced to further improve the current catalyst complex.[3,4,5,6]

The catalyst complexes utilized for the Monsanto acetic acid process have also evolved from the original cobalt catalyst system, $[Co(CO)_2I_2]^-$, operating at high temperatures and pressures (> 200 ˚C and 700 bar) to a low pressure rhodium catalyst, $[Rh(CO)_2I_2]^-$, which catalyses the carbonylation of methanol to acetic acid under relatively mild conditions (150 – 200 ˚C and 30 – 50 bar pressure).[7,8,9] This rhodium based system, as well as the Ir based Cativa process, is now the dominant technology in the field.

Hydrogenation reactions use Wilkinson's catalyst based on a $[Rh(Cl)(PPh_3)_3]$ system.[10] These few examples illustrate the extensive use of rhodium complexes as catalysts, particularly when combined with phosphorous ligand systems.

1.2 PHOSPHORUS AND STIBINE LIGAND SYSTEMS

Recently, the interest in hydroformylation catalyst ligand systems has shifted from σ donating phosphine ligands to the more π accepting phosphite systems. This is a result of a number of factors, including the following:

- The synthesis of phosphite ligands is relatively simple compared to the corresponding phosphine analogues,

[2] M. Chanon, *J. Mol. Cat.*, **32**, 1985, 27
[3] I. Odinets, T. Kegl, *J. Organomet. Chem.*, 2005 – Article in Press
[4] M. Haumann, R. Meijboom, J.R. Moss, A. Roodt, *Dalton Trans*., 2004, 1679
[5] R. Meijboom, M. Haumann, A. Roodt, L. Damoense, *Helv. Chim. Acta*, **88**, 2005, 676
[6] R. Crous, M. Datt, D. Foster, L. Bennie, C. Steenkamp, J. Huyser, L. Kirsten, G. Steyl, A. Roodt, *Dalton Trans*., 2005, 1108
[7] F.E. Paulik, *J. Chem. Soc., Chem. Commun.*, 1968, 1578
[8] J.F. Roth, *Chem. Technol.*, 1971, 600
[9] R.T. Eby, *Appl. Ind. Cat.*, 1971, 483
[10] J.F. Young, J.A. Osborn, F.H. Jardine, G. Wilkinson, *Chem. Commun.*, 1965, 131

- Phosphites are not as electron rich as phosphines and are thus less prone to oxidation on the phosphorus atom,
- Metal complexes formed with phosphite ligand systems are generally more stabile than the corresponding metal phosphine systems.[3]

Triphenylphosphite[4] as well as several more sterically demanding phosphites,[5,6] such as tris(2,4-di-^{t}butylphenyl)phosphite, have been incorporated into cobalt catalyst systems for hydroformylation reactions. These ligands as well as cyclic phosphites[3] have also been introduced into rhodium catalysts for hydroformylation.

Stibine systems have been incorporated into modified cobalt catalysts for amidocarbonylation reactions. Recent publications have compared various cobalt – stibine systems to the classical cobalt – phosphine precursors. They show the addition of stibine dramatically improved catalytic activity and increased the yields of aldehydes with an appreciable n / iso ratio.[11]

This prompted us to look at rhodium systems with simple phosphite / stibine ligands. Since these ligands have different π acceptor properties when compared to phosphines, the reactants, intermediates and products were studied.

1.3 AIM OF STUDY

A brief glance at the available literature shows that phosphine and arsine ligand systems have been intensively studied. However, in comparison, the coordination chemistry of the heavier Group 15 metals, stibine and bismuthine have received relatively little attention.[12,13,14]

[11] A. Cabrera, P. Sharma, *J. Mol. Cat.*, **212**, 2004, 19
[12] C.A. McAuliffe, ed., 'Transition Metal Complexes of Phosphine, Arsenic, and Antimony Ligands', Wiley, New York, 1973
[13] W. Levason, C.A. McAuliffe, 'Phosphine, Arsine, and Stabine Complexes of Transition Elements', Elsevier, 1978
[14] N.R. Champness, *Coord. Chem. Rev.*, **133**, 1994, 115

With this in mind, this study was designed to investigate a number of stibine systems to determine their coordinating ability and reactivity on both Rh(I) and Rh(III) metal centers. The recent interest in phosphite ligands for hydroformylation catalyst systems led us to include these donors in order to study novel mixed stibine–phosphite rhodium complexes.

A range of phosphite ligand systems are available, providing a selection of small and sterically hindered systems based on their Tolman cone angles.[15] As a result, it is possible to study the coordinating ability of both phosphite and stibine ligands on the mixed rhodium complex as a function of steric bulk. The relative *trans* effect of stibine versus that of phosphorus, as well as the electronic similarity between stibines and phosphites leads to interesting opportunities for kinetic and mechanistic investigation of these mixed stibine – phosphite systems.

With the above in mind, the following aims were set out for this study:

- Synthesis of mixed stibine–phosphite Vaska type complexes, *trans*-[Rh(Cl)(CO)($SbPh_3$){$P(OR)_3$}] utilizing triphenylstibine and a range of phosphite ligands.

- Synthesis of *bis*-phosphite Vaska type complexes, *trans*-[Rh(Cl)(CO){$P(OR)_3$}$_2$].

- Solution state investigation of the reaction of *trans*-[Rh(Cl)(CO)($SbPh_3$)$_2$] with various small and bulky phosphites.

- Synthesis of Rh(III)-stibine, -phosphite and -phosphine complexes.

- Characterisation of complexes using IR, UV-Vis and NMR, with further characterisation of selected complexes by X-ray crystallography.

[15] C.A. Tolman, *Chem. Rev.*, ***77***, 1977, 313

CHAPTER 1 INTRODUCTION

- Kinetic and mechanistic investigation of the substitution reaction forming *trans*-[Rh(Cl)(CO)($SbPh_3$){$P(OR)_3$}] and *trans*-[Rh(Cl)(CO){$P(OR)_3$}$_2$] from *trans*-[Rh(Cl)(CO)($SbPh_3$)$_2$], where $P(OR)_3$ = tris(2,4-di-^{t}butylphenyl)phosphite.

- Analysis of results with respect to stibine, phosphite and phosphine reactivity and coordinating ability.

2. ORGANOMETALLIC CHEMISTRY

2.1 INTRODUCTION

Transition metal complexes have been intensively studied over the past century. This is a result of their widespread and diverse use in chemical processes and their rich chemistries. They play a particularly important role as transition metal catalysts in industrial processes, such as hydroformylation, hydrogenation and polymerization reactions.

The applicability and effectiveness of the catalyst system selected for each of these processes is determined by a number of factors. These include the inherent characteristics of each transition metal center as well as a combination of contributing factors from the corresponding ligand system.

This chapter aims to expand on these concepts, while focusing attention on rhodium metal complexes and stibine ligand systems, as well as the broad catalytic applicability of the transition metal catalysts as organometallic catalysts.

2.2 RHODIUM IN ORGANOMETALLIC CHEMISTRY

2.2.1 Rhodium Metal

Rhodium, as a bulk metal, is highly resistant to oxidation and corrosion. It is unaffected by all acids, including aqua regia, and is particularly inert to attack by oxygen, unless at red heat, where it reacts rather slowly.[1]

Rhodium is frequently used as an alloy with platinum,[2] producing materials with high hardness and chemical resistance. These alloys are used in electric ovens in the glass industry; in turbine reactors; in the production of thermocouples and in furnace windings. Rhodium metal also finds some application in the production of projectors and emitting and receiving circuit components, etc. In the jewellery industry, rhodium is used as a fine film coating of white gold jewels, by electrolytic deposit. The process of electrolytic deposition improves the 'aspect' of the jewels, turning them white and adding to their resistance.[3]

Rhodium can be used as an adsorption catalyst for reactions requiring high temperatures and oxidising conditions. This is well illustrated by the use of platinum-rhodium gauze to catalyse the oxidation of ammonia to nitric acid at 850 ˚C.[4] Rhodium metal is also an important catalyst at lower temperatures, and under reducing conditions.

2.2.2 Oxidation States of Rhodium

Rhodium metal can be converted to the anhydrous chlorides, $RhCl_3$ and RhI_3 etc., by direct reaction with the respective halide. These Rh(III) halides are insoluble in water and

[1] R.S. Dickson, 'Organometallic Chemistry of Rhodium and Iridium – Organometallic Chemistry, A Series of Monographs', Academic Press, London, 1983
[2] G.C. Bond, *Platinum Met. Rev.*, **23**, 1979, 46
[3] http://nautilus.fis.uc.pt/st2.5/scenes-e/elem/e04530.html
[4] J. Perez-Ramirez, *J. of Cat.*, **229**, 2, 2005, 303

are relatively inert. The usual starting material for preparing complexes of rhodium, however, is the hydrated chloride, $RhCl_3.3H_2O$. This can be obtained by dissolving Rh_2O_3 in aqueous hydrochloric acid, and by electrolytic dissolution of the metal in hydrochloric acid. The hydrate dissolves readily in a variety of organic solvents as well as in water.[1] Figure 2.1 illustrates selected reactions of rhodium trichloride.[5]

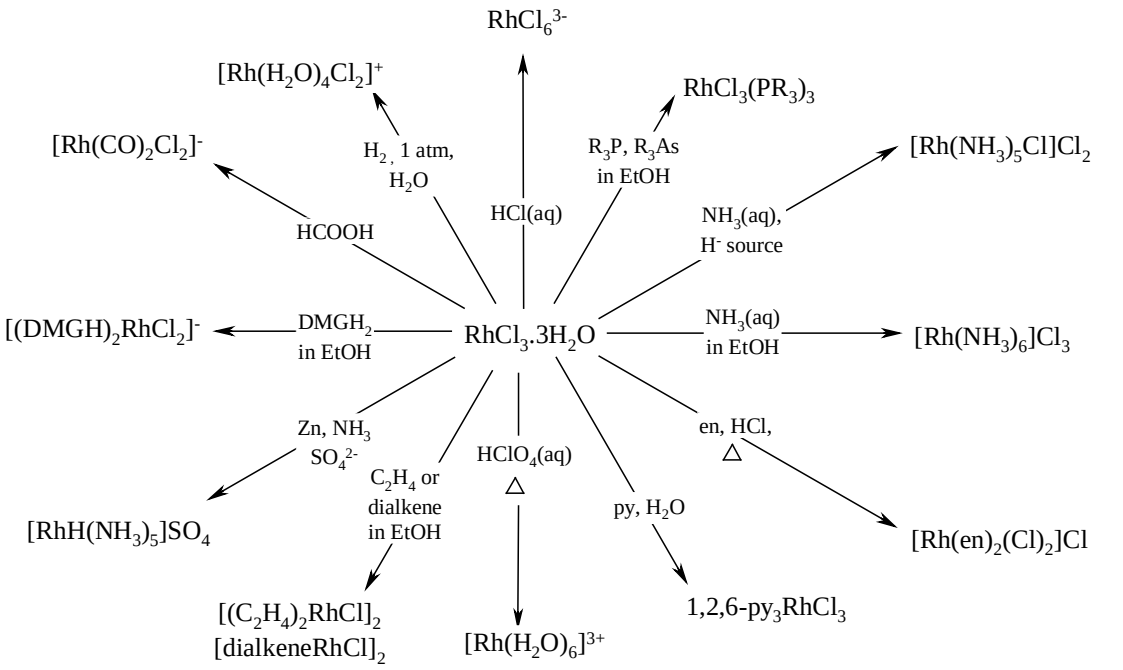

py: pyridine
en: ethylenediamine
$DMGH_2$: dimethylgloxime

Figure 2.1: Selected reactions of rhodium trichloride [5]

Rhodium(I) complexes can be obtained from $RhCl_3.3H_2O$ by reduction of the metal halide. For instance, treatment of $RhCl_3.3H_2O$ with excess triphenylphosphine in ethanol yields $RhCl(PPh_3)_3$, Wilkinsons catalyst.[5] This reaction, as well as others associated with rhodium(I) centers is illustrated in Figure 2.2. In the presence of stabilising π-acceptor ligands, further reduction to zero or negative formal oxidation states can be

[5] F.A. Cotton, G. Wilkinson, 'Advanced Inorganic Chemistry' 5th Ed., John Wiley, 1988

accommodated. The cluster carbonyl $[Rh_4(CO)_{12}]$ and the carbonylate anion $[Rh(CO)_4]^-$ are examples of complexes with the metal in the oxidation state 0 and –1 respectively.[1]

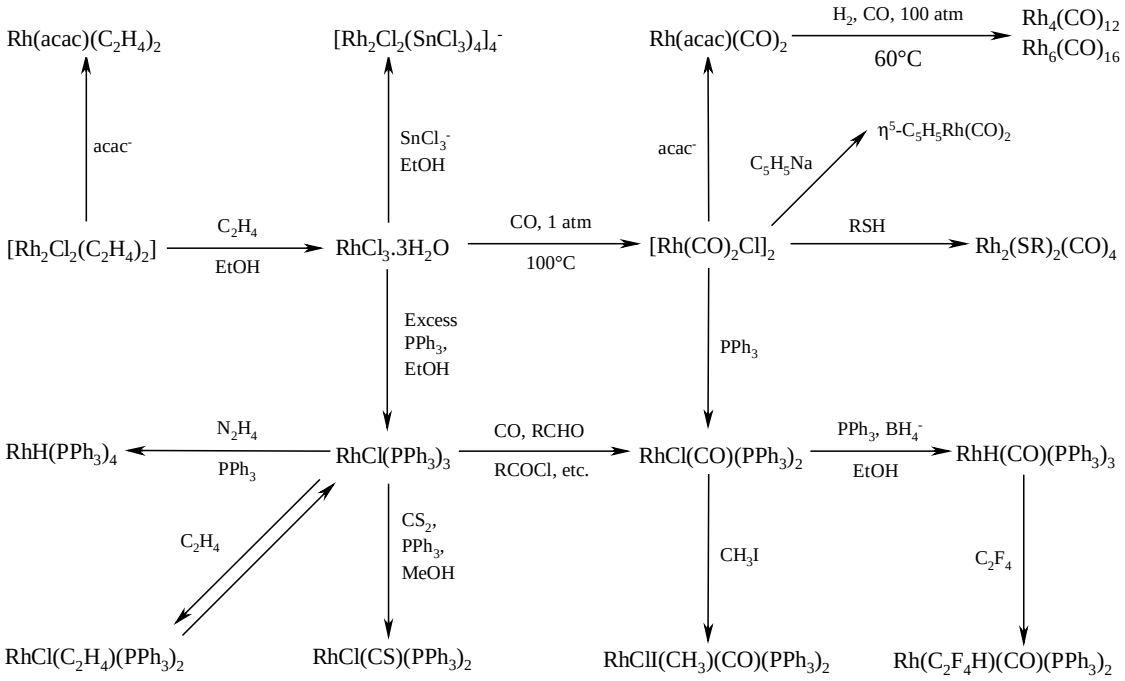

acac-: acetyl acetonate anion

Figure 2.2: Some preparations and reactions of Rh(I) [5]

2.2.3 Rhodium in Catalysis

Four coordinate complexes of rhodium(I) are coordinatively unsaturated and undergo an important series of reactions that provide the basis for our understanding of metal catalysis.[6] The main reaction types are termed coordinative-addition, oxidative-addition, reductive-elimination and *cis*-migration. The scope of these reactions is extensive and significant.

[6] J.P. Collman, L.S. Hegedus, 'Principals and Applications of Organotransition Metal Chemistry', University Science Books, Calif., 1980

CHAPTER 2 ORGANOMETALLIC CHEMISTRY

Complexes of metals with a *d*8 (Rh(I)) or *d*6 (Rh(III)) *d* electron orbital configuration are coordinatively saturated when the coordination number is 5 or 6 respectively. Consequently, species such as $RhCl(PPh_3)_3$ (*d*8, 4-coordinate), or $H_2RhCl(PPh_3)_2$ (*d*6, 5-coordinate), are classified as coordinatively unsaturated complexes.[7] These unsaturated complexes are essential for catalytic reactions and allow for entering substrate molecules to bind and consequently activate the metal. This binding also determines the stereospecificity of the reaction by controlling the coordination of two or more different ligands in specific orientation.

Ligand binding can occur by coordinative-addition, where there is an increase in the coordination number, but not in the oxidation state of the metal. An important consequence of this type of addition is that the coordinated ligand is often kinetically more reactive than the free ligand. An example of this change in reactivity is present in coordinated ethene, which is susceptible to electrophilic attack by HCl while free ethene is relatively inert to such attack.

Addition to coordinatively unsaturated complexes may also occur with concomitant oxidation of the metal. This process is known as oxidative-addition. The reverse process is termed reductive-elimination. When various substrates are bound to the same metal, interaction between neighbouring groups sometimes occurs. This may occur as *cis*-migration or insertion reactions.[8]

[7] C.A. Tolman, *Chem. Soc. Rev.*, ***1***, 1972, 337
[8] J.K. Stille, K.S.Y. Lau, *Accts. Chem. Res.*, **10**, 1977, 434

2.3 ORGANOMETALLIC LIGAND SYSTEMS

2.3.1 Ligand Types

The term 'ligand' refers to any molecule or ion that has at least one electron pair that can be donated. Ligands may also be called Lewis bases;[9] while organic chemists often use the term nucleophile. Metal ions or molecules such as BF_3, with incomplete valence electron shells, are Lewis acids or electrophiles.

There are two main classes of ligands:

1) *Classical* or *simple donor ligands*[5] act as electron pair donors to acceptor ions or molecules, and form complexes with all types of Lewis acids, metal ions, or molecules. These *classical* ligands are numerous and include halogen, oxygen, sulfur and nitrogen. These ligand types form bonds with transition metals in both high and low oxidation states.

2) *Nonclassical ligands*,[5] *π-bonding* or *π–acid ligands* form compounds largely if not entirely with transition metal atoms. This is a result of the inherent orbital properties of both metal and ligand. The metal has *d* orbitals that are utilised in bonding, while the ligand has donor capacity as well as acceptor orbitals. As a result, the ligand is capable of accepting an appreciable amount of π-electron density from the metal atom into empty π or π* orbitals. The bonding interaction of carbon monoxide to metal centers best describes this behavior. The effect is also evident with ligands such as the linear nitrosyl (NO^+) and the isocyanide ligand CNR, amongst others.

The bonding of carbon monoxide to a metal center consists of the overlap of a filled carbon σ-orbital with a σ–type orbital on the metal atom, as in Figure 2.3. Carbon to

[9] D M.P. Mingos ' Essentials of Inorganic Chemistry', Oxford University Press, Oxford, 1995

metal electron flow in such an overlap would result in impossibly high electron density on the metal atom if the metal were not +2 or a more highly charged ion. The metal reduces this charge by donating electron density back to the ligand resulting in back-bonding. This is of course only possible if the ligand has suitable acceptor orbitals. Second overlap of a filled $d\pi$ or hybrid $dp\pi$ metal orbital with the empty $p\pi$ orbital on carbon monoxide acts as a receptor of electron density.[5]

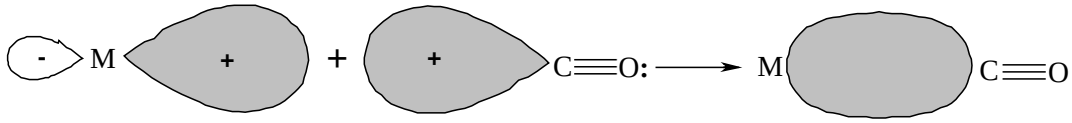

(a)

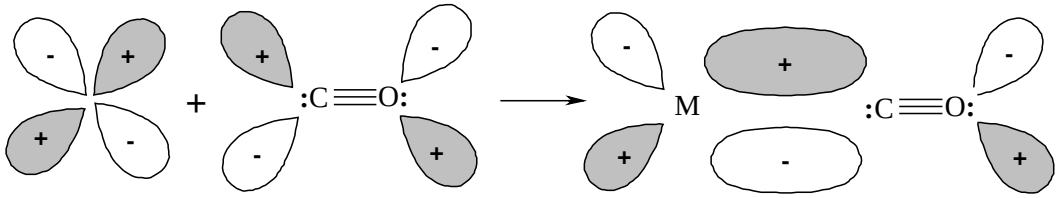

(b)

(a) The formation of the metal ← carbon σ bond using an unshared pair on the C atom

(b) The formation of the metal → carbon π bond. The other orbitals on the CO are omitted for clarity

Figure 2.3: Orbital interactions of metal – carbonyl bonds

Classical Lewis base ligands can be divided into unidentate and multidentate types, according to whether one or more donor atoms are present. Multidentate ligands can form chelate rings, of which the five-membered metallacycle is the most stable.[10] Some examples of five- and six-membered chelate rings are shown in Figure 2.4.

[10] J.E. Huheey, E.A. Keiter, 'Inorganic Chemistry' Fourth Edition, Harper College, New York, 1993

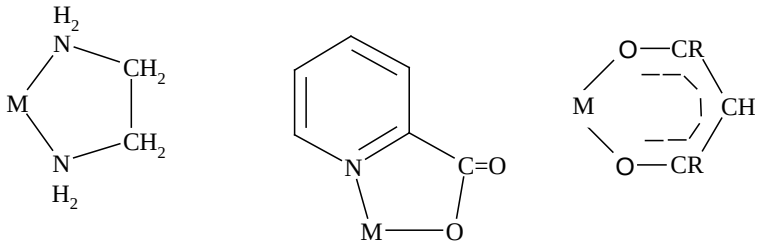

Figure 2.4: Examples of chelate rings

As a general rule, polarisable donor atoms such as S, Se, etc., (sometimes referred to as 'soft' bases)[9] form stronger bonds with third row transition metals, with metals to the right of the transition series, and with metals in lower oxidation states, i.e.: 'soft' metals. Alternatively, 'hard' bases, such as N, O, etc, have a greater affinity for earlier, more electropositive transition metals and metals in high formal oxidation states.[11]

A few of the classic Lewis base donors, chosen for their applicability to the organometallic systems discussed later, will be described here in further detail.

2.3.1.1 Halogen Donors

All halide ions have the ability to function as ligands and form complexes such as SiF_6^{2-}, $FeCl_4^-$, and HgI_4^{2-} with various metal ions or covalent halides. They also form mixed complexes with other ligands, for example, $[Co(NH_3)_4Cl_2]^+$.[5] Of these complex types, the organotransition-metal fluorides are the least common.

Halides readily form bridges, which may be easily broken by other ligands.[12] The formation of these bridges is an important structural feature not only in complex compounds, but also in many simple molecular compounds. Among the simplest example

[11] D.L. Kepert, 'The Early Transition Metals', Academic Press, London, 1972
[12] D.M. Barlex, *J. Organomet. Chem.*, **43**, 2, 1972, 425

is $PdCl_2$, which is an insoluble polymer with square planar geometry. This dissolves in CH_3CN to form a reactive square planar complex,[6] Scheme 2.1.

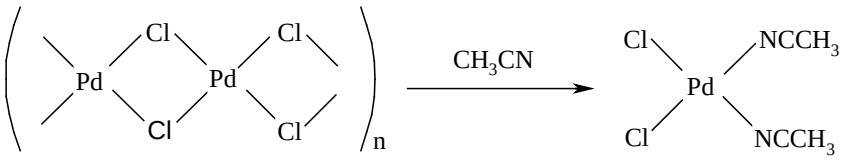

Scheme 2.1

The available literature on these complexes is at best ambiguous as to the order of stability of the halide complexes. It generally shows the stability to decrease in the series F > Cl > Br > I, but with some metal ions the order is the opposite. There is little theoretical justification for either series, however it is likely that charge-radius ratio, polarisability, and the ability to use empty outer *d* orbitals for back-bonding are significant factors.[5]

2.3.1.2 Oxygen Donors

Often, the source of oxygen donors to metal complexes comes in the form of solvent molecules, for example H_2O, THF, MeOH, DMSO and acetone. These ligands act as unidentate, weakly basic 'hard' donors, which coordinate weakly to low-valent transition metals. As a result of the weak ligand - metal interaction, these donors often act as sources of vacant coordination sites in catalysis

2.3.1.3 Phosphines and Other Group 15 Ligands

Transition metals exhibit a pronounced tendency to coordinate trivalent compounds of phosphorus and arsenic as well as to a lesser extent, antimony and bismuth.[5]

CHAPTER 2 ORGANOMETALLIC CHEMISTRY

The number of known transition metal complexes containing tertiary phosphine ligands is truly immense, and includes monodentate, bidentate, tridentate, and higher chelating phosphines.[13,14,15,16,17,18,19]

Compounds of the type PX_3 (as well as AsX_3, SbX_3, SX_2 and SeX_2) are important π–bonding ligands, especially when X is relatively electronegative, i.e. Ph, OR, Cl, or F etc. The Lewis basicities of the PX_3 ligands vary considerably and not entirely predictably[20] with X, however, the extent of both donation from the lone pair on the P atom, and back-donation, depends on the nature of X. As an example, for PH_3 and $P(alkyl)_3$ ligands, π-acceptor ability is very low. While the most electronegative substituent, F in PF_3, will reduce the σ–donor character substantially so that there will be less P → M electron transfer, and M*d*π → P*d*π transfer should be aided. This trend, dependent on X, is similar for the analogous AsX_3 and SbX_3 complexes.[5]

Steric factors are of at least as great importance to the chemistry of PX_3 (X = aryl, alkyl, aroyl, etc.) compounds as the electronic factors.[15] The steric effects on phosphorus may be dominant in determining the stereochemistry and structures of PX_3 complexes. Tertiary phosphines have been extensively studied in catalytic reactions, where selectivity can be controlled by steric factors, and chiral syntheses can be facilitated by use of dissymmetric phosphines. Steric factors also affect rates and equilibria of dissociation reactions such as the one shown in Scheme 2.2, and the propensity of phosphine complexes to undergo oxidative addition reactions, or form alkene complexes.[5]

---

[13] C.A. Tolman, *Chem. Rev.*, **77**, 1977, 313
[14] C.A. McAuliffe, ed., 'Transition Metal Complexes of Phosphine, Arsenic, and Antimony Ligands', Wiley, New York, 1973
[15] W. Levason, C.A. McAuliffe, 'Phosphine, Arsine, and Stabine Complexes of Transition Elements', Elsevier, 1978
[16] W. Levason, C.A. McAuliffe, *Acs. Chem. Res.*, **11**, 1978, 363
[17] W. Levason, C.A. McAuliffe, *Adv. Inorg. Chem. Radiochem.*, **14**, 1972, 173
[18] G. Booth, *Adv. Inorg. Chem. Radiochem.*, **6**, 1964, 1
[19] T.T. Derencsengi, *Inorg. Chem.*, **20**, 1981, 665
[20] G M. Bancroft, *Inorg. Chem.*, **25**, 1986, 3675

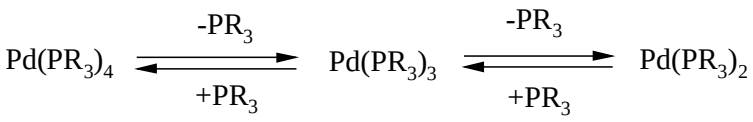

Scheme 2.2

Chelating (bidentate) phosphine ligands have widespread use. Figure 2.5 shows the five-membered ring chelates DIPHOS[21], DIARS[22] and others, with the conformation of the bonding interaction holding the phosphine groups in mutually *cis* positions.

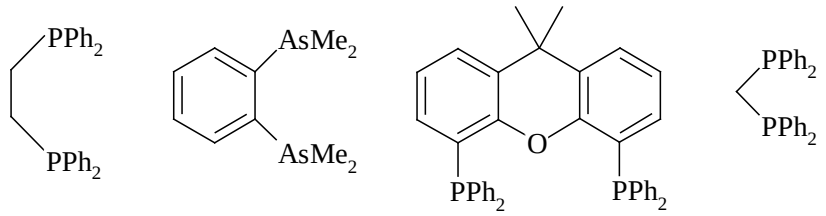

(a): DIPHOS, 1,2-bis(diphenylphosphino)ethane

(b): DIARS, *o*-phenylenebis(dimethylarsine)

(c): XANTPHOS, 9,9-dimethyl-4,5-bis(diphenylphosphino)xanthene

(d): DPPM, diphenylphosphinomethane

Figure 2.5: Examples of *cis* Chelating phosphine ligands

Other bidentate phosphines are designed to keep the two phosphine donors in a *trans* position. Bidentate phosphine ligands with long chains between the P atoms, for example, $^{t}Bu_2P(CH_2)_{5\text{-}8}P^{t}Bu_2$ can span trans positions in square complexes or give large ring systems.[23]

[21] H. Kunkely, *Inorg. Chem. Comm.*, **7**, 6, 2004, 767
[22] A M.F. Benial, *Spectrochemica Acta,* **57**, 6, 2001, 1199
[23] B.L. Shaw, *J. Chem. Soc., Dalton Trans.*, 1979, 1972

Chiral phosphines are known that exhibit chirality at the P atom as well as within the carbon framework, Figure 2.6.

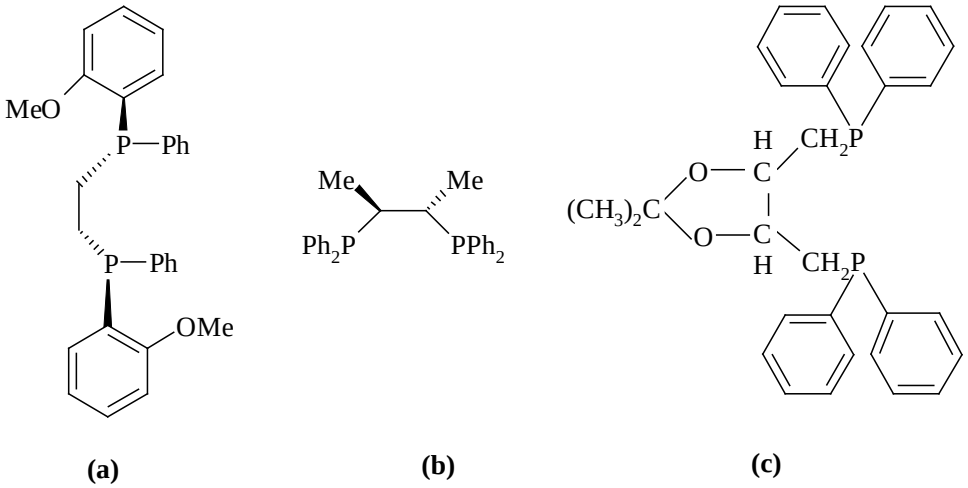

(a) **(b)** **(c)**

(a): (S,S)-DIPAMP, (1S,2S)-(+)-bis[(2-methoxyphenyl)phenylphosphino]ethane

(b): (S,S)-CHIRAPHOS, (2S,3S)-(-)-bis(diphenylphosphino)butane

(c): (S,S)-DIOP,

(4S,5S)-[(2,2-dimethyl-1,3-dioxolane-4,5-diyl)bis(methylene)]diphenylphosphane

Figure 2.6: Some chiral phosphine ligands

These optically active diphosphinoethanes,[24] such as S,S-chiraphos[25] (Figure 2.6), can be used to impose chirality[26] on complexes and then on products formed, when the chiral complexes serve as catalysts,[27] i.e. with chiral hydrogenation.

2.3.2 Stibine Ligand Systems

Transition metal complexes of tertiary phosphine ligands remain one of the most frequently studied areas of coordination chemistry, and there extensive literature on

[24] L.J. Higham, *J. Organomet. Chem.,* **690**, 1, 2005, 211
[25] W.A. Schenk, *J. Organomet. Chem.,* **560**, 1, 1998, 3987
[26] F.A. Cotton, *J. Am. Chem. Soc.*, **106**, 1984, 1851
[27] J. Halpern, *Science,* **217**, 1982, 401

tertiary arsine complexes.[14,28,29] In contrast, the coordination chemistries of the heavier Group 15 analogues, stibines and bismuthines, have received limited attention. In part, this reflects their significantly weaker coordinating ability, studies being often confined to soft metals in low oxidation states. In contrast to phosphines, the heavier ligands lack an NMR probe analogous to the ^{31}P nucleus. Although naturally occurring antimony and bismuth nuclei have nuclear spins and reasonable sensitivities (^{121}Sb $I = 5/2$, 57.3%, ^{123}Sb $I = 7/2$, 42.7%,^{209}Bi $I = 9/2$, 100%), these are associated with substantial quadrupole moments,[30] which result in unobservably broad resonances unless in cubic symmetry environments.[31] As a result, in practical terms, no resonances have been observed of their coordination complexes. Fast quadrupolar relaxation also prevents observation of 1-bond coupling constants between Sb or Bi and other NMR active nuclei.

Commercially available stibine and bismuthine complexes are limited to Ph_3Sb, $^nBu_3Sb$, Ph_3Bi and to ultra-pure (and correspondingly highly expensive) "electronic grade" Me_3Sb. Trialkyl- and alkylaryl-stibines are air-sensitive liquids, with characteristic odours, which must be handled under an inert atmosphere. The lower trialkylstibines are pyrophoric, while triarylstibines are air stable solids.[32]

Arsenic, stibine and bismuth trihalides comprise 12 compounds that exhibit diversity in their physical and chemical properties, as well as considerable variations in their structures. Some, such as AsF_3, $SbCl_3$ and $SbBr_3$ are essentially molecular, and they give pyramidal EX_3 molecules readily in the vapour phase. For the iodides, the solids have close-packed arrays of I atoms with E atoms in octahedral interstices but located off-center so EI_3 molecules can be considered to exhist.[5]

Arsenic trifluoride and SbF_3 (called Swartz reagent) are very useful reagents for fluorination of various nonmetallic substrates, while arsenic trichloride and $SbCl_3$ have

[28] W. Levason, 'The Chemistry of Organophosphorus Compounds, Vol. 1' Wiley, New York, 1990
[29] C.A. McAuliffe, W. Levason, 'Phosphine, Arsine and Stibine Complexes of the Transition Elements', Elsevier, Amsterdam, 1979
[30] J.A. Iggo, 'NMR Spectroscopy in Inorganic Chemistry', Oxford University Press, 1999
[31] J. Mason, 'Multinuclear NMR', Plenum Press, New York, 1987
[32] N.R. Champness, *Coord. Chem. Rev.*, **133**, 1994, 115

some use as non-aqueous solvents.[33] It is doubtful that they undergo significant self-ionization (although this has been proposed as to form $ECl_2^+ + ECl_4^-$) but they have low viscosities, high dielectric constants, liquid ranges of ~150˚C, and are good media for Cl^- transfer reactions.

The overwhelming majority of reported coordination complexes of monodentate stibines contain Ph_3Sb. Trialkystibine and phenylalkylstibine ($Ph_{3-n}R_nSb$) complexes are much less common, perhaps a reflection of the air-sensitivity of the free ligands and correspondingly increased difficulties in handling, coupled with commercial unavailability. A few complexes of stibane (SbH_3) have been prepared, but no reports of complexes of primary ($RSbH_2$) or secondary (R_2SbH) stibines were found.[32]

2.3.2.1 Applications of Stibine Ligands

Recently, stibine has been incorporated into modified cobalt catalyst systems for amidocarbonylation reactions.[34] These reactions, originally discovered by Wakamatsu *et al*. in 1971 constitute a good method for the synthesis of amino acids using olefins,[35] aldehydes,[36] allylic alcohols,[37] oxiranes[38] and acetals[34] as substrates.

The newly awakened interest in this reaction reflects the fact that C_1 chemistry, which in the past has mainly made its appearance in the synthesis of bulk chemicals, is receiving greater attention in the area of fine and speciality chemicals for a number of economic and ecological reasons.[39]

[33] G.P. Smith, *J. Am. Chem. Soc*., **108**, 1986, 654
[34] R.M. Gomez, P. Sharma, LJ.L Arias, J. Perez-Flores, *J. Molec. Cat. A: Chem*., **170**, 2001, 271
[35] H. Wakamatsu, J. Uda, N. Yamakani, *Chem. Commun*., 1971, 1540
[36] J.J. Lui, J.F. Kifton, *Chemtechnology*, 1992, 248
[37] R. Stern, A. Herschnaner, D. Commerenc, Y. Chauvin, US Patent 426, 451, 1981
[38] K. Herai, Y. Takahashi, I. Gima, *Tetrahedron Lett.*, **23**, 1982, 2491
[39] W. Keim, 'Catalysis in C_1 Chemistry', D. Reidel, Dordrecht, 1983

A publication by Cabrera and Sharma[40] compared various cobalt – stibine systems to the classical cobalt – phosphine precursors. They found the incorporation of stibine dramatically improved the catalytic activity and yields of aldehydes produced with an appreciable n/iso ratio. They postulated that the good π–acceptor character and *trans* effect of the stibine species is responsible for enhancing the exchange of ligands, giving the appropriate cobalt intermediates needed for the process. The inclusion of a stibine ligand in the coordination sphere of cobalt gave special chemo- and region-selectivity to the reaction.

Sb*i*Pr_3 has been used as a bridging ligand in dinuclear rhodium complexes, such as [$Rh_2(acac)_2$ μ-$C(p\text{-}tol)_2$ $_2$(μ-Sb*i*Pr_3)] (with acac = acetylacetonato and tol = tolyl), to investigate phosphine substitution reactions. Reactions with bulky phosphines, such as P*i*Pr_3 or PPh_3 result in the substitution of Sb*i*Pr_3 for P*i*Pr_3 or PPh_3 as well as, most unusually, the migration of one acetylacetonato ligand from one metal center to the next. Other Lewis Bases, such as CO, CN^tBu and $SbEt_3$ as well as sterically less demanding phosphines, like PMe_3 react by displacement of the tripropylstibine ligand and formation of the analogous dinuclear rhodium complexes, in which the ligand, like Sb*i*Pr_3 in the starting material, occupies a bridging position.[41]

Metal stibine complexes have not been intensively investigated in oxidative addition reactions, even though they are readily available for rhodium(I). Square-planar *trans*-[Rh(Cl)(CO)$(SbPh_3)_2$] was successfully used by Chin[42] in the synthesis of rhodium(III) allyl complexes, and Kayan[43] has reported reactions of [Rh(X)(CO)$(SbPh_3)_3$] (X = Cl, Br) with propargyl halides and tosylates. The reaction with tosylates generally gives the expected rhodium(III) η^1-allenyl and η^1-propargyl complexes, while those with propargyl halides surprisingly afford rhodiacyclopent-3-ene-2-one products, Scheme 2.3

[40] A. Cabrera, P. Sharma, *J. Molec. Cat. A: Chem.*, **212**, 2004, 19
[41] U. Herber, *J. Organomet. Chem.*, **689**, 26, 2004, 4917
[42] C.S. Chin, S.Y. Shin, C. Lee, *J. Chem. Soc., Dalton Trans.*, 1992, 1323
[43] A. Kayan, J. Gallucci, *J. Organomet. Chem.*, **630**, 1, 2001, 44

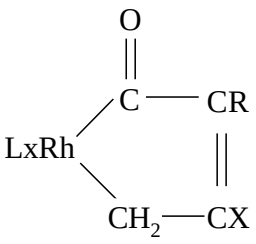

Scheme 2.3

Some η^1-allenyl and rhodiacyclic complexes were reported to interconvert under appropriate experimental conditions.

Square-planar carbenerhodium(I) complexes, such as *trans*-[Rh(Cl)(=CRR^1)(Sb*i*Pr$_3$)$_2$], can be obtained from *trans*-[Rh(Cl)(C_2H_4)(Sb*i*Pr$_3$)$_2$] and diazoalkanes RR^{1}CN$_2$ as precursors. These rhodium carbenes provide a rich chemistry, including unusual C-C coupling reactions. Iridium counterparts have been prepared, such as *trans*-[Ir(Cl)(C_2H_4)(Sb*i*Pr$_3$)$_2$], however it was found that, in contrast to their rhodium analogues, square-planar (olefin)iridium(I) complexes are surprisingly labile and, at least in the case of cyclooctene, propene and 1-hexene as ligands, rapidly rearrange to the (η^3-allyl)hydridoiridium(III) isomers.[44,45]

The structural and electronic differences between stibine and phosphine, as well as their inherent similarities have resulted in new synthetic routes being developed, where the reaction of stibines, or phosphines, alone do not provide the required product.

For example, the carbene complex *trans*-[Rh(Cl)(=CPh_2)(P*i*Pr$_3$)$_2$] is the parent member of a series of rhodium(I) compounds with the general composition *trans*-[Rh(Cl){=C(=C)$_n$$Ph_2$}(P*i*Pr$_3$)$_2$] (n =1, 2 and 4). These square-planar vinylidene and allenylidene rhodium(I) complexes are quite stable and offer a rich chemistry, including the chance to perform novel metal-assisted C-C coupling reactions as a result of their high reactivity towards nucleophiles.[46]

[44] D.A. Ortmann, *Organometallics*, **20**, 2001, 1776
[45] P. Schwab, *Angew. Chem., Int. Ed. Engl.*, **32**, 1993, 1480
[46] E. Bleuel, *J. Organomet. Chem.*, **617**, 2001, 502

In attempting to prepare the carbene complex *trans*-[Rh(Cl)(=CPh_2)(P*i*Pr_3)$_2$], the dimer [Rh(P*i*Pr_3)$_2$(μ-Cl)]$_2$ was reacted with Ph_2CN_2, but instead of the above, the diazoalkane derivative *trans*-[Rh(Cl)(N_2CPh_2)(P*i*Pr_3)$_3$] was obtained in excellent yield.

The successful route to obtain the carbene complex was to prepare, in the initial step, the bis(stibine) complex *trans*-[Rh(Cl)(=CPh_3)(Sb*i*Pr_3)$_2$] from *trans*-[Rh(Cl)(C_2H_4)(Sb*i*Pr_3)$_2$] and Ph_2CN_2 and then displace the two stibine molecules for two phosphine ligands.[47]

2.3.2.2 Pharmaceutical Application of Stibine Ligands

It has been known for at least two decades that some compounds of Rh(I) and Rh(III) have anti-cancer and antibacterial activities.[48,49,50] The synthesis of Rh complexes with the ability to bind nucleobases has become an area of considerable interest, specifically in the field of antineoplastic and antiviral research.[51] Once inside the cell the complex molecule can release one or more donor atoms, and the free sites can then bind to nucleobases. General nucleophilic substitution reactions at the metal centre are modulated by a series of factors, like *trans* influence, steric hindrance and concentration of the ligands.[52]

It is with this in mind, that Cini and co-workers[52] investigated the Rh(III) complex, [Rh(Cl)$_2$(Ph)($SbPh_3$)$_3$]. The insertion of η^1-bound phenyl groups in the Rh coordination sphere opens up new promising synthetic routes to complexes with potential anticancer properties, by taking advantage of the high *trans* influence exerted by the phenyl ligand itself. They have been able to selectively substitute the stibine ligand *trans* to the phenyl group by various nucleophilic agents.[52,53,54,55]

---

[47] T. Pechmann, *Organometallics,* **22**, 2003, 3004
[48] J. Reedijk, *Chem. Commun.,* 1996, 801
[49] M.J. Cleare, 'Recent Results in Cancer Research', Eds. T.A. Connors, J.J. Roberts, New York, 1974
[50] T. Giraldi, G. Sava, *Cancer Res.,* **37**, 1977, 2662
[51] a, L.M. Torres, L.G. Marzilli, *J. Am. Chem. Soc.,* **113**, 1991, 4678
b, S. Mukundan, Jr., Y. Xu, G. Zon, *J. Am. Chem. Soc*., **113**, 1991, 3021
c, M. Krumm, I. Mutikainen, B. Lippert, *Inorg. Chem.*, **30**, 1991, 890
[52] R. Cini, G. Giorgi, L. Pasquini, *Inorg. Chim. Acta,* **196,** 1992, 7
[53] R. Cini, G. Giorgi, *Acta Cryst.,* **C47**, 1991, 716
[54] A. Cavaglioni, R. Cini, *J. Chem. Soc., Dalton Trans*., 1997, 1149
[55] A. Cavaglioni, R. Cini, *Polyhedron,* **16**, 1997, 4045

2.4 ORGANOMETALLIC CATALYSIS

2.4.1 Introduction

A thermodynamically favourable reaction may be slow at low temperatures and thus have little value for synthesis. Increasing the temperature of the reaction may significantly accelerate its rate, but providing the energy for this is expensive and higher temperatures may induce competing side reactions that greatly reduce the product yield. An alternative approach to increase the reaction rate would involve the use of a catalyst.[56,57]

The German scientist, Wilheim Ostwald, provided the first modern definition of a catalyst in 1865 as 'a substance that changes the rate of the reaction without itself appearing in the product'. Today the most widely accepted definition of a catalyst is a substance that increases the rate of approach to equilibrium of a chemical reaction, without being consumed in the reaction itself.[9]

The latter definition suggests that a catalyst can never change the thermodynamic equilibrium of a reaction and only the rate by which the equilibrium is reached is changed. The acceleration of the rate is possible since the catalyst allows for a new reaction pathway for the equilibrium state to be reached. The overall reaction is divided into several individual steps of which the rate-determining step has a lower activation energy than that of the un-catalyzed reaction, hence the increased reaction rate. The definition also indicates that a catalyst must not be consumed in the reaction, thus the ideal catalyst would be endlessly efficient or should be recyclable.

Catalytic reactions are classified as homogeneous when all the compounds present, or at least one of them, are miscible with the catalysts; and heterogeneous when a solid catalyst is in contact with a reactive liquid or gaseous phase. Each type has its advantages

[56] B. Cornils, 'Catalysis from A to Z: A Concise Encyclopedia', Wiley, New York, 2000
[57] R. Pearse, 'Catalysis and Chemical Processes', Leonard Hill, 1981

and disadvantages. Heterogenous catalysts are easily separated from the reaction products but tend to require rather high temperatures and pressures and frequently lead to mixtures of products i.e., they have low selectivity.

Homogeneous catalysts must be separated from the product but operate at low temperatures and pressures, and usually give good selectivity. Attempts to overcome the technical problems associated with homogeneously catalysed reactions are:[5]

a) Phase transfer reactions, where the catalyst is in the aqueous, fluorous or ionic liquid phase while substrates and products exist in an organic phase
b) The supporting of a well defined homogenous catalyst on surfaces that may in addition be functionalized to act as ligands. This has been done by incorporating tertiary phosphine, pyridine, thiol, or other ligands into styrenedivinylbenzene or other polymeric materials, as well as by supporting complexes on carbon, silica, alumina, ion-exchange resins, or molecular sieves.[58a-h]

Many important chemicals are produced commercially by reactions which are catalysed by organometallic compounds and this fact provides one of the motivating forces for studying organometallic chemistry. Most organic chemicals produced in bulk quantities are oxygenated compounds such as alcohols, ketones, and carboxylic acids, and hydrocarbons such as ethene, propene, and butadiene that may be polymerised to higher alkenes, which include polyethene, polypropene, and rubbers. Many are used as starting materials for other syntheses.[5]

---

[58] [a] F.R. Hartley, *Adv. Organomet. Chem*., **15**, 1977, 189
[b] R.H. Grubbs, *Chemtech*, 1977, 512
[c] Z.M. Michalska, *Chemtech*, 1975, 117
[d] E.M. Cernia, *J. Appl. Polym. Sci*., **18**, 1974, 2725
[e] C.U. Pittman, Jr., *Chemtech*, 1973, 560
[f] P. Hodge, *Chem. Brit.*, **14**, 1978, 237
[g] A.L. Robinson, *Science*, **194**, 1976, 1261
[h] J.C. Balair, *Catal. Rev., Sci. Eng*., **10**, 1974, 17

2.4.2 Synthesis gas

Synthesis gas, a mixture of CO and H_2 along with CO_2 may be obtained by controlled oxidation or catalytic steam "re-forming" of CH_4 or light petroleums, or by gasification of coal with oxygen and/or steam at ~1500 ˚C. Carbon dioxide is removed by scrubbing with monoethanolamine or by arsenite solutions, from which it is recovered. The ratios of H_2 and CO vary in the different routes from 0.9 for coal gasification, to 1.8 for oxidation of CH_4.[5] There are several reasons for wanting to alter the hydrogen concentration. Firstly, hydrogen is a more versatile industrial chemical than water gas. Secondly, small organic molecules tend to have roughly three to four times as many hydrogen atoms as carbon atoms, so if the H_2/CO mole ratio can be changed to about two, a good feedstock is obtained.

The water-gas shift (WGS) reaction, Scheme 2.4, is used to convert CO and H_2O into H_2 and the byproduct CO_2.[59] This equilibrium process is catalysed by many soluble transition-metal complexes; however the commercial catalysts are typically heterogenous: Cr_2O_3 at 350 ˚C, or Cu-Zn-oxide at 200-300 ˚.[60]

$$CO + H_2O \rightleftharpoons CO_2 + H_2$$

Scheme 2.4

Many homogenous WGS catalysts have been studied, including $[Ru_3(CO)_{12}]$, $[Pt(PR_3)_3]$, $[Rh(CO)_2I_2]^-$, and $[HFe(CO)_4]^-$. On the basis of studies involving these homogenous WGS catalysts, a mechanism for the water-gas shift reaction has been proposed, Scheme 2.5.

[59] C. Rhodes, *Catal. Commun.*, **3**, 2002, 381
[60] H.M. Colquhoun, D.J. Thompson, 'Carbonylation – Direct Synthesis of Carbonyl Compounds', Plenum Press, New York, 1991

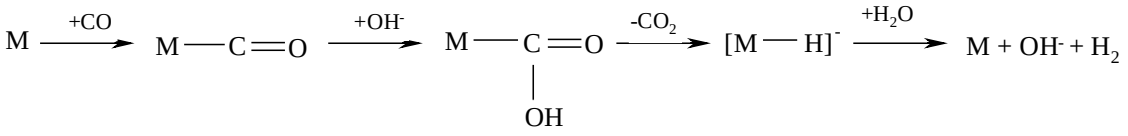

Scheme 2.5

A scheme for the reaction catalysed by $[Ru(bipy)_2(CO)Cl]^+$ is illustrated in Figure 2.7. This particular scheme is important because all the key intermediates have been isolated.[60]

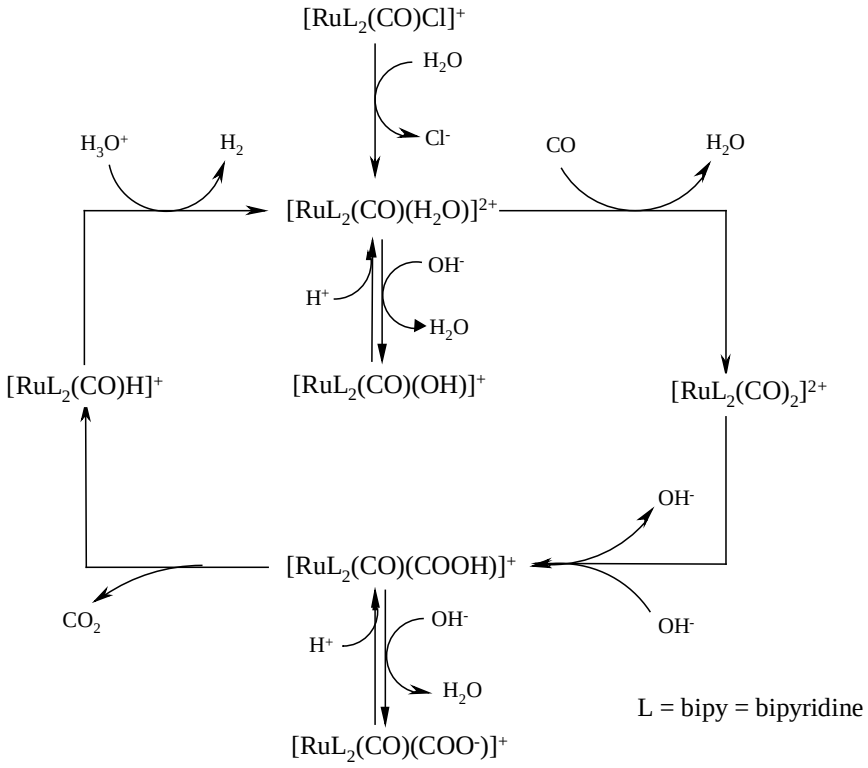

Figure 2.7: Ruthenium catalysed Water Gas Shift reaction

Whatever the source of synthesis gas, it is the starting point for many industrial chemicals. Some examples to be discussed are the hydroformylation processes for converting alkenes to aldehydes and alcohols and the "Monsanto" and "Cativa" processes for the production of acetic acid from methanol. Other generalised reactions using CO in

the presence of water (a synthesis gas equivalent via the WGS), alcohols, amines, and so on, are loosely termed carbonylations, and are summarised in Figure 2.8.[60]

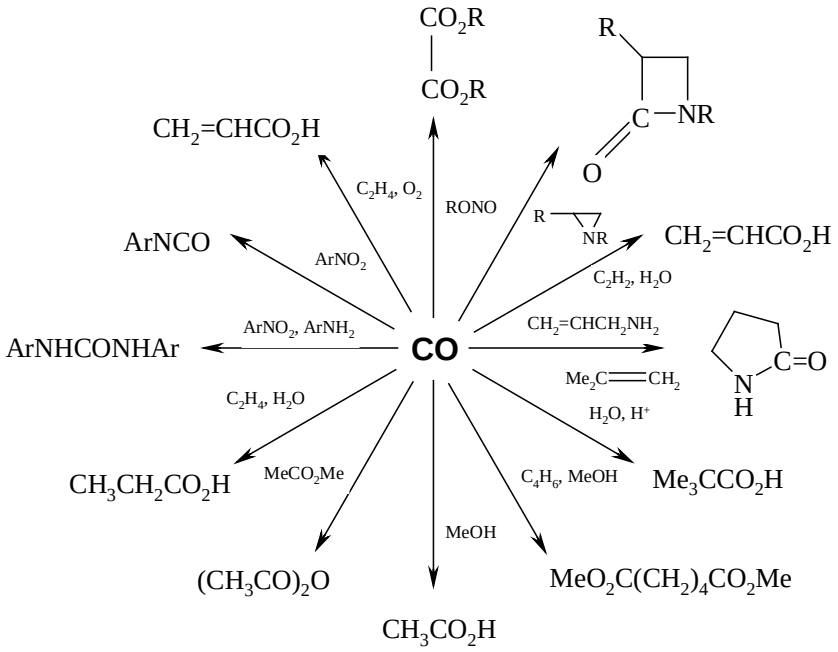

Figure 2.8: Examples of some carbonylation reactions

2.4.3 Hydroformylation

Hydroformylation is the process whereby alkenes react with synthesis gas to produce aldehydes in the presence of certain homogenous transition metal catalysts, namely cobalt and rhodium salts. The process was discovered by Otto Roelen of Ruhrchemie in 1938 and is the oldest and largest volume catalytic reaction of alkenes, with the conversion of propylene to butyraldehyde being the most important.[61,62] Several million tons of aldehydes and aldehyde derivatives are produced annually worldwide, making the process the most important industrial synthesis using a metal carbonyl complex as a

[61] B. Cornils, W.A. Herrman, *Angew. Chem*., **106**, 1994, 2219
[62] B. Cornils, J. Falbe, 'New Synthesis with Carbon Monoxide', Springer-Verlag, Berlin, 1980

homogeneous catalyst. The name stems from the nature of the reaction, which formally involves adding H and the formyl group (CHO), derived from H_2 and CO to an alkene, Scheme 2.6. The net result of the process is extension of the carbon chain by one, and more importantly, introduction of oxygen into the molecule.[5]

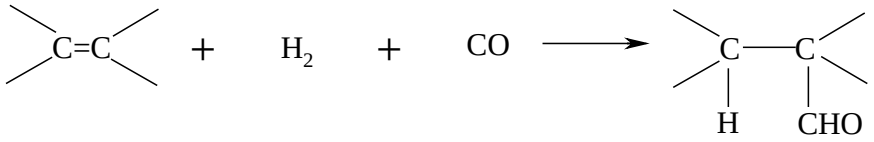

Scheme 2.6

In subsequent steps *n*-butyraldehyde is converted into either *n*-butanol, 2-ethylhexanol, or 2-ethylhexanoic acid (Scheme 2.7). The principal commercial product, 2-ethylhexanol, is transformed into pthalate esters which are used as plasticisers for polyvinylchloride resins.

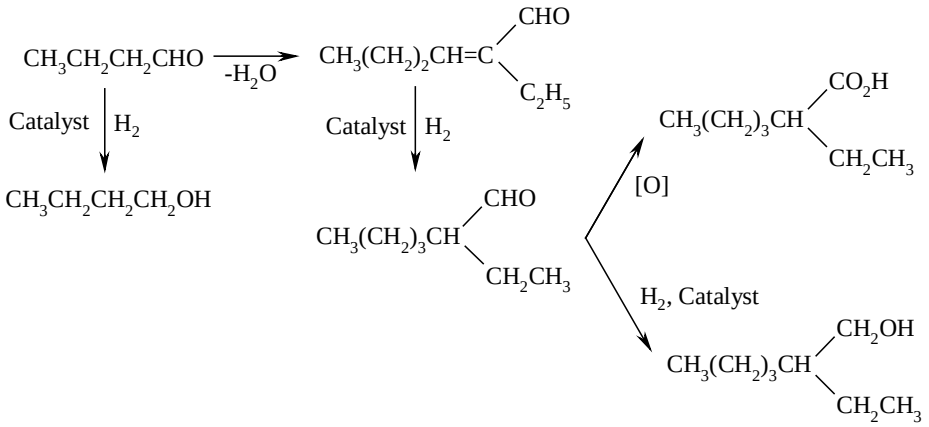

Scheme 2.7

The original hydroformylation catalyst [$Co_2(CO)_8$] requires process conditions of 150 – 180 ˚C and syngas pressures exceeding 200 atm. Besides the obvious disadvantages of such extreme reaction conditions, this catalyst produces predominantly branched chain aldehydes over linear molecules.[5] The linear products are more desirable as a result of the

increased biodegradability of linear detergents over branched ones. The Cobalt process is technically difficult to operate because the hydrocarbonyl, [$HCo(CO)_4$], participating in the catalyst cycle, is volatile and must be separated from the alcohol products, and the Co must be recovered as sulfate and recycled. Another disadvantage is that ~15% of the alkene is lost by hydrogenation, while condensation and ketone by-products are also formed.[5]

The most widely accepted mechanism for the catalytic cycle was proposed by Heck and Breslow[63] in the early 1960's and is depicted as Figure 2.9, below.[64]

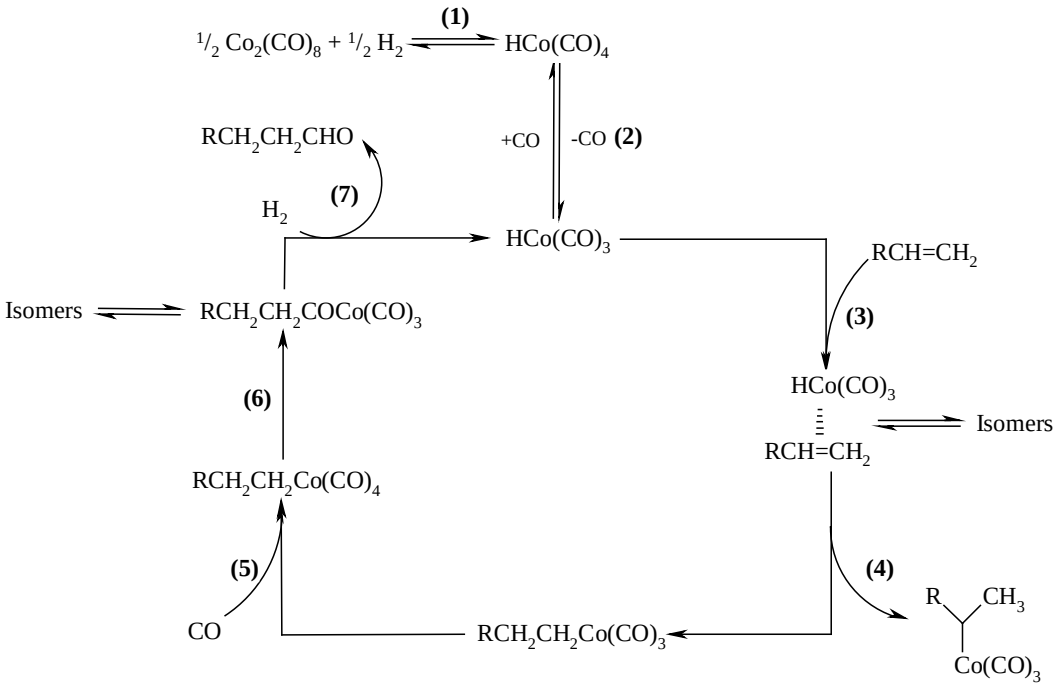

Figure 2.9: Catalytic cycle of hydroformylation with unmodified cobalt catalysts

[63] R.F. Heck, D.S. Breslow, *J. Am. Chem. Soc.*, **83**, 1961, 4023
[64] B. Cornils, W.A. Herrmann, 'Applied Homogenous Catalysis with Organometallic Compounds', Volume 1, Wiley, 2002

The steps labeled (1) to (7) in Figure 2.9 correspond to the following:

(1) Formation of the active hydridometal carbonyl species via reaction of the metal carbonyl [$Co_2(CO)_8$] with hydrogen.
(2) CO dissociation to form the unsaturated 16e species, [$HCo(CO)_3$]
(3) Alkene coordination to form the saturated 18e complex.
(4) β–Hydrogen transfer to form the 16e alkylmetal carbonyl species.
(5) Coordination of CO to form the 18e complex.
(6) Carbonyl insertion reaction to form the 16e acylmetal carbonyl species.
(7) Hydrogen cleavage of the acylmetal species to form the desired aldehyde and regeneration of the hydridometal carbonyl.

Since its discovery in 1938, the hydroformylation process has been fine tuned by way of catalyst modification to improve the reaction conditions, linear to branched ratio of the products, as well as other process parameters. These modifications involved introducing phosphine ligands to the Co metal center, moving from Co to Rh metal and subsequent ligand modification of the Rh center. The following discussions provide further details and the results of these modifications.

2.4.3.1 Shell Modification of the Cobalt Catalyst System

The modified Co catalyst, [$HCo(CO)_3PBu_3$], developed by Shell, produces improved linear to branched ratios of ~ 3, but gives lower reaction rates and thus requires higher reaction temperatures. However, the modified catalyst is far more stable to decomposition than [$Co_2(CO)_8$] and can thus be used at lower pressures (~100 atm). An additional advantage of the modified catalysts increased stability is that the aldehyde can be distilled from the catalyst, thus simplifying the process engineering. Apart from the increased temperatures, a further drawback of the modified catalyst is the tendency to promote alkene hydrogenation, which is an undesirable side reaction. As a result of these factors, the phosphine-modified catalyst is superior when linear alcohols are the desired

product; otherwise the simple cobalt carbonyl catalyst is preferable, for example, in the manufacture of 2-ethylhexanol.

2.4.3.2 Unmodified Rhodium Catalysts

Simple rhodium carbonyl derivatives have found little use as hydroformylation catalysts. This is a result of the competing equilibria of the carbonyl species to form the thermodynamically stable, but catalytically inactive tetrameric and hexameric rhodium carbonyl clusters. It is, however, possible to form a catalytically active rhodium carbonyl species, $[HRh(CO)_4]$ under CO/H_2 pressure[65] (Scheme 2.8). This species has very high catalytic activity but tends to hydrogenate and isomerise alkenes, and produce lower linear to branched ratios than the cobalt analogues.

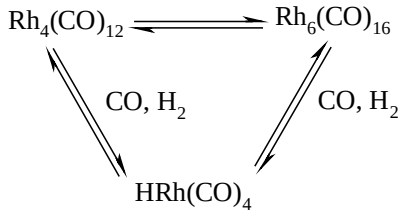

Scheme 2.8

2.4.3.3 Modified Rhodium Catalysts

The replacement of cobalt by modified rhodium catalysts has allowed development of processes which operate under much milder conditions, below 100 ˚C and at only a few atmospheres pressure. The addition of phosphine ligands to rhodium carbonyl catalyst precursors produces highly active catalysts (rates comparable to unmodified rhodium catalysts) with excellent selectivity for the formation of the desired linear aldehydes (ratio of 30:1, linear to branched).

[65] R. Whyman, *J. Organomet. Chem.*, **94**, 1975, 303

An additional advantage of these systems is that they produce aldehydes without loss of alkene by hydrogenation.

The rhodium system based on $[HRh(CO)(PPh_3)_3]$ has allowed a fairly detailed picture of the mechanism to be obtained.[66]

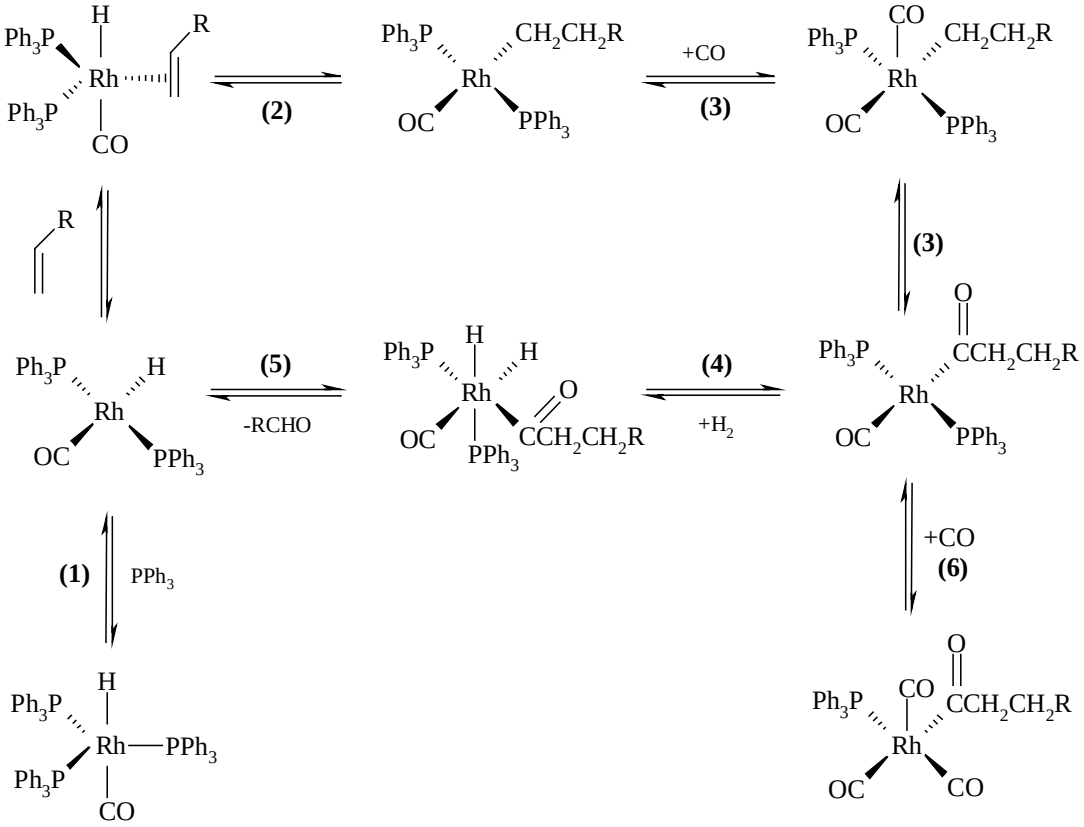

Figure 2.10: Simplified catalytic cycle for hydroformylation using modified rhodium catalysts

[66] M. Chanon, *J. Mol. Catal.*, **32**, 1985, 27

The steps labeled (1**)** to (6) in Figure 2.10 correspond to the following:[5]

(1) Formation of catalytically active 16e species.

(2) After alkene coordination, β-hydride migration leads to the alkylmetal complex.

(3) CO coordination and acyl migration yields the acylmetal derivitave.

(4) Acylmetal complex undergoes oxidative-addition of molecular hydrogen to give the dihydridoacyl complex.

(5) Rate determining step of hydride transfer to carbon atom of acyl group, followed by reductive elimination to aldehyde and active species .

(6) Excess of CO over H_2 inhibits hydroformylation through formation of five-coordinate dicarbonyl acyls, which is unable to react with dihydrogen.

There are several convenient rhodium precatalysts for hydroformylation reactions. These include rhodium metal on carbon, $[RhCl(CO)(PPh_3)_2]$ + EtN_3, $[Rh(CO)_2(acac)]$, and $[HRh(CO)(PPh_3)_3]$. These modified rhodium hydroformylation catalysts were introduced into commercial production by Union Carbide in 1976 and have been used subsequently by several other companies. A few years ago the company announced a new low-pressure hydroformylation rhodium catalyst modified with phosphites, $P(OR)_3$, which works with less active alkenes such as 2-butene and 2-methylpropene. The relatively high expense of rhodium requires that this catalyst be long lived and not lost from the reaction system.

As a result of the above factors, even though rhodium costs much more than cobalt (300:1), the moderate conditions, high selectivity, good yields, improved catalyst stability, ease of product separation, and higher reaction rates combine to make the rhodium catalyst commercially competitive with cobalt systems. It is expected that the use of rhodium catalysts will continue to increase in hydroformylation chemistry.

2.4.4 The Monsanto Acetic Acid Process

The carbonylation of methanol to form acetic acid, developed by workers at Monsanto, stands out as the technologically most successful example of homogeneous catalysis. This route for the industrial manufacture of acetic acid accounts for approximately 60% of the world acetic acid manufacturing capacity,[67] with over a million tons per year of acetic acid being produced.

This extremely selective, high-yield reaction is also very fast, with rates in the enzymatic range. The original process, commercialized by BASF in 1960, used a homogenous cobalt catalyst with an iodide co-catalyst. This combination required the use of high temperatures (> 200 ˚C) and pressures (about 700 bar),[68,69] with the selectivity to acetic acid at about 90% based upon methanol. But in 1971 the low-pressure rhodium-catalysed reaction was commercialised by Monsanto at Texas City.[70] This system, again with an iodine co-catalyst, is a highly selective (>99% based on methanol) catalyst for the carbonylation of methanol to acetic acid under relatively mild conditions (150 – 200 ˚C and 30 – 50 bar pressure)[70,71,72] and is now the dominant technology in the field.

The key elements of these carbonylation processes is the ability of a metal complex to undergo facile oxidative addition with methyl iodide, carbon monoxide insertion into the methyl-metal bond, and reductive elimination of the acetyl group as the acetyl halide.[73]

A common catalytic pathway is proposed which involves the nucleophilic attack of the active Rh catalyst complex, $[Rh(CO)_2I_2]^-$, on methyl iodide (CH_3I) to form a methylrhodium(III) intermediate, $[Rh(CH_3)(CO)_2(I)_3]^-$. Rapid methyl migration in this complex generates the acylrhodium(III) intermediate, $[Rh(CH_3CO)(CO)I_3]^-$, which reacts with CO to form $[Rh(CH_3CO)(CO)_2I_3]^-$ and subsequently reductively eliminates acetyl

[67] G. Sunley, D.J. Watson, *Catalysis Today*, **58**, 2000, 293
[68] H. Hohenschutz, *Hydrocarbon Process*, **45**, 1996, 141
[69] N. von Kutepow, *Chem. Ing. Tech*., **37**, 1965, 383
[70] J.F. Roth, J.H. Craddock, *Chem. Technol.*, 1971, 600
[71] F.E. Paulik, *J. Chem. Soc., Chem. Commun*., 1968, 1578
[72] R.T. Eby, *Appl. Ind. Catal.*, 1971, 483
[73] S.L. Cook, *Chem. Ind.*, **49**, 1993, 145

iodide and regenerates the rhodium(I) anion,[64] see Figure 2.11, below. This catalytic cycle[74] was proposed on the basis of selected data from the structures of reactants and intermediates which have been identified by X-ray crystallography,[75] infrared and NMR spectroscopy.[76]

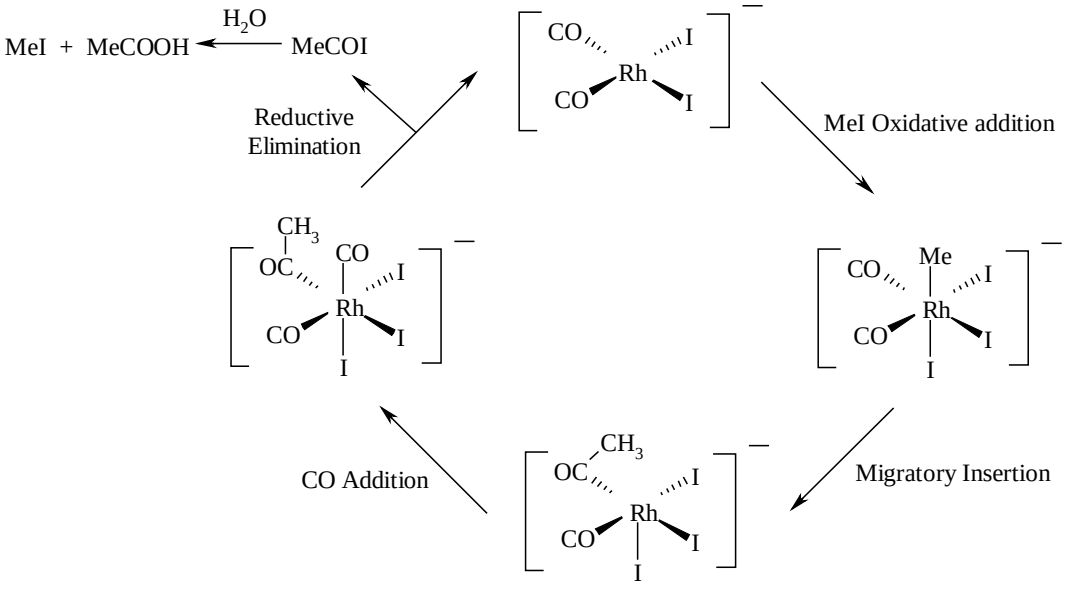

Figure 2.11: The Monsanto Acetic Acid Process

The final reaction of acetyl iodide with compounds containing hydroxyl groups such as water, methanol or acetic acid leads to the formation of hydrogen iodide and the corresponding acetyl derivatives. This final reaction step of the carbonylation mechanism is the primary distinguishing feature of each carbonylation process. A sufficient concentration of water or acetic acid in the reactor is therefore necessary to achieve high acetic acid or acetic anhydride formation rates respectively. The hydrogen iodide liberated then reacts with methanol or methyl acetate (or dimethyl ether) to regenerate the methyl iodide promoter.[64] Since methanol would insert CO into the O-H bond (to give

[74] D. Forster, *J. Am. Chem. Soc.*, **98**, 1976, 846
[75] D. Forster, *Adv. Organomet. Chem.*, **17**, 1979, 255
[76] A. Haynes, *J. Am. Chem. Soc.*, **115**, 1993, 4093

methyl formate) and not into the C-O bond (to give acetic acid), the presence of iodide is necessary to convert methanol into methyl iodide prior to carbonylation.[77]

The reaction rate is essentially independent of methanol concentration and carbon monoxide pressure[78] (so the process can be operated, if required, at atmospheric pressure). The rate-determining step appears to be oxidative addition of iodomethane to the anionic square planar complex, and the reaction rate is essentially of first order in both catalyst and methyl iodide concentrations under normal conditions.[77] The subsequent steps in the catalytic cycle are migratory insertion and reductive elimination. These reactions are fast and therefore not rate-limiting in this catalytic reaction.

A substantial amount of water (14 – 15 wt.%) is required to achieve high catalyst activity and also to maintain good catalyst stability.[76] Water serves to maintain the catalyst in its active form [as the rhodium(I) complex] and decreases the formation of inactive rhodium(III) complexes such as $[Rh(CO)_2I_4]^-$ or $[Rh(PEt_3)_2(CO)I_3]$.[77] In fact, if the water content is less than 14 – 15 wt.%, the rate determining step becomes the reductive elimination of the acetyl species. However, as rhodium also catalyses the water-gas shift reaction, the side reaction leading to CO_2 and H_2 is significantly affected by water and hydrogen iodide concentration in the reaction liquid.[79,80]

The various ligands bound to the metal center affect the reactivity of the complex by increasing or decreasing the electron density on the center and can thus be used to control the outcome, rate and stereoselectivity of a catalytic reaction. Increasing the electron density at the Rh center should promote oxidative addition, and consequently increase the overall rate of the reaction. This factor has initialized an intensive study into the development of systems containing simple phosphine ligands such as PEt_3[81,82] and other

[77] C. Thomas, *Coord. Chem. Rev.*, **243**, 2003, 125
[78] J. Hjortkjaer, *Ind. Eng. Chem. Prod. Res. Dev.*, **15**, 1976, 46
[79] D. Forster, *J. Chem. Ed.*, **63**, 1986, 204
[80] D.J. Watson, 'Catalysis of Organic Reactions', Marcel Deker, New York, 1998
[81] J. Rankin, *Chem. Commun.*, **19**, 1997, 1835
[82] J. Rankin, *J. Chem. Soc., Dalton Trans*., 1999, 3771

trialkylphosphines as promoters for rhodium-based carbonylation catalysts, because they are strongly electron donating ligands.[77]

The iodine ions acting as ligands for the Monsanto catalyst are good nucleophiles, very weak proton bases, good leaving groups and generally good ligands for transition metals in lower oxidation states, however the corrosive nature of iodine is a major engineering problem with the Monsanto process.[6]

Another factor to consider regarding the catalytic activity is the geometrical arrangement of the ligands. The rate of the oxidative addition, rate determining step has been shown to be enhanced by the presence of *trans*-$[Rh(CO)_2I_2]^-$. The *cis* form of the active species is nearly exactly square planar while the *trans* structure is twisted. It has also been shown that *cis* to *trans* isomerizations are possible and reasonable paths to the formation of previously unidentified *trans* forms. The presence of $[Rh(CO)_2I_3]^{2-}$ is also thought to enhance the addition even more. These points show that the geometrical arrangement of the ligands has a very large effect on the catalytic activity of the complexes and this suggests possible improvements to these industrially important processes.[83]

2.4.5 The Cativa Process

Despite the successes of the rhodium catalysed Monsanto processes, there was still a need for a catalytic system that would offer improved catalyst stability, allowing operation under even milder conditions and at lower water concentrations. Lowering the water content of the reaction process results in reduced production of CO_2 and of hydrogenated by-products via the water-gas shift reaction. Lower water content also reduces the concentration of HI and thus the corrosion risk as well as decreases the steam consumption.[77]

[83] T. Kinnunen, *J. of Mol. Struct. (Theochem),* **542**, 2001, 273

During the development of the Monsanto process it was discovered that iodide promoted iridium catalysts were effective as carbonylation catalysts, although the reaction rate exhibited by the rhodium catalyst system was superior to that of iridium. However, recently it was shown that an improved iridium catalyst based on $[Ir(CO)_2I_2]^-$, in combination with a promoter metal such as ruthenium in the form of $[Ru(CO)_4I_2]$, has a higher activity and selectivity than reported in previous iridium systems.[84,85]

This system and its use in the production of acetic acid was commercialized as the 'Cativa' process in 1996 and besides achieving all the aims of the previous section, this process is also characterised by reduced formation of liquid by-products and improved yield on carbon monoxide.[67]

The Cativa process holds several advantages over its Monsanto analogue. The system is able to operate at reduced water levels (< 8 wt.%), compared to the Monsanto process (14 – 15 wt.%) and the iridium catalyst has a far superior stability[86] to the rhodium catalyst at these low water levels. The iridium catalyst has also been found to remain stable under a wide range of conditions that would cause the rhodium analogues to decompose completely to inactive and largely unrecoverable rhodium salts. The iridium is also far more soluble than rhodium in the reaction medium, and thus a higher catalyst concentration can be obtained, making much higher reaction rates achievable. A rate maximum exists at commercially attractive low water conditions, and optimization of the process parameters gives acetic acid with a selectivity in excess of 99% based on methanol.[77]

Mechanistic studies of the iridium-catalysed methanol carbonylation show many similarities to the rhodium system, but with a greater degree of complexity. The rhodium system comprises only anionic components, while the iridium-based cycle involves both anionic and neutral intermediates.[64] The kinetics of the two systems also differ, where the rate determining step of the Monsanto process is the oxidative addition of methyl iodide

[84] M.J. Howard, M.D. Jones, *Catal. Today*, **18**, 1993, 325
[85] D.J. Watson, *Chem. Ind.*, **75**, 1998, 369
[86] K.E. Clode, European Patent to BP Chemicals, 1994, 616997

to the metal center, in the Cativa process, the 1,1-insertion is the rate determining step.[83] Model studies have shown that the oxidative addition step on an iridium metal center occurs about 150 times faster than the equivalent addition on the rhodium center. This represents a dramatic improvement in reaction rates.[87]

The rate of the Cativa cycle also holds an inverse dependence on the concentration of ionic iodide. So species capable of removing iodide should promote the rate limiting step. These promoters fall into two distinct groups: simple iodide complexes of zinc, cadmium, mercury, gallium and indium, and carbonyl-iodo complexes of tungsten, rhenium, osmium and rhuthenium. The presence of the promoter leads to a substantial increase in the proportion of the active anionic species $[Ir(CH_3)(CO)_2I_3]^-$ and a substantial decrease in the loss of iridium by the formation of inactive $[Ir(CO)_3I_3]$ and $[Ir(CO)_2I_4]^-$ species.[77]

The Cativa process has now been successfully commercialized on three world scale plants. However, on the other hand, recent advances in the design of suitable ligands, mainly based on phosphorous-containing systems, has led to the synthesis of highly active and stable rhodium complexes, so that new advances in the rhodium-catalysed carbonylation of methanol is to be expected.

[87] P.M. Maitless, *J. Chem. Soc. Dalton Trans*., 1996, 2187

3. SYNTHESIS AND CHARACTERISATION OF RHODIUM COMPLEXES

3.1 INTRODUCTION

This chapter contains the synthetic protocols utilized for the production of the Rh(I) and Rh(III) stibine complexes and the spectroscopic characterisation thereof. Various techniques were used for complex characterisation, including infrared (IR), UV – Visible (UV-Vis) and Nuclear Magnetic Resonance (NMR) spectroscopy, and the synthesis section is precluded by a brief introduction to each of these techniques.

For the purpose of this study, various phosphorous ligand systems were reacted with the rhodium - stibine complexes, and the chapter details the methods of reaction as well as identification and characterisation of the various products formed.

Several of the complexes synthesised were also characterised by means of X–ray crystallography. Theoretical aspects of the technique as well as a detailed look at each crystal structure will follow.

3.2 SPECTROSCOPIC CHARACTERISATION TECHNIQUES

3.2.1 Infrared Spectroscopy

Infrared spectroscopy is one of the most important analytical techniques available to chemists. The technique is based on the vibration modes of atoms in a molecule. This vibration results in the formation of a peak in the absorption spectrum and the energy of

the peak corresponds to the frequency of the particular vibration. An infrared spectrum is obtained by passing infrared radiation through a sample and determining what fraction of the incident radiation is absorbed at a particular energy.[1]

A molecule can only absorb radiation when the incoming infrared radiation is at the same frequency as one of the fundamental modes of vibration of the molecule. This means that the vibrational motion of a small part of the molecule is increased, while the rest of the molecule is left unaffected. For a vibration to give rise to absorption of infrared radiation, it must cause a change in the dipole moment of the molecule. The larger this change, the more intense the absorption band will be.

As a result of the difference in electronegativity between carbon and oxygen, the carbonyl group is permanently polarized, and vibrational stretching of this bond will therefore increase the dipole moment. As a result of these factors, C≡O stretching produces a distinct absorption peak and the carbonyl group is frequently used for complex characterisation.

The C≡O stretching frequency, *v*(CO), is dependant on the groups bonded to the C atom, e.g.: free C≡O produces an absorption peak around 2200 cm^{-1}, however the stretching frequency of metal – carbonyl complexes are shifted to lower wavelengths, for example 1979 cm^{-1} and 1975 cm^{-1} for *trans*-[Rh(Cl)(CO)(PPh_3)$_2$] and *trans*-[Rh(Cl)(CO)($AsPh_3$)$_2$], respectively.[2] This shift is a result of electron back donation from the metal orbitals to the carbon anti-bonding orbitals, which weakens the C≡O bond, lowering the frequency of the bond vibration.

The infrared spectrum can be divided into three regions: the far infrared (400 – 0 cm^{-1}), the mid infrared (4 000 – 400 cm^{-1}) and the near infrared (14 285 – 4 000 cm^{-1}). Most infrared applications employ the mid infrared region, where resonances with molecular

[1] B. Stuart, 'Modern Infrared Spectroscopy', Wiley, New York, 1996
[2] A. Roodt, S. Otto, G. Steyl, *Coord. Chem. Rev.* **245**, 2003, 121

vibrational frequencies occur,[3] but the near and far regions can also provide information about certain materials.

The mid infrared spectrum can be divided into four regions:

The X – H stretching region (4 000 – 2 500 cm^{-1})
The triple bond region (2 500 – 2 000 cm^{-1})
The double bond region (2 000 – 1 500 cm^{-1})
The fingerprint region (1 500 – 600 cm^{-1})

For the purpose of this study, the spectra were produced using the double and triple bond regions. The principal bonds in this region are due to C=C and C≡O stretching. Since the *v*(CO) of metal carbonyl complexes is generally free from coupling with other modes and is not obscured by the presence of other vibrations, studies of *v*(CO) alone often provides valuable information about the structure and bonding of carbonyl complexes.[4]

3.2.2 Ultraviolet - Visible Spectroscopy

The technique of Ultraviolet – Visible (UV – Vis) spectroscopy (200 - 800 nm) is based on the electronic excitations between energy levels of molecular orbitals of molecular systems. When sample molecules are exposed to light having an energy matching that of a possible electronic transition within the molecule, part of the light energy becomes absorbed and the electron is promoted to an empty, higher energy orbital. As a rule, energetically favored electron transitions will be from the highest occupied molecular orbital (HOMO) to the lowest unoccupied molecular orbital (LUMO), creating an excited state.

[3] W.N. Delgass, 'Spectroscopy in Heterogenous Catalysis', Academic Press, New York, 1979
[4] K. Nakamoto, 'Infrared and Raman Spectra of Inorganic Coordination Compounds', 3rd Ed., Wiley-Interscience, New York, 1978

Transitions involving π orbitals and lone pairs tend to have stronger absorptions, and are thus useful for identifying conjugated systems. The more highly conjugated the system, the smaller the HOMO – LUMO gap, ΔE, and the lower the frequency and longer the wavelength.

The unit of the molecule responsible for absorption is called the chromophore. These chromophore functional groups contain valence electrons of low excitation energy. The most common chromophore systems are the C=C and C≡O groups.[5]

UV – Vis spectroscopy has many uses, including the detection of eluting components in high performance liquid chromatography (HPLC), determination of the oxidation state of a metal center of a cofactor (such as heme), or following reaction profiles corresponding to the formation or disappearance of different colored reaction components.[5]

3.2.3 Nuclear Magnetic Resonance

Nuclear Magnetic Resonance (NMR) spectroscopy is one of the most powerful tools in modern science. Since its discovery 60 years ago, in 1945, it has spread from physics to chemistry, biosciences, material research and medical diagnosis. NMR and IR spectroscopy are powerful methods for structure determination of molecules in liquid state and challenge X-ray spectroscopy in the field of solid state structure analysis.

NMR makes use of the quantum mechanical property, called spin (*I*), of a nucleus in an atom. A nucleus must have a non-zero spin to be observed by NMR. The most commonly observed nuclei have $I = ½$, (^{1}H, ^{13}C, ^{19}F, ^{31}P). Nuclei that have spins greater than ½ are called quadrupolar and normally give broad NMR lines,[6] for example, the stibine nucleus.

[5] www.cem.msu.edu/~reusch/VirtualText/ Spectrpy/UV-Vis/spectrum.htm
[6] J.A. Iggo, 'NMR Spectroscopy in Inorganic Chemistry', Oxford University Press, 1999

Nuclear spin, although not really a physical 'spinning' has an associated magnetic moment vector that will interact with a magnetic field, B. When a sample is set in a strong magnetic field, it is possible to transfer energy into the spin system in the form of radio frequency pulses and change the state of the system. After the pulse, the system relaxes back to its state of equilibrium, sending a weak signal that can be recorded.
Under the influence of the external magnetic field, the spin state of the nuclear magnetic field may align with the external field or give rise to an opposing field. This results in a low energy state (E_1) and a high energy state (E_2) respectively. Radio frequency waves at this energy (ΔE) will interconvert the two states, Figure 3.1.

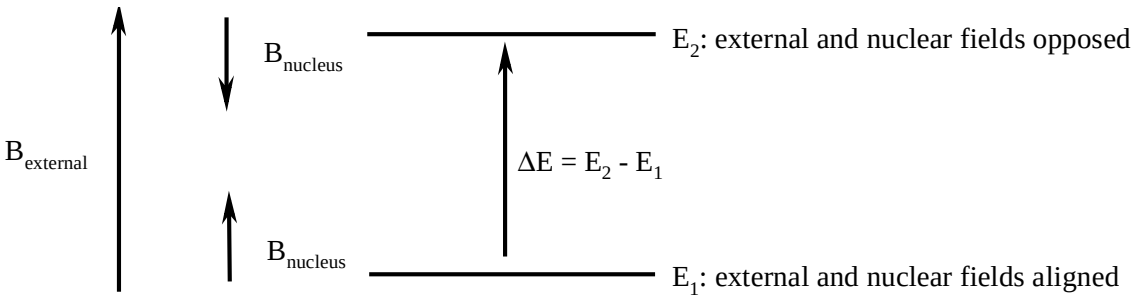

Figure 3.1: Energy Transition States associated with NMR Spectroscopy

An NMR spectrum arises because nuclei in different parts of the molecule experience different local magnetic fields according to the molecular structure, and therefore have different frequencies at which they absorb. The other nuclei and electrons in the molecule shield the nuclei from some of the magnetic field, so the effective magnetic field felt is somewhat less than the applied field. This results in signals having varying chemical shifts, δ. Several factors, including co-ordination number, oxidation state, and geometry influence the shielding of the nuclei and hence the chemical shift. An increase in shielding, σ, results in a decrease in the chemical shift, i.e. in a shift upfield.

Other nearby spin-active nuclei also effect the local magnetic field about a nucleus. This is referred to as coupling and leads to additional splitting of the resonances for groups of

coupled nuclei.[6] Coupling is transmitted by the valence electrons of a molecule. The magnitude of coupling is related to the number of bonds separating the coupled nuclei. Coupling between nuclei separated by four or more bonds is not generally observed. Various factors affect the extent of coupling and include the σ-orbital character of the bond, hybridization, the coordination number, electronegativity, *trans*-influence and oxidation state of the coupled nuclei.

The concepts of chemical shift and coupling play a vital role in the assigning of NMR signals to different chemical species, as indicated later in this chapter.

3.3 SYNTHESIS AND SPECTROSCOPIC CHARACTERISATION

3.3.1 Chemicals and Instrumentation

All chemicals used for synthesis and characterisation were reagent grade. The following chemicals were commercially available from Sigma-Aldrich and were used without further purification: $SbPh_3$, $Ag(CF_3SO_3)$, $(CH_3)_2C_6H_3OH$, Et_3N, PCl_3, $P(O\text{-}2,4\text{-}{}^tBu_2C_6H_3)_3$, $P(OPh)_3$, PPh_3. The $RhCl_3.3H_2O$ was purchased from Next Chimica.

The additional phosphites: $P(O\text{-}2,6\text{-}Me_2C_6H_3)_3$, $P(O\text{-}4\text{-}ClC_6H_4)_3$, $P(O\text{-}4\text{-}{}^tBuC_6H_4)_3$ and $P(O\text{-}4\text{-}OMeC_6H_4)_3$ were synthesised in cooperation with Dr R. Meijboom.[7] A representative synthetic route has been included in section 3.3.2.5. Table 3.1 gives the abbreviated forms of each phosphite to be used later in the text.

All infrared spectra were recorded as KBr disks or in $CHCl_3$ using a Bruker Equinox FT-IR spectrophotometer and analysed using Bruker OPUS-NT software. The UV-Vis spectra were obtained using a Varian Cary 50 spectrophotometer with 1.00 cm path length. The complexes were further characterised using ^1H, ^{31}P and ^{13}C NMR on a 300

[7] To be published

MHz Gemini 2000 spectrometer operating at 300, 121 and 75 MHz for each nucleus respectively. The spectra were recorded in $CDCl_3$, with the ^1H spectra calibrated relative to TMS using the $CHCl_3$ peak (7.24 ppm) and the ^{31}P spectrum relative to 85% H_3PO_4 as an external standard in a capillary at 0 ppm. Low temperature ^{31}P NMR spectra were conducted using a Varian Inova spectrometer at 121 MHz.

Table 3.1: Phosphite ligands and their associated abbreviations

Phosphite Name	Chemical Formula	Abbreviation
Tris(2,6-dimethylphenyl)phosphite	$P(O\text{-}2,6\text{-}Me_2C_6H_3)_3$	2,6-MPP
Tris(2,4-di-^{t}butylphenyl)phosphite	$P(O\text{-}2,4\text{-}^tBu_2C_6H_3)_3$	2,4-TBPP
Triphenylphosphite	$P(OC_6H_5)_3$	TPP
Tris(4-chlorophenyl)phosphite	$P(O\text{-}4\text{-}ClC_6H_4)_3$	4-ClPP
Tris(4-methoxyphenyl)phosphite	$P(O\text{-}4\text{-}OMeC_6H_4)_3$	4-MPP
Tris(4-^{t}butylphenyl)phosphite	$P(O\text{-}4\text{-}^tBuC_6H_4)_3$	4-BPP

3.3.2 Synthesis of Rh(I) and Rh(III) Complexes

The following sections provide the synthesis protocols for the complexes discussed later in the chapter.

3.3.2.1 Synthesis of $[Rh(\mu\text{-}Cl)(CO)_2]_2$

Tetracarbonyldichlorodirhodium $[Rh(\mu\text{-}Cl)(CO)_2]_2$, was synthesised according to the procedure developed by McCleverty and Wilkinson.[8]

[8] J.A. McCleverty, G. Wilkinson, *Inorg. Synth.*, **28**, 1990, 84

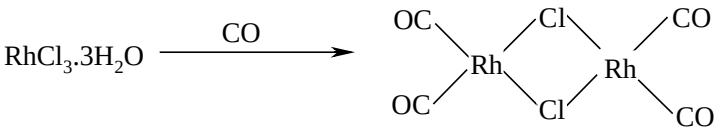

Scheme 3.1

Rhodium trichloride trihydrate (1.00 g, 3.81 mmol) was pulverized and placed on top of a porous disk sealed at the end of a 20 cm x 2 cm tube. The apparatus was flushed with carbon monoxide and lowered into an oil bath maintained at 97 ˚C. Bath temperatures above 100 ˚C were avoided to prevent the formation of anhydrous rhodium trichloride, which is inert to carbon monoxide. Carbon monoxide was then flushed through the system over a period of 15 hours, while red needle-like crystals of the dimer sublimed on the inner surfaces of the tube. The crystals were recrystalised from hexane (Yield: 388 mg, 62 %).

IR (ν(CO)/KBr): 1967 and 1991 cm^{-1}

3.3.2.2 Synthesis of *trans*-[Rh(Cl)(CO)($SbPh_3$)$_2$] (1)

The complex was prepared according the procedure of Otto and Roodt.[9]

(1)

Scheme 3.2

[Rh(μ-Cl)(CO)$_2$]$_2$ (50 mg, 0.13 mmol) was dissolved in diethyl ether (20 cm^3) and maintained at 0 ˚C with the aid of a salt/ice bath. A solution of $SbPh_3$ (172 mg, 0.49 mmol) in diethyl ether (25 cm^3) was added drop-wise, where after a yellow precipitate of

[9] S. Otto, A. Roodt, *Inorg. Chim. Acta,* **331**, 2002, 199

trans-[Rh(Cl)(CO)($SbPh_3$)$_2$] formed. The product was collected in fractions by decanting the reaction solution to prevent contamination by unreacted rhodium starting material (Yield: 185 mg, 85 %).

IR (ν(CO)/KBr): 1952 cm^{-1}

(ν(CO)/$CHCl_3$): 1969 cm^{-1}

UV-Vis (CH_2Cl_2) [λ_{max}, nm (log ε, M^{-1} cm^{-1})]: 307 (3.15), 366 (3.44)

^{1}H NMR ($CDCl_3$): δ (ppm) 7.36 – 7.46 (m, 18H), 7.62 – 7.70 (m, 12H)

3.3.2.3 Synthesis of *trans*-[Rh(Cl)(CO)($SbPh_3$)$_3$] (2)

The procedure described is according to that of Otto and Roodt.[9]

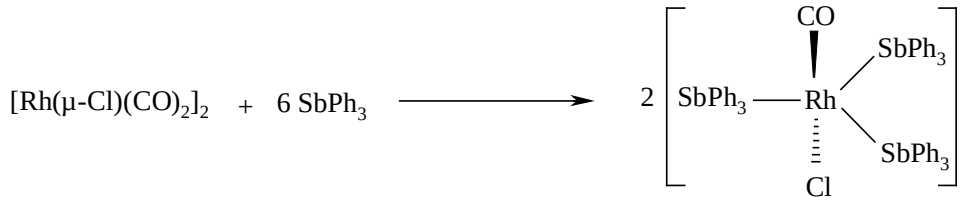

(2)

Scheme 3.3

[Rh(μ-Cl)(CO)$_2$]$_2$ (50 mg, 0.13 mmol) was dissolved in acetone (10 cm^3) at room temperature and solid $SbPh_3$ (340 mg, 0.96 mmol) was added in small portions. The yellow solution turned a darker red with each addition of ligand. Large red crystals of *trans*-[Rh(Cl)(CO)($SbPh_3$)$_3$] formed with solvent evaporation (Yield: 215 mg, 68%).

IR (ν(CO)/KBr): 1967 cm^{-1}

(ν(CO)/$CHCl_3$): 1971 cm^{-1}

UV-Vis (CH_2Cl_2) [λ_{max}, nm (log ε, M^{-1} cm^{-1})]: 418 (3.46), 488 (3.07)

^{1}H NMR ($CDCl_3$): δ (ppm) 7.25 – 7.38 (m, 27H), 7.48 – 7.56 (m, 18H)

3.3.2.4 Synthesis of *trans-mer*-[Rh(Cl)$_2$(Ph)(SbPh$_3$)$_3$] (3)

The complex was synthesised using two independent methods, starting from Rh(I) and Rh(III), respectively. Synthesis A gives the procedure starting from $RhCl_3.3H_2O$ and Synthesis B details the synthesis of (**3**) from *trans*-[Rh(Cl)(CO)(SbPh$_3$)$_2$].

Synthesis A:

The procedure described is according to that of Cini and co-workers.[10]

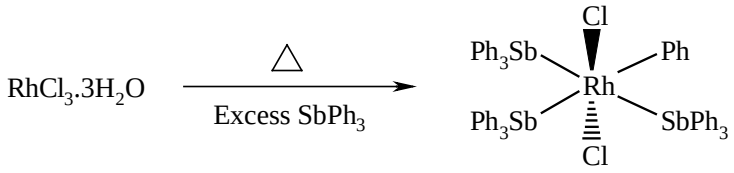

(3)

Scheme 3.4

$RhCl_3.3H_2O$ (527 mg, 2.00 mmol) was dissolved in warm absolute ethanol (8 cm^3) and the solution was filtered. This rhodium solution was then added to a mixture of $SbPh_3$ (2.82 g, 8.00 mmol) in absolute ethanol (30 cm^3) and heated under reflux while stirring. After 3 hours, the yellow suspension was allowed to cool where after a solution of $Ag(CF_3SO_3)$ (513 mg, 2.00 mmol) in ethanol (6 cm^3) was added. The mixture was heated under reflux for a further 3 hours in the dark and then it was allowed to cool to room temperature. The yellow crystalline solid was filtered and washed with ethanol. The crude product was mixed with CH_2Cl_2 (20 cm^3), AgCl was filtered off and the solution was treated with ethanol. The solid was then purified through recrystallisation from acetone (Yield 1.502 g, 56%).

[10] R. Cini, G. Giorgi, L. Pasquini, *Inorg. Chim. Acta*, **196,** 1992, 7

UV-Vis (CH_2Cl_2) [λ_{max}, nm (log ε, M^{-1} cm^{-1})]: 383 (3.25), 481 (3.06)
^1H NMR ($CDCl_3$): δ (ppm) 6.77 – 7.23 (m, 45H), 6.33 (t, 1H, $^1J_{H-H}$ = 15 Hz, $^2J_{H-H}$ = 8 Hz), 6.53 (t, 2H, $^1J_{H-H}$ = 14 Hz, $^2J_{H-H}$ = 7 Hz), 6.69 (d, 1H, $^1J_{H-H}$ = 8 Hz), 7.45 (d, 1H, $^1J_{H-H}$ = 8 Hz)

The reaction components produced from refluxing $RhCl_3.3H_2O$ with $SbPh_3$ correspond to a mixture of $[Rh(Cl)_2(Ph)(SbPh_3)_3]$ and $[Rh(Cl)_3(SbPh_3)_3]$. The addition of $Ag(CF_3SO_3)$ aids in removing the Cl^- ligand *trans* to the $SbPh_3$ in the latter complex and thus increases the yield of $[Rh(Cl)_2(Ph)(SbPh_3)_3]$. The addition of excess Cl^- would thus inhibit the formation of $[Rh(Cl)_2(Ph)(SbPh_3)_3]$, (**3**).

Cini *et. al*. investigated the reaction under various conditions and were able to conclude that free benzene is not responsible for producing (**3**) and the Ph ligand must come from $SbPh_3$. It seems reasonable to assume the reaction of $RhCl_3.3H_2O$ with $SbPh_3$ in ethanol first produces the *mer* isomer, $[Rh(Cl)_3(SbPh_3)_3]$. The Cl^- donor, which experiences a strong *trans* influence from Sb, is then replaced by a Ph group from a $SbPh_3$ molecule, and $[Rh(Cl)_2(Ph)(SbPh_3)_3]$ and a $ClSbPh_2$ molecule are formed.

Synthesis B:

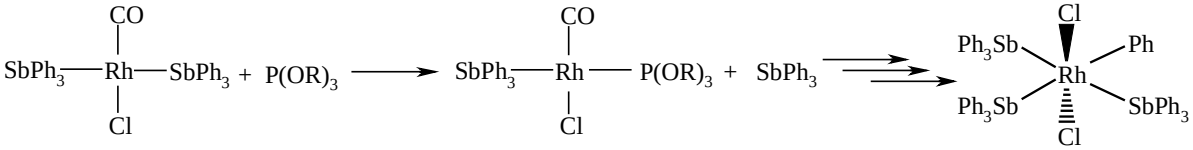

$P(OR)_3$ = 2,4-TBPP, 2,6-MPP and 4-BPP

Scheme 3.5

trans-$[Rh(Cl)(CO)(SbPh_3)_2]$ (50 mg, 0.057 mmol) was dissolved in chloroform (5 cm^3) and a solution of $P(O\text{-}2,4\text{-}^tBu_2C_6H_3)_3$ (37 mg, 0.057 mmol) in chloroform (10 cm^3) was added drop-wise to form *trans*-$[Rh(Cl)(CO)(SbPh_3)(2,4\text{-TBPP})]$. Slow addition ensured

the reaction did not form the *bis* phosphite, *trans*-[Rh(Cl)(CO)(2,4-TBPP)$_2$] species. IR spectroscopy was used to confirm the formation of *trans*-[Rh(Cl)(CO)($SbPh_3$)(2,4-TBPP)].

The reaction solution was left to evaporate and an orange semi-solid residue remained. The residue was washed with hexane, filtered and re-dissolved in dichloromethane. The solution was then was left to crystallize overnight. Orange crystals formed in an oily residue and were rinsed in acetone. The crystals were characterised crystallographicaly as *trans-mer*-[$Rh(Cl)_2(Ph)(SbPh_3)_3$].2CH_2Cl_2 (Yield 36 g, 42%). The crystallographic results can be found in Section 3.4.2.3.

The same procedure was followed using an equivalent of P(O-2,6-$Me_2C_6H_3)_3$ as well as P(O-4-^{t}Bu$C_6H_4)_3$, and the same orange crystals were produced. Preliminary structure refinement showed each of these crystals corresponded to *trans-mer*-[$Rh(Cl)_2(Ph)(SbPh_3)_3$]. Initial investigation shows complex (**3**) forms in the presence of phosphite ligands from *trans*-[Rh(Cl)(CO)($SbPh_3$){$P(OR)_3$}], however the formation is not dependant on the type of phosphite ligand used. A more complete study will be conducted to determine the actual mechanism for the formation of (**3**) at a later stage.

3.3.2.5 Synthesis of Tris(2,6-dimethylphenyl)phosphite

The procedure described is analogous to that of van Leeuwen and Roobeek[11] for the synthesis of tris(2-butylphenyl)phosphite.

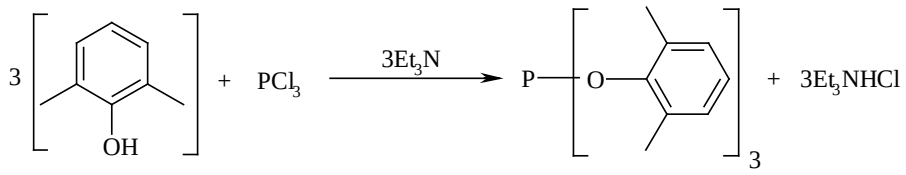

Scheme 3.6

[11] P.W.N.M. van Leeuwen, C.F. Roobeek, *J. Organomet. Chem.*, **258**, 1983, 343

2,6-Dimethylphenol (50 g, 0.41 mol) was mixed with xylene (435 g, 4.09 mol) under an inert atmosphere. Triethylamine (0.73 g, 7 mmol) and phosphorous trichloride (19.7 g, 0.143 mol) were added and the system was stirred and heated under reflux for an hour. The reaction mixture was then left to stir overnight, where after it was placed in a freezer for a day. Freezing induced the precipitation of a white crystalline solid, which was dried following evaporation of the volatiles. The solid was then purified through recrystallisation from pentane (Yield 53 g, 95 %).

^{31}P NMR ($CDCl_3$): δ (ppm) 103 (s)

3.3.2.6 Synthesis of *trans*-[Rh(Cl)(CO)($SbPh_3$)(2,4-TBPP)] (4)

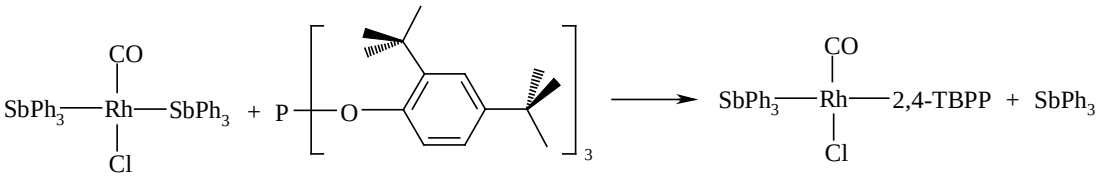

(4)

Scheme 3.7

trans-[Rh(Cl)(CO)($SbPh_3$)$_2$] (50 mg, 0.057 mmol) was dissolved in chloroform (5 cm^3) and a solution of P(O-2,4-^{t}Bu$_2$C$_6$H$_3$)$_3$ (37 mg, 0.057 mmol) in chloroform (10 cm^3) was added drop-wise. The yellow solution became increasingly orange with each drop of phosphite.

It was not possible to isolate the complex for % yield determination and the ^{1}H NMR characterisation was not included due to extensive signal overlapping resulting from the free triphenylstibine present.

IR (ν(CO)/$CHCl_3$): 1994 cm^{-1}

UV-Vis (CH_2Cl_2) [λ_{max}, nm (log ε, M^{-1} cm^{-1})]: 358 (3.40)

^{31}P NMR ($CDCl_3$): δ (ppm) 106 (d, $^1J_{Rh-P}$ = 275 Hz)

3.3.2.7 Synthesis of *trans*-[Rh(Cl)(CO)(2,4-TBPP)$_2$] (5)

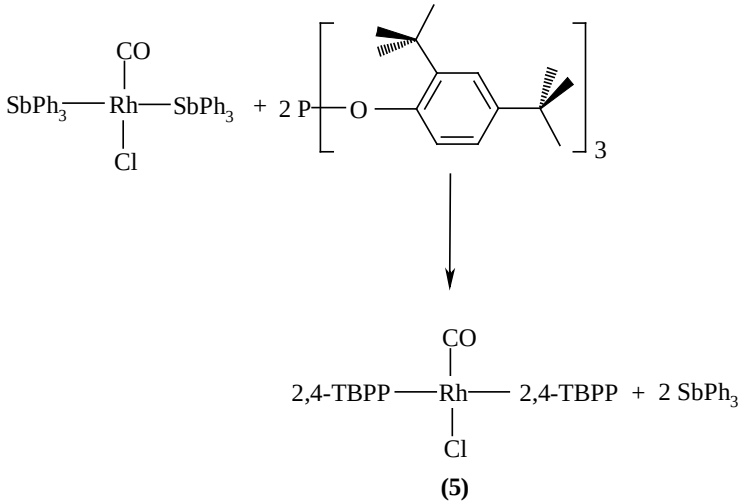

(5)

Scheme 3.8

trans-[Rh(Cl)(CO)($SbPh_3$)$_2$] (50 mg, 0.057 mmol) was dissolved in chloroform (5 cm^3) and a solution of P(O-2,4-$^tBu_2C_6H_3$)$_3$ (74 mg, 0.114 mmol) in chloroform (10 cm^3) was added. On addition of the phosphite, the solution turned orange and then became pale yellow in colour, indicating the initial formation of *trans*-[Rh(Cl)(CO)($SbPh_3$)(2,4-TBPP)] followed by *trans*-[Rh(Cl)(CO)(2,4-TBPP)$_2$]. After solvent evaporation, the residue was washed with acetone to remove the excess $SbPh_3$, leaving the purified yellow powdery product (Yield: 78 mg, 94%).

IR (ν(CO)/$CHCl_3$): 2010 cm^{-1}

UV-Vis (CH_2Cl_2) [λ_{max}, nm (log ε, M^{-1} cm^{-1})]: 356 (3.27)

^{31}P NMR ($CDCl_3$): δ (ppm) 111 (d, $^1J_{Rh-P}$ = 212 Hz)

^{1}H NMR ($CDCl_3$): δ (ppm) 7.6 (d, 4H, $^2J_{H-H}$ = 8.4Hz), 7.2 (s, 2H), 6.8 (d, 4H, $^2J_{H-H}$ = 8.4Hz), 1.3 (s, 18H), 1.2 (s, 18H)

^{13}C NMR ($CDCl_3$): δ (ppm) 148.2 (s, 6C), 147.2 (s, 6C), 145.9 (s, 6C), 124.4 (s, 6C), 123.1 (s, 6C), 120.1 (s, 6C), 35.1 (s, 2C), 34.5 (s, 2C), 1.6 (s, 6C), 30.5 (s 6C)

3.3.2.8 Synthesis of *trans*-[Rh(Cl)(CO)($SbPh_3$)(2,6-MPP)] (6)

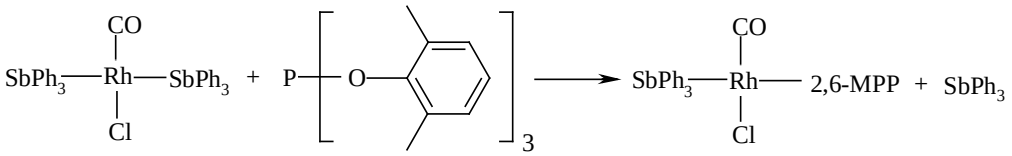

(6)

Scheme 3.9

Using the same method as for *trans*-[Rh(Cl)(CO)($SbPh_3$)(2,6-MPP)], the reaction of *trans*-[Rh(Cl)(CO)($SbPh_3$)$_2$] (50 mg, 0.057 mmol) with P(O-2,6-$Me_2C_6H_3$)$_3$ (23 mg, 0.057 mmol) produced an orange solution of *trans*-[Rh(Cl)(CO)($SbPh_3$)(2,6-MPP)]
It was not possible to isolate the complex for % yield determination and ^{1}H NMR characterisation.

IR (ν(CO)/$CHCl_3$): 1992 cm^{-1}
UV-Vis (CH_2Cl_2) [λ_{max}, nm (log ε, M^{-1} cm^{-1})]: 361 (3.42)
^{31}P NMR ($CDCl_3$): δ (ppm) 109 (d, $^1J_{Rh-P}$ = 274 Hz)

3.3.2.9 Synthesis of *trans*-[Rh(Cl)(CO)(2,6-MPP)$_2$] (7)

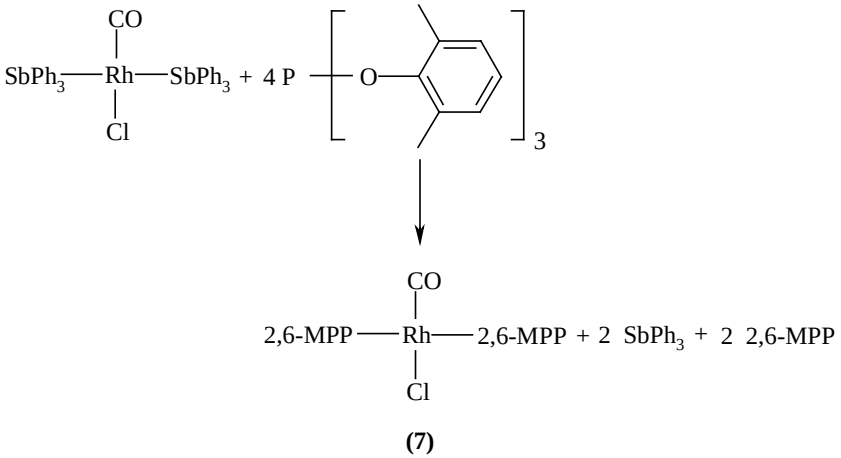

(7)

Scheme 3.10

Using a similar method as for *trans*-[Rh(Cl)(CO)(2,4-TBPP)$_2$], the reaction of *trans*-[Rh(Cl)(CO)(SbPh$_3$)$_2$] (50 mg, 0.057 mmol) with a large excess of P(O-2,6-Me$_2$C$_6$H$_3$)$_3$ (90 mg, 0.228 mmol), produced a yellow solution of *trans*-[Rh(Cl)(CO)(2,6-MPP)$_2$]. Excess phosphite was required in order to force the very bulky phosphite into the coordination sphere of the rhodium. It was not possible to isolate the complex for % yield determination.

IR (ν(CO)/CHCl$_3$): 2004 cm^{-1}
UV-Vis (CH$_2$Cl$_2$) [λ_{max}, nm (log ε, M^{-1} cm^{-1})]: 358 (3.11)
^{31}P NMR (CDCl$_3$): δ (ppm) 111 (d, $^1J_{Rh-P}$ = 212 Hz)
^{1}H NMR (CDCl$_3$): δ (ppm) 6.97 (s, 18H), 2.29 (s, 36H)

3.3.2.10 Synthesis of *trans*-[Rh(Cl)(CO)(SbPh$_3$){P(OR)$_3$}] where P(OR)$_3$ = TPP, 4-ClPP, 4-MPP and 4-BPP

The complexes were prepared using a protocol analogous to that followed for the synthesis of *trans*-[Rh(Cl)(CO)(SbPh$_3$)(2,4-TBPP)] (**4**).

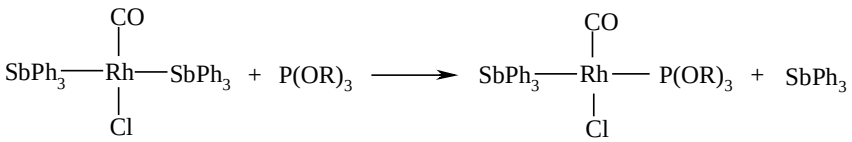

Scheme 3.11

trans-[Rh(Cl)(CO)(SbPh$_3$)$_2$] (50 mg, 0.057 mmol) was dissolved in chloroform (5 cm^3) and a solution containing a single molar equivalent of each phosphite in chloroform (10 cm^3) was added drop-wise to form each phosphite complex respectively. The yellow solution became increasingly orange with each drop of phosphite. The masses of each phosphite used were as follows:

TPP = 18 mg

4-ClPP = 24 mg

4-MPP = 23 mg

4-BPP = 27 mg

It was not possible to isolate any of the four complexes for % yield determination. The IR and low temperature (-50 ºC) ^{31}P NMR characterisations are as follows:

[Rh(Cl)(CO)(SbPh$_3$)(TPP)]

IR (ν(CO)/$CHCl_3$): 1998 cm^{-1}

^{31}P NMR ($CDCl_3$): δ (ppm) 124 (d, $^1J_{Rh-P}$ = 270 Hz)

[Rh(Cl)(CO)(SbPh$_3$)(4-ClPP)]

IR (ν(CO)/$CHCl_3$): 2000 cm^{-1}

^{31}P NMR ($CDCl_3$): δ (ppm) 126 (d, $^1J_{Rh-P}$ = 275 Hz)

[Rh(Cl)(CO)(SbPh$_3$)(4-MPP)]

IR (ν(CO)/$CHCl_3$): 1997 cm^{-1}

^{31}P NMR ($CDCl_3$): δ (ppm) 126 (d, $^1J_{Rh-P}$ = 278 Hz)

[Rh(Cl)(CO)(SbPh$_3$)(4-BPP)]

IR (ν(CO)/$CHCl_3$): 1997 cm^{-1}

^{31}P NMR ($CDCl_3$): δ (ppm) 125 (d, $^1J_{Rh-P}$ = 280 Hz)

3.3.2.11 Synthesis of *trans*-[Rh(Cl)(CO){P(OR)$_3$}$_2$] where P(OR)$_3$ = TPP, 4-ClPP, 4-MPP and 4-BPP

Similarly to 3.3.2.10, the complexes were prepared using a protocol analogous to that for the synthesis of [Rh(Cl)(CO)(2,4-TBPP)$_2$] (**5**).

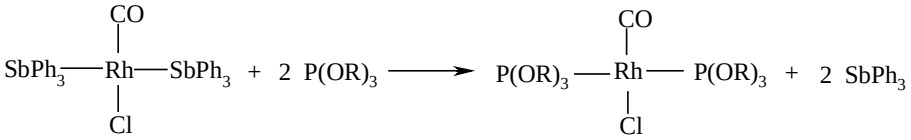

Scheme 3.12

trans-[Rh(Cl)(CO)($SbPh_3$)$_2$] (50 mg, 0.057 mmol) was dissolved in chloroform (5 cm^3) and a solution containing two molar equivalents of each phosphite in chloroform (10 cm^3) was added drop-wise to form each phosphite complex respectively. On addition of each phosphite, the solution initially turned orange in color, then became a light yellow. The masses of each phosphite used were as follows:

TPP = 36 mg
4-ClPP = 48 mg
4-MPP = 46 mg
4-BPP = 54 mg

It was not possible to isolate any of the four complexes for % yield determination. The IR and low temperature (-50 ºC) ^{31}P NMR characterisations are as follows:

[Rh(Cl)(CO)(TPP)$_2$]
IR (ν(CO)/$CHCl_3$): 2017 cm^{-1}
^{31}P NMR ($CDCl_3$): δ (ppm) 116 (d, $^1J_{Rh-P}$ = 213 Hz)

[Rh(Cl)(CO)(4-ClPP)$_2$]
IR (ν(CO)/$CHCl_3$): 2021 cm^{-1}
^{31}P NMR ($CDCl_3$): δ (ppm) 116 (d, $^1J_{Rh-P}$ = 214 Hz)

[Rh(Cl)(CO)(4-MPP)$_2$]
IR (ν(CO)/$CHCl_3$): 2014 cm^{-1}
^{31}P NMR ($CDCl_3$): δ (ppm) 117 (d, $^1J_{Rh-P}$ = 212 Hz)

[Rh(Cl)(CO)(4-BPP)$_2$]

IR (ν(CO)/$CHCl_3$): 2016 cm^{-1}

^{31}P NMR ($CDCl_3$): δ (ppm) 115 (d, $^1J_{Rh-P}$ = 212 Hz)

3.3.2.12 Synthesis of *trans*-[Rh(Cl)$_2$(Ph)(PPh$_3$)$_2$] (8)

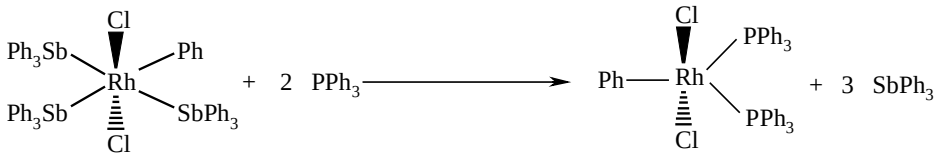

(8)

Scheme 3.13

trans-mer-[Rh(Cl)$_2$(Ph)(SbPh$_3$)$_3$] (50.0 mg, 0.038 mmol) was dissolved in $CHCl_3$ (10 cm^3) and a solution of PPh_3 (19.9 mg, 0.076 mmol) in $CHCl_3$ (10 cm^3) was added. The orange solution turned yellow on addition of the phosphine. After solvent evaporation, the product was recrystallised from CH_2Cl_2 (Yield, 11 mg, 38 %).

UV-Vis ($CHCl_3$) [λ_{max}, nm (log ε, M^{-1} cm^{-1})]: 365 (3.20)

^{31}P NMR ($CDCl_3$): δ (ppm) 21 (d, $^1J_{Rh-P}$ = 103 Hz)

3.3.3 Results and Discussion

3.3.3.1 Rh(I) Stibine Complexes

Both the solid and solution state IR spectra of the four (**1**) and five (**2**) coordinate rhodium-stibine complexes exhibit carbonyl stretching frequencies between 1950 and 1971 cm^{-1}. These values are within the expected range for these type of complexes, with two triaryl ligands in *cis* positions with respect to the OC–Rh–Cl core. The analogous

phosphine[12] and arsine[13] complexes have solution state carbonyl absorption frequencies of 1979 and 1975 cm^{-1} respectively. This decrease in wavenumber as the donor ligand moves down the Group 15 series is in accordance with the changing electron density on the metal center. The electron-donating ability of the Group 15 donor ligands increases down the series, the electron density on the metal increases accordingly and thus more electron density is available to the C≡O moiety via π-back-bonding into the carbon π*-orbitals. The result is a stronger M-CO bond (weaker C≡O bond) and therefore a decrease in ν(CO).[2]

In solution, a dynamic equilibrium exists between the four and five coordinate stibine complexes, according to equation 3.1.

$$\underset{\textbf{(1)}}{[Rh(Cl)(CO)(SbPh_3)_2]} + SbPh_3 \overset{K_{eq}}{\rightleftharpoons} \underset{\textbf{(2)}}{[Rh(Cl)(CO)(SbPh_3)_3]} \qquad (3.1)$$

This equilibrium was investigated by Otto and Roodt,[9] where they determined the equilibrium constants for the reaction in a number of solvents. The equilibrium constants, presented in Table 3.2, indicate that the formation of (**1**) is more favoured in less polar/non coordinating solvents.

Table 3.2: Equilibrium constants calculated by Otto and Roodt[9] for the reaction of $[Rh(Cl)(CO)(SbPh_3)_2]$ with $SbPh_3$ in different solvents

Solvent	K (M^{-1})
Dichloromethane	163 ± 8
Diethylether	744 ± 34
Acetone	1043 ± 95
Ethyl Acetate	1261 ± 96

[12] K. Dunbar, S. Haefner, *Inorg. Chem.*, **31**, 1992, 3676
[13] S. Otto, A. Roodt, *Inorg. Chim. Acta*, **357**, 2004, 1

It is not certain whether the inherent characteristics of the solvent are necessarily responsible for the isolation of *trans*-[Rh(Cl)(CO)($SbPh_3$)$_2$] (**1**) from solution, as per Sec. 3.3.2.2, or if the lower crystallisation energy of (**1**) in diethyl ether adds some driving force for obtaining (**1**) over (**2**).

As a result of this equilibrium, a mixed solution of (**1**) and (**2**) gives a single carbonyl stretching frequency at 1969 cm^{-1} corresponding to the *bis*-stibine complex (**1**).

The infrared spectra of Figure 3.2 show that the addition of excess triphenylstibine to a solution of (**1**) pushes the equilibrium to the right, with the formation of the red, five coordinate complex, (**2**).

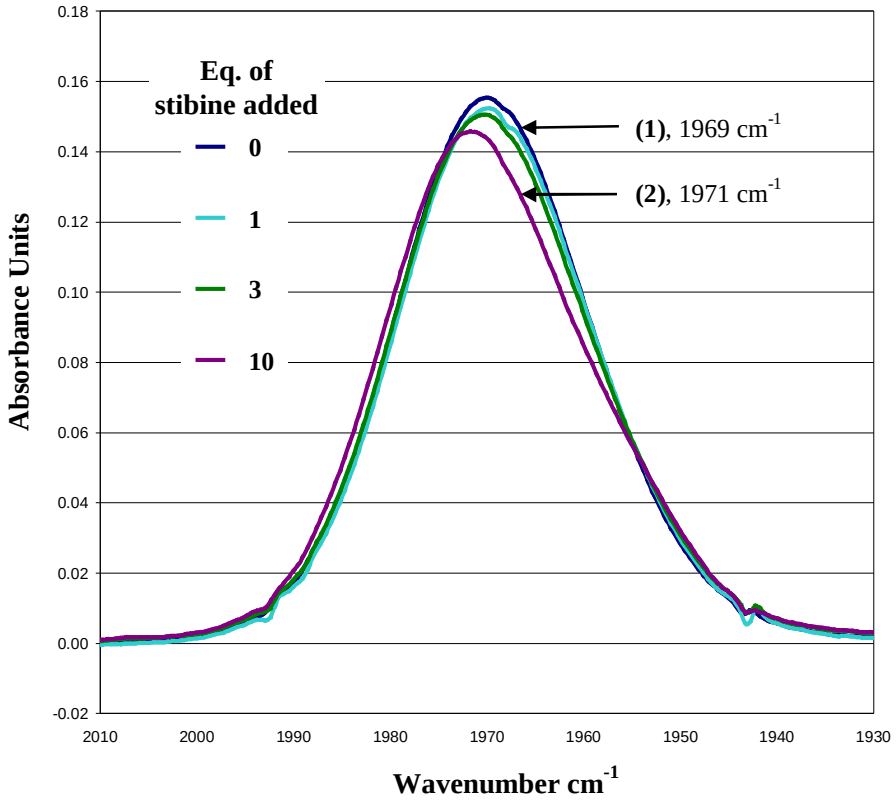

Figure 3.2: Spectral change in the IR spectra for the addition of $SbPh_3$ to [Rh(Cl)(CO)($SbPh_3$)$_2$] (1) in $CHCl_3$ at T = 25 ˚C. [Rh] = 2.3 mM, [$SbPh_3$] = 0, 2.3, 6.9 and 23 mM for 0, 1, 3 and 10 equivalents respectively

3.3.3.2 Rh(I) Phosphite Complexes

In order to study the reactivity of the four coordinate, *bis*-stibine system (**1**), the complex was reacted with a variety of phosphites. The phosphites were selected in order to provide a range of sterically demanding ligand systems and were grouped as 'large/bulky' or 'small' according to their Tolman cone angles.[14] Table 3.3 lists these phosphites and their respective cone angles, θ.

Table 3.3: Phosphite ligands selected for investigation and their corresponding Tolman cone angles[14]

Phosphite System	Abbreviation	Tolman Cone Angle, θ (˚)	Phosphite Source
Bulky Phosphites $P(O\text{-}2,6\text{-}Me_2C_6H_3)_3$	2,6-MPP	190[15]	Dr Meijboom[7]
$P(O\text{-}2,4\text{-}^tBu_2C_6H_3)_3$	2,4-TBPP	175[16]	Sigma-Aldrich
Small Phosphites $P(OC_6H_5)_3$	TPP	128[14] 123[17]	Sigma-Aldrich
$P(O\text{-}4\text{-}ClC_6H_4)_3$	4-ClPP	128[18]	Dr Meijboom[7]
$P(O\text{-}4\text{-}^tBuC_6H_4)_3$	4-BPP	128[17]	Dr Meijboom[7]
$P(O\text{-}4\text{-}OMeC_6H_4)_3$	4-MPP	128[17]	Dr Meijboom[7]

[14] C.A. Tolman, *Chem. Rev.*, **77**, 1977, 313
[15] P.B. Dias, M.E. Minas de Piedale, J.A. Martinho Simoes, *Coord. Chem. Rev.*, **125**, 1994, 737
[16] J.F. Piniella, A. Alvarez-Larena, *Organomet.*, **17**, 1998, 2857
[17] W.C. Trogler, *J. Am. Chem. Soc.*, **96**, 1974, 7589
[18] M.M. Rahman, H.Y. Liu, A. Prock, W.P. Giering, *Organomet.*, **8**, 1989, 1

Spectroscopic analysis revealed there are two different reaction profiles for the reaction of (**1**) with the two phosphite groups. It was evident that the large phosphites reacted by two consecutive substitution reactions to form a *mono*-stibine *mono*-phosphite intermediate, followed by a *bis*-phosphite product.

However, the small phosphites reacted by a series of addition and elimination reactions to form a range of four and five coordinate intermediates, as well as the two phosphite complexes described above. These species appeared to be in fast exchange at room temperature and it was not possible to isolate them for individual characterisation. However, some of the species can be detected using infrared and low temperature ^{31}P NMR and are illustrated in Section 3.3.3.4 (A) and (B).

3.3.3.3 Reaction of *trans*-[Rh(Cl)(CO)(SbPh$_3$)$_2$] with Bulky Phosphites

The synthesis protocol for the formation of the *mono*-stibine *mono*-phosphite, *trans*-[Rh(Cl)(CO)(SbPh$_3$){P(OR)$_3$}], and *bis*-phosphite, *trans*- [Rh(Cl)(CO){P(OR)$_3$}$_2$], complexes from the two large phosphites, can be found in Sections 3.3.2.6 to 3.3.2.9. It was not possible to isolate the *mono*-stibine *mono*-phosphite complexes, therefore solid state characterisation and % yields were not determined.

The *bis* phosphite complex, *trans*-[Rh(Cl)(CO)(2,4-TBPP)$_2$], (**5**) can be synthesised directly from the tetracarbonyldichlorodirhodium dimer.[19] The IR and ^{31}P NMR characterisation of this complex compares well with the data obtained for (**5**).

The addition of small increments of tris(2,4-di-^{t}butylphenyl)phosphite to (**1**) was followed spectroscopically using infrared and ^{31}P NMR spectroscopy, the results of which will be discussed below in section 3.3.3.3 (A) and 3.3.3.3 (B) respectively.

[19] L. Kirsten, M.S.c Thesis, University of Johannesburg, 2005

CHAPTER 3 SYNTHESIS AND CHARACTERISATION

(A) IR Spectroscopy

Figure 3.3 shows the infrared spectrum following the addition of tris(2,4-di-^{t}butylphenyl)phosphite to *trans*-[Rh(Cl)(CO)($SbPh_3$)$_2$] (**1**). The spectra show the carbonyl absorption peak shifting from the *bis*-stibine complex (**1**) to the *mono*-stibine *mono*-phosphite species, *trans*-[Rh(Cl)(CO)($SbPh_3$)(2,4-TBPP)] (**4**)**,** followed by the formation of the *bis*-phosphite, *trans*-[Rh(Cl)(CO)(2,4-TBPP)$_2$] (**5**) with increasing additions of phosphite. The peak shift to higher wavenumbers follows the trend expected with the metal center becoming significantly less electron dense with each stibine substitution and phosphite incorporation. The metal center in complex (**1**) contains far more electron density than in the corresponding *bis*-phosphite (**5**), as a result of the difference in σ donating/π accepting properties of Sb relative to P. Therefore, there is stronger π-back donation into the M-C bond of (**1**), resulting in a weaker C≡O bond and a lower *v*(CO) for the *bis*-stibine complex.[2]

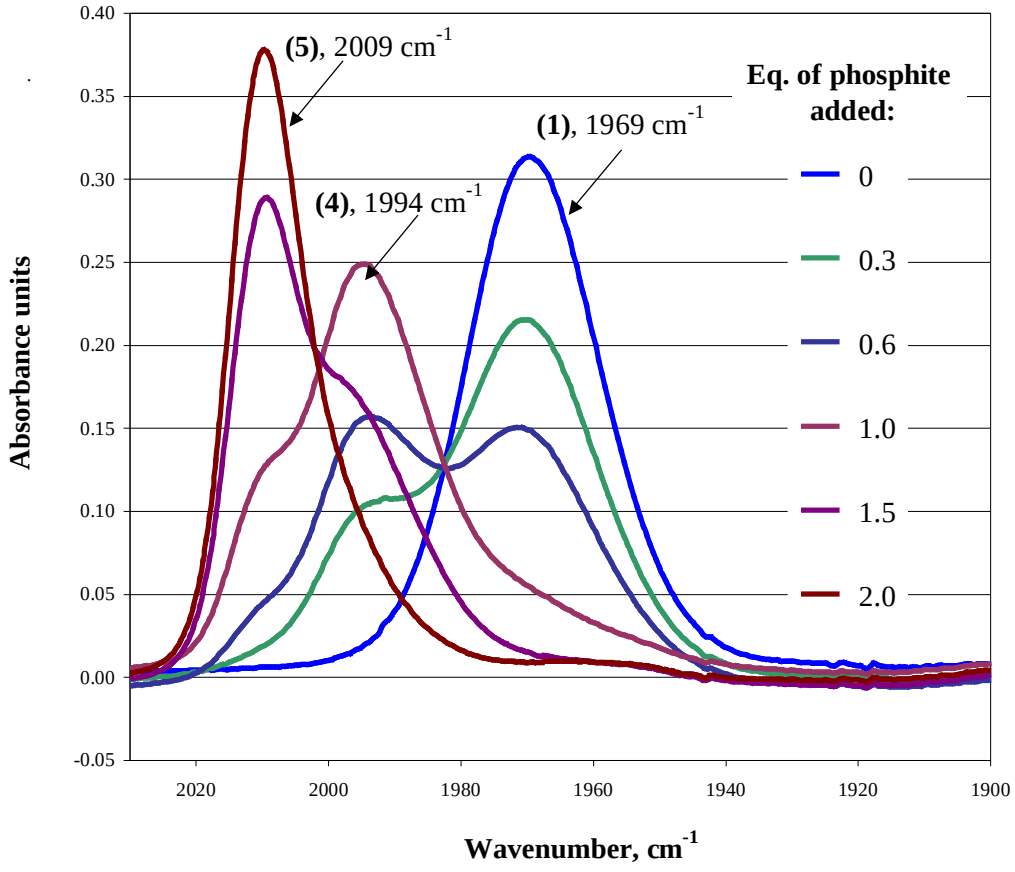

Figure 3.3: Spectral change in the IR spectra for the addition of 2,4-TBPP to *trans*-[Rh(Cl)(CO)(SbPh$_3$)$_2$] (1) in CHCl$_3$ at T = 25 ˚C. [Rh] = 5 mM, [2,4-TBPP] correspond to = 0, 1.5, 3, 5, 7.5 and 10 mM for 0, 0.3, 0.6, 1.0, 1.5 and 2.0 equivalents respectively

The infrared spectrum clearly shows two isosbestic points corresponding to the consecutive stibine/phosphite substitution reactions. This indicates that the sum of the concentrations of each reacting species was constant throughout the experiment, and thus no side reactions occurred.[20]

In an attempt to study the stability of *trans*-[Rh(Cl)(CO)(SbPh$_3$)(2,4-TBPP)] (**4**), we synthesised a solution of the intermediate (by the addition of a single equivalent of

[20] L. Meites, 'An Introduction to Chemical Equilibrium and Kinetics', Permagon Press, New York, 1981

phosphite to (**1**), Section 3.3.2.6), and observed the infrared spectrum over time. Figure 3.4 shows the ν(CO) carbonyl absorption band for the complex at 0 and 24 hours. The plot clearly shows species (**4**) undergoes a disproportionation reaction to form complexes (**1**) and (**5**). This disproportionation only occurs when a single equivalent of phosphite is added. Excess phosphite shifts the system irreversibly to (**5**).

The disproportionation may occur either by the formation of transient bridged complexes, or by phosphite migration. The latter process is postulated to occur as follows: the free stibine released after phosphite substitution on (**1**) may weakly recoordinate to (**4**) (we have already shown the tendency of stibine to form five coordinate systems). This sterically crowded species may then release a phosphite, which can in turn displace a stibine from a second *trans*-[Rh(Cl)(CO)($SbPh_3$)(2,4-TBPP)] complex, thus releasing an additional stibine molecule. This results in the formation of the stable complexes, (**1**) and (**5**).

The stability study was not extended to include ^{31}P NMR spectroscopy as complex (**1**) is not ^{31}P NMR active and the infrared results effectively illustrate the disproportionation reaction.

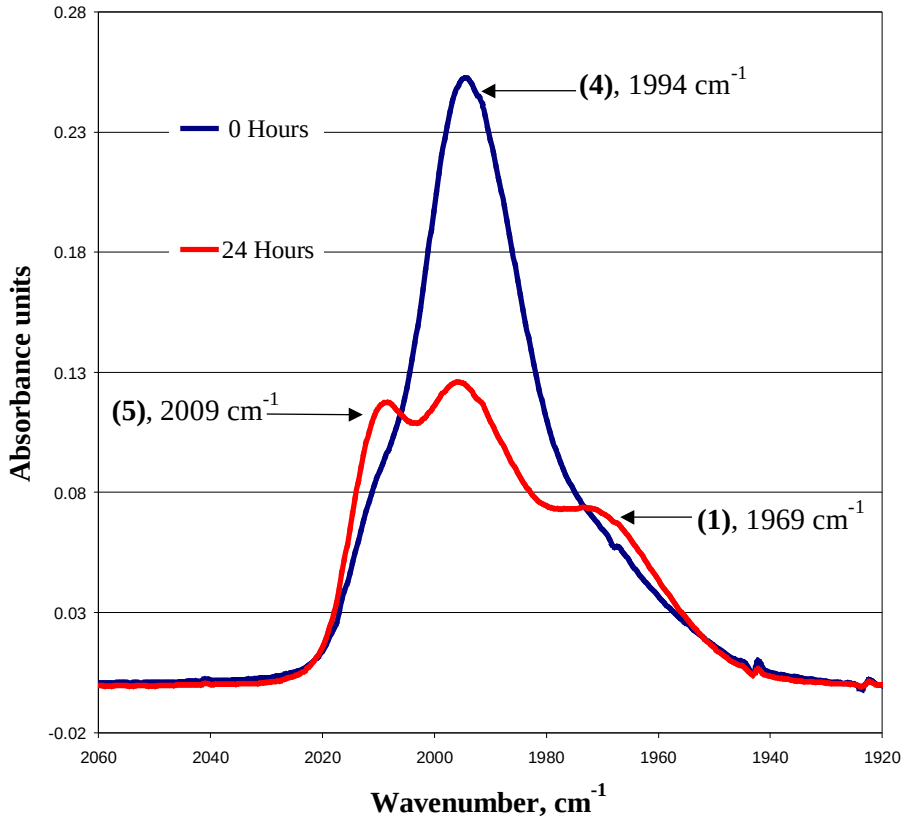

Figure 3.4: Carbonyl shift for a [Rh(Cl)(CO)($SbPh_3$)(2,4-TBPP)] solution in $CHCl_3$ at zero and 24 hours after synthesis. T = 25 ˚C, [Rh] = 5 mM, [2,4-TBPP] = 5 mM

(B) ^{31}P NMR Spectroscopy

Figure 3.5 shows a stacked plot of the ^{31}P NMR spectra for a similar phosphite addition experiment as described in Fig. 3.3. Phosphite incorporation forms the ^{31}P NMR active *mono*-stibine *mono*-phosphite *trans*-[Rh(Cl)(CO)($SbPh_3$)(2,4-TBPP)] (**4**), which reacts to form the *bis* phosphite *trans*-[Rh(Cl)(CO)(2,4-TBPP)$_2$] (**5**) complex with further additions of phosphite. The chemical shift changes observed in Figure 3.5 indicate the environment of the NMR active nuclei is becoming less electron dense as the reaction procedes, with the signals shifting downfield, i.e. the second stibine ligand being replaced by a less electron rich phosphite ligand.

The change in coupling constants show the metal phosphorus bonds are lengthened moving from (**4**) to (**5**). Although we would expect the bonds to shorten as a result of the lower *trans* effect of phosphine relative to stibine, the steric bulk of the 2,4-TBPP may cause the ligands to be pushed out from the metal center.

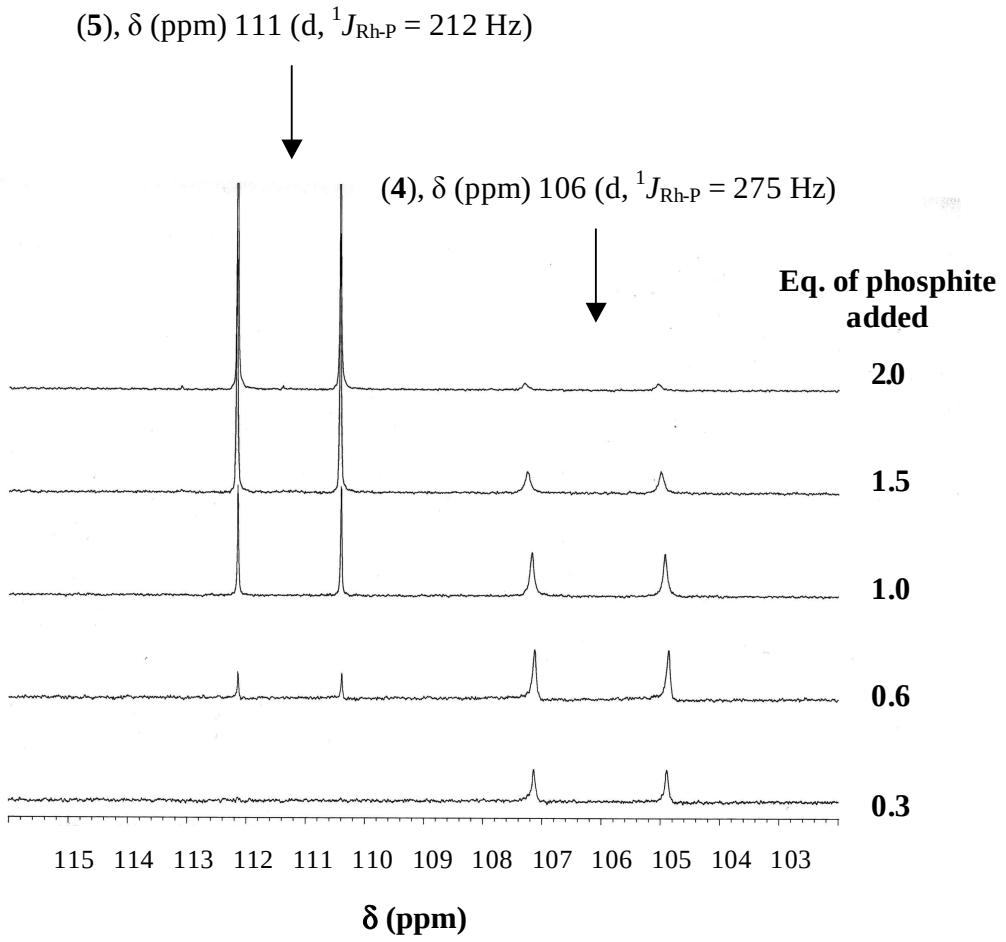

Figure 3.5: ^{31}P NMR following 2,4-TBPP addition to [Rh(Cl)(CO)(SbPh$_3$)$_2$] (1) in CDCl$_3$ at 25 ˚C. [Rh] = 11.5 mM, [2,4-TBPP] = 3.5, 6.9, 11.5, 17.3 and 23 mM for 0.3, 0.6, 1, 1,5 and 2 respectively

The addition of excess stibine to a solution of (**4**) and (**5**) has little effect on the infrared and ^{31}P NMR spectra, indicating irreversible reaction steps. Figure 3.6 depicts the ^{31}P NMR for a solution of (**4**) and (**5**) before and after the addition of excess stibine. The

spectra show there is little effect on the chemical shift or peak area of either species. Thus the amount of phosphite species formed is not governed by an equilibrium reaction but is quantitatively formed based on the amount of $P(OR)_3$ added.

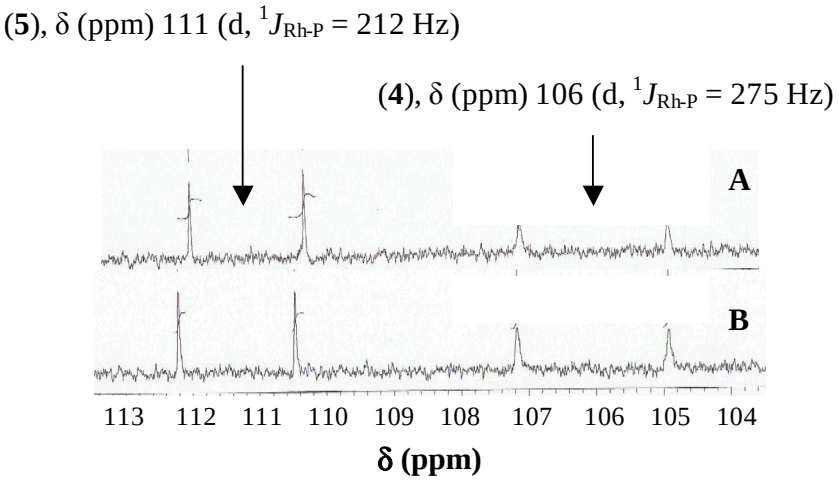

Figure 3.6: **^{31}P NMR showing addition of excess $SbPh_3$ to a solution of [Rh(Cl)(CO)($SbPh_3$)(2,4-TBPP)] (4) and [Rh(Cl)(CO)(2,4-TBPP)$_2$] (5) in $CDCl_3$ at 25 ˚C. [Rh] = 11.5 mM, [2,4-TBPP] = 17.3 mM, [$SbPh_3$] = 0 and 46 mM for A and B respectively.**

(C) Conclusions and Stoichiometric Mechanism

From the spectroscopic results obtained, we proposed a reaction mechanism as per Scheme 3.14.

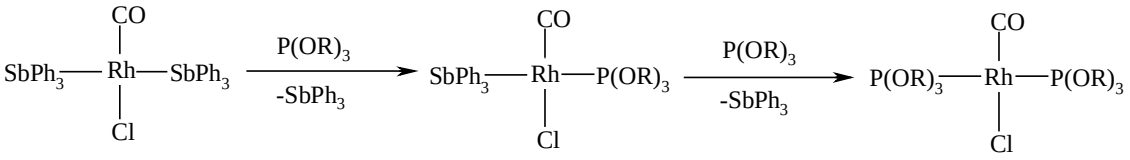

$P(OR)_3$ = 2,4-TBPP

Scheme 3.14: Proposed mechanism for the reaction of *trans*-[Rh(Cl)(CO)($SbPh_3$)$_2$] (1) with bulky phosphites

A similar IR and ^{31}P NMR spectroscopic investigation was conducted using tris(2,6-dimethylphenyl)phosphite. The investigation yielded similar results to those obtained for tris(2,4-di-^{t}butylphenyl)phosphite, the main difference being the four-fold excess of tris(2,6-dimethylphenyl)phosphite that was required in order to substitute the second triphenylstibine molecule by an additional phosphite ligand. This is presumably the result of steric crowding around the rhodium center that is introduced with the incorporation of the first phosphite group. The tris(2,6-dimethylphenyl)phosphite ligand has a significantly larger cone angle than tris(2,4-di-^{t}butylphenyl)phosphite, (190˚ vs 175˚, see Table 3.2). Tris(2,4-di-^{t}butylphenyl)phosphite formed *trans*-[Rh(Cl)(CO)(2,4-TBPP)$_2$] from *trans*-[Rh(Cl)(CO)($SbPh_3$)(2,4-TBPP)] with a single additional equivalent of phosphite ligand.

The IR and ^{31}P NMR spectra for the phosphite additions can be found in Appendix A.1. As a result of the similar spectroscopic results, it is concluded that the reaction mechanism given in Scheme 3.14 can be extended to include tris(2,6-dimethylphenyl)phosphite.

3.3.3.4 Reaction of *trans*-[Rh(Cl)(CO)($SbPh_3$)$_2$] with Small Cone Angle Phosphites

It was mentioned in Section 3.3.3.2 that the addition of small phosphites to *trans*-[Rh(Cl)(CO)($SbPh_3$)$_2$] resulted in the formation of a range of four and five coordinate Rh(I) species. The addition reactions were followed using IR and the species formed were observed using low temperature ^{31}P NMR. The results obtained will be discussed below.

(A) IR Spectroscopy

The addition of small equimolar increments of the small phosphites to (**1**), followed by IR spectroscopy at room temperature, only shows the formation of the dominating *mono*-stibine *mono*-phosphite and *bis*-phosphite complexes. The reaction components are in fast exchange at room temperature and this results in the *v*(CO) absorption bands shifting towards the dominating species, and causing peak broadening. Figure 3.7 gives a representative example of this addition using triphenylphosphite.

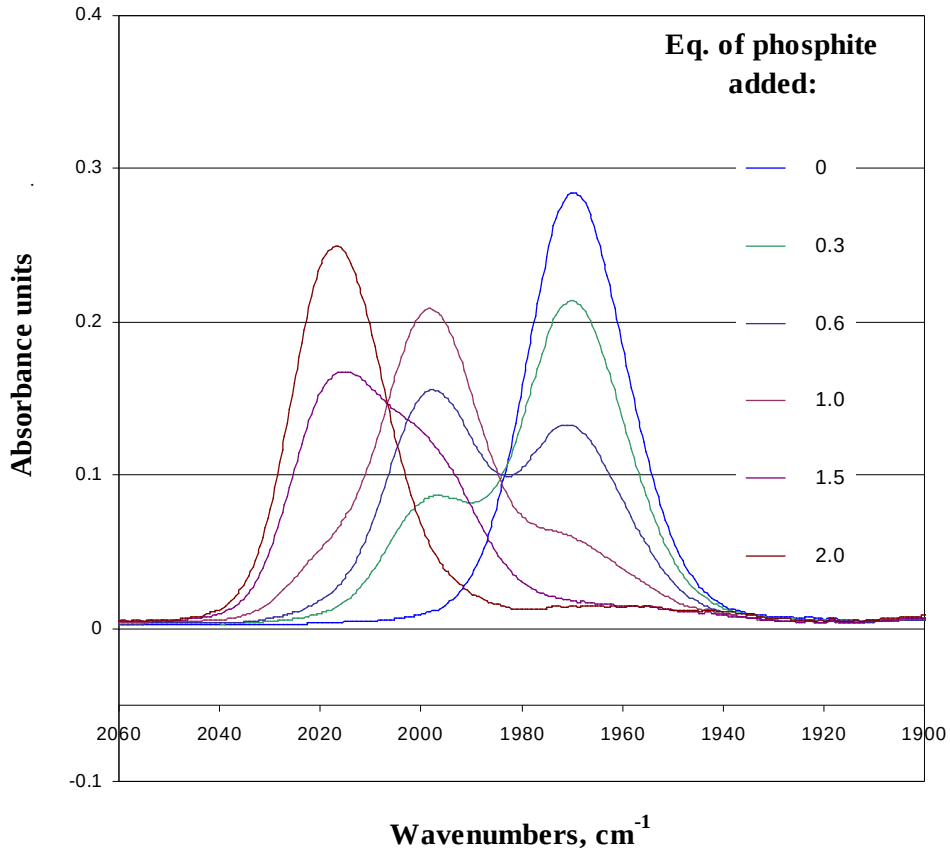

Figure 3.7: Spectral change in the IR spectra for the addition of TPP to *trans*-[Rh(Cl)(CO)(SbPh$_3$)$_2$] (1) in CHCl$_3$ at T = 25 ˚C. [Rh] = 5 mM, [TPP] correspond to = 0, 1.5, 3, 5, 7.5 and 10 mM for 0, 0.3, 0.6, 1.0, 1.5 and 2.0 equivalents respectively

(B) ^{31}P NMR Spectroscopy

Room temperature ^{31}P NMR of a solution containing both the *mono*-stibine *mono*-phosphite and *bis*-phosphite complexes for each ligand system gave a broad band of signals in fast exchange, see Figure 3.8. The ^{31}P NMR experiment was then repeated at –50 ˚C, where the bands resolved into a range of signals containing doublets and triplets. See Figures 3.9 and 3.10 for the low temperature ^{31}P NMR spectra.

These results indicate that the IR spectra do not give a good representation of the relative amounts of each species present. The spectra show broad peaks for the *mono*-stibine

mono-phosphite and *bis*-phosphite complexes. While theses species are present, they are not the predominant species and there is a large contribution to these peak areas from the other 4 and 5 coordinate species in solution, as seen by the ^{31}P NMR of Figures 3.9 and 3.10.

Alternatively, if we consider the equilibrium constants of the reactions forming the various phosphite containing species, it is also possible that these constants differ at the two temperatures, thus accounting for the mono- and bis-phosphite species dominating at room temperature.

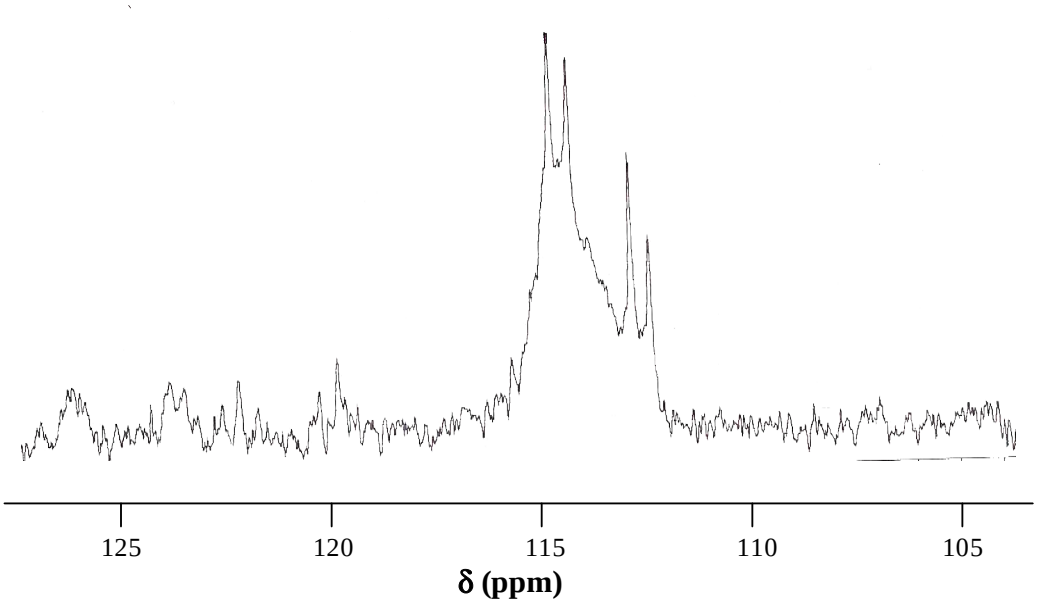

Figure 3.8 Room temperature ^{31}P NMR spectrum of *trans*-[Rh(Cl)(CO)(SbPh$_3$)$_2$] (1) with added P(OPh)$_3$ in CDCl$_3$. Corresponding IR shows υ(CO) peaks for *trans*-[Rh(Cl)(CO)(SbPh$_3$){P(OPh)$_3$}] and *trans*-[Rh(Cl)(CO){P(OPh)$_3$}$_2$] species present. [Rh] = 15.3 mM, [P(OPh)$_3$] = 23.0 mM

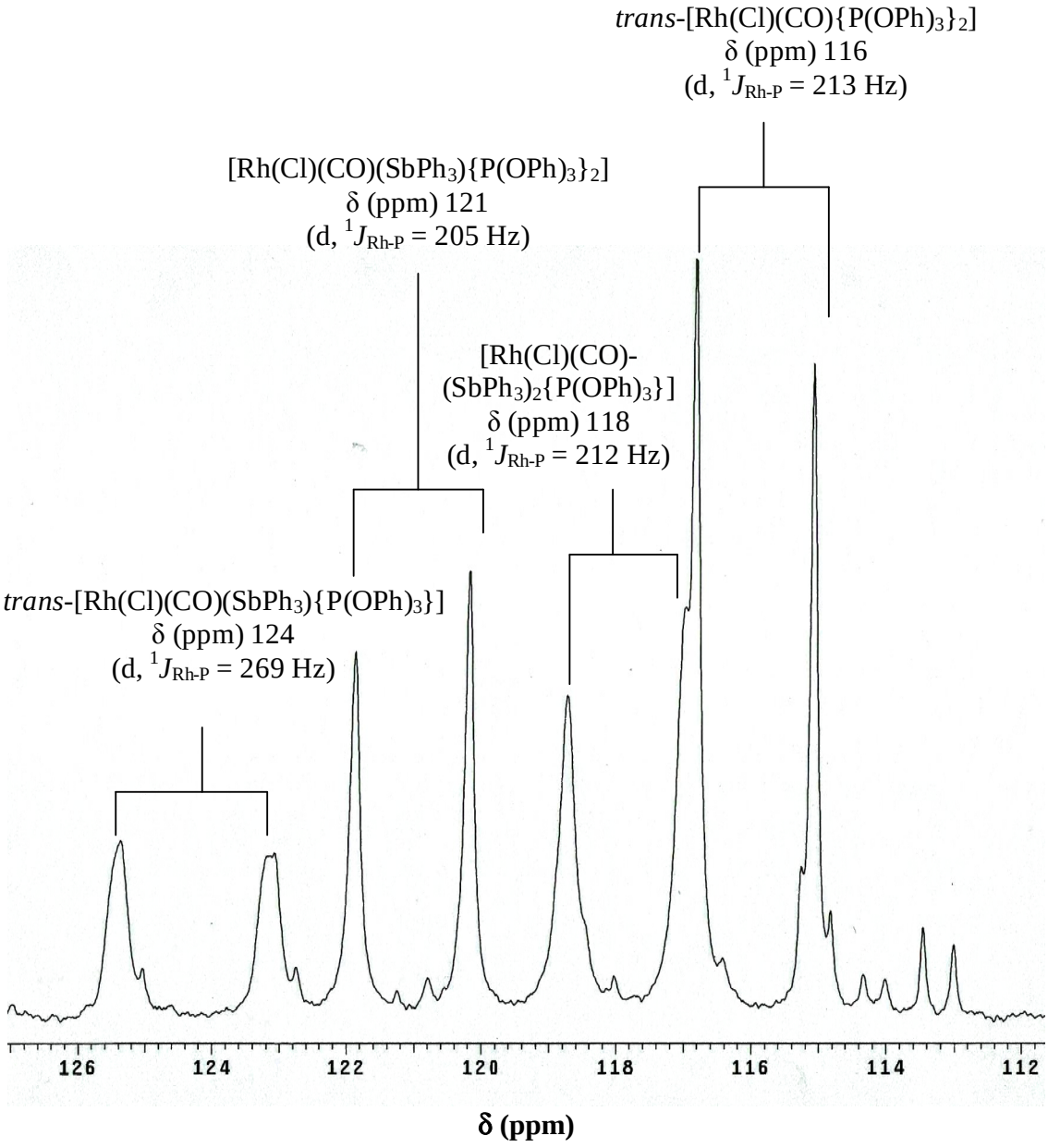

Figure 3.9: Low temperature ^{31}P NMR spectrum of *trans*-[Rh(Cl)(CO)(SbPh$_3$)$_2$] (1) with added P(OPh)$_3$ and SbPh$_3$. [Rh] = 15.3 mM in CDCl$_3$, [P(OPh)$_3$] = 19.1 mM and [SbPh$_3$] = 23 mM, T = -50 ˚C

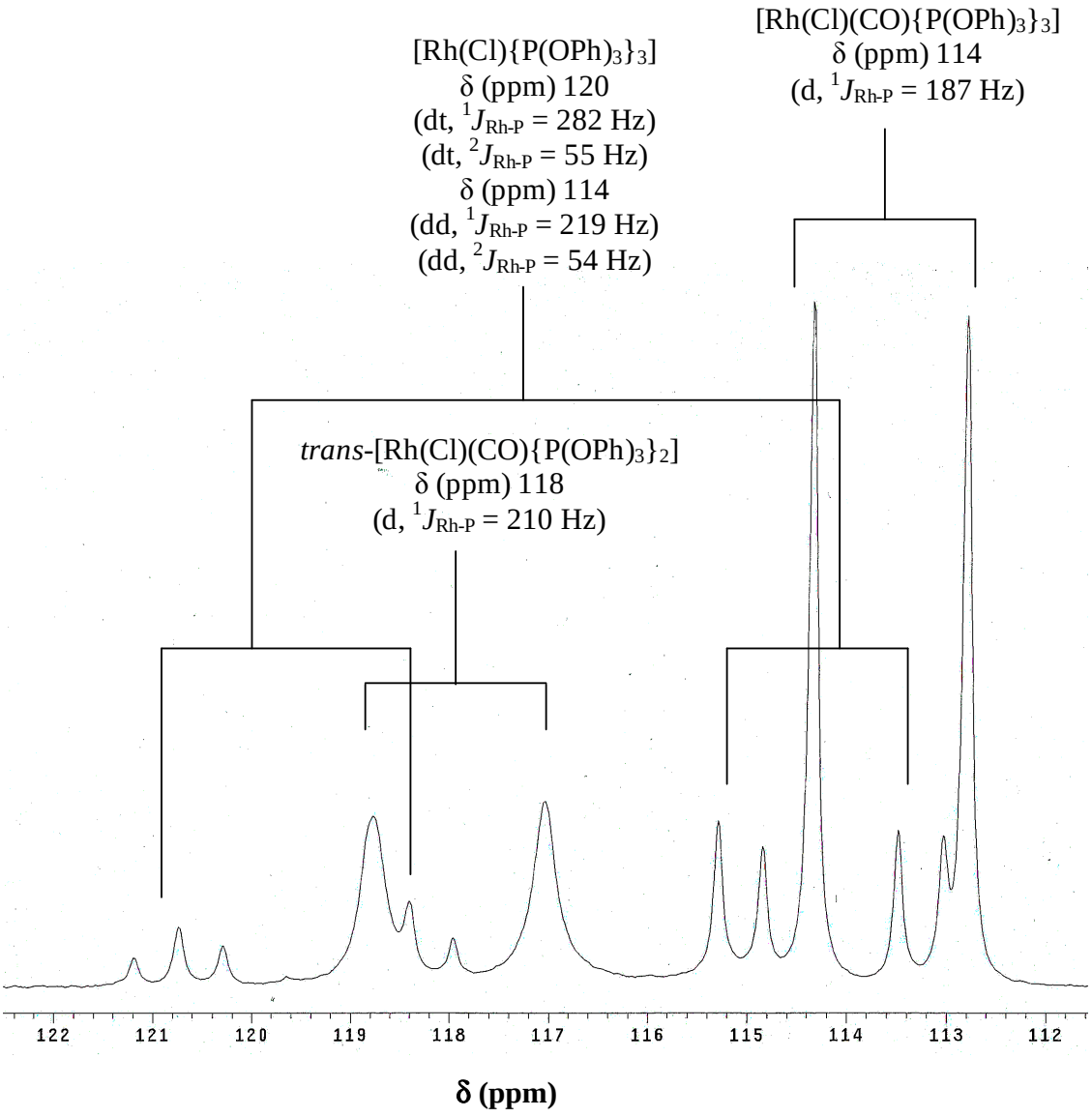

Figure 3.10: Low temperature ^{31}P NMR spectra of *trans*-[Rh(Cl)(CO)($SbPh_3$)$_2$] (1) with added $P(OPh)_3$ and $SbPh_3$. [Rh] = 15.3 mM in $CDCl_3$, [$P(OPh)_3$] = 45.9 mM and [$SbPh_3$] = 23 mM, T = -50 ˚C

Using coupling constant calculations, and a knowledge of the factors that influence chemical shift,[6] these NMR signals were assigned to the various reaction intermediates. The signals could be manipulated by the addition of triphenylstibine or the corresponding phosphite, which aided in the assignment of signals to species.

Table 3.4 contains the ^{31}P NMR spectroscopic data for the intermediate species formed from the reaction of (**1**) with the small cone angle phosphite ligands. Unfortunately, due to the large number of NMR signals produced over such a small chemical shift range, extensive signal over-lapping occurred and a few of the peaks could not be resolved clearly for peak assignment.

Table 3.4: ^{31}P spectroscopic assignment of intermediates observed upon reaction of *trans*-[Rh(Cl)(CO)(SbPh$_3$)$_2$] with the small cone angle phosphite ligands. [Rh] = 1.5 mM, CDCl$_3$ at T = -50˚C

P(OR)$_3$ =	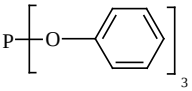		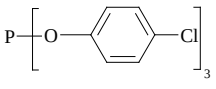		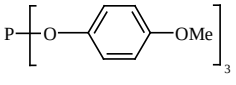		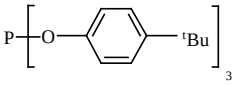	
Assigned Structure	**δ[a] (ppm)**	**$^1J_{Rh-P}$ (Hz)**	**δ (ppm)**	**$^1J_{Rh-P}$ (Hz)**	**δ (ppm)**	**$^1J_{Rh-P}$ (Hz)**	**δ (ppm)**	**$^1J_{Rh-P}$ (Hz)**
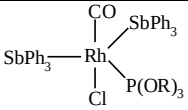	121.0 (d)	205	115.1 (d)	204	-	-	118.5 (d)	213
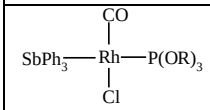	124.3 (d)	270	126.0 (d)	275	125.9 (d)	278	124.6 (d)	280
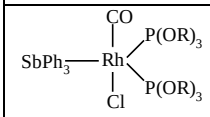	117.8 (d)	212	-	-	-	-	120.6 (d)	218
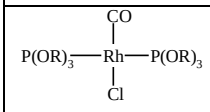	115.9 (d)	213[b]	116.2 (d)	214	116.9 (d)	212	115.4 (d)	212
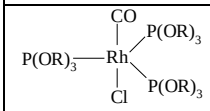	113.5 (d)	187	123.8 (d)	199	122.4 (d)	193	-	-
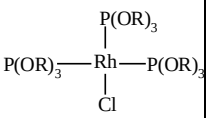	119.5 (dt) 114.1 (dd)	282[c] (dt) 219[d] (dd)	120.7 (dt) 114.7 (dd)	281[e] (dt) 220[f] (dd)	116.1 (dd)	218[g]	-	-

[a]: (d) = doublet, (dt) = doublet of triplets (dd) = doublet of doublets
[b]: Structure solved previously[21]
[c]: $^2J_{P-P}$ = 55 Hz
[d]: $^2J_{P-P}$ = 54 Hz
[e]: $^2J_{P-P}$ = 53 Hz
[f]: $^2J_{P-P}$ = 53 Hz
[g]: $^2J_{P-P}$ = 53 Hz

[21] A. Muller, Ph.D. Thesis, University of Johannesburg, 2005

It is significant to note the formation of the *tris*-phosphite complex, [Rh(Cl)(CO){P(OR)$_3$}$_3$]. This illustrates the electronic similarity between triphenylstibine and tertiary arylphosphite ligands that becomes evident when they are sterically equivalent. However, also of importance is the fact that the CO-ligand can also be substituted to eventually yield the [Rh(Cl){P(OR)$_3$}$_3$] complex. This species is a phosphite analogue of Wilkinsons catalyst[22] and terminates the reaction mechanism. The signal in the ^{31}P NMR spectrum for this species is clearly seen in Figure 3.10 and becomes more pronounced with increasing phosphite added.

(C) Conclusions and Stoichiometric Mechanism

Following this, a stoichiometric reaction mechanism for the formation of the different species was proposed, as given in Scheme 3.15. The mechanism shows addition reactions forming the five coordinate species followed by elimination reactions to produce the four coordinate *mono*-stibine *mono*-phosphite as well as the *bis*-phosphite complexes.

[22] J.F. Young, J.A. Osborn, F.H. Jardine, G. Wilkinson, *Chem. Commun.*, 1965, 131

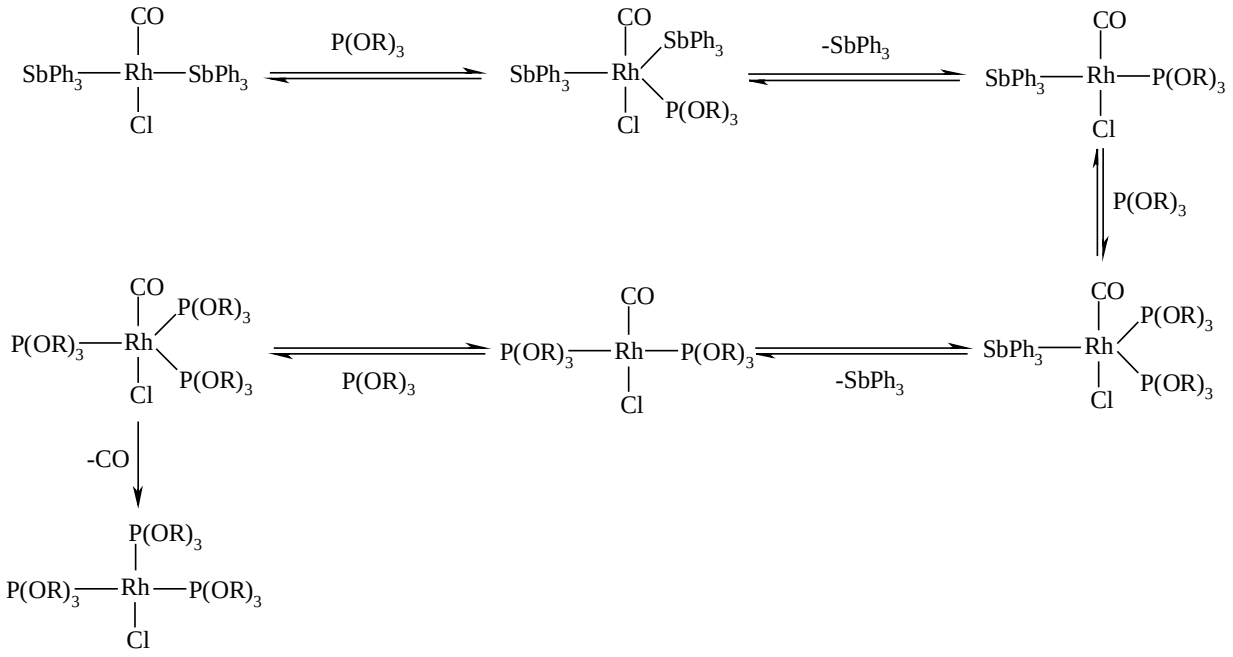

$P(OR)_3$ = TPP, 4-ClPP, 4-MPP and 4-BPP

Scheme 3.15: Proposed mechanism for the reaction of *trans*-[Rh(Cl)(CO)($SbPh_3$)$_2$] (1) with less bulky, small cone angle phosphites

The results indicate that two different reaction mechanisms occur depending on the steric characteristics of the incoming ligand, however, in principal the same mechanism could be operating for both bulky and small phosphates, with the only difference being the longevity of the five-coordinate intermediates. Bulky phosphites react irreversibly to form complexes (**4**) and (**5**), while the smaller tertiary aryl phosphites have illustrated their electronic similarity to triphenylstibine by readily forming five coordinate complexes as well as a *tris*-phosphite species.

It is clear that in the case of the small cone angle phosphite ligands, a complicated range of intermediates are formed, and only a qualitative assignment of the species was possible. A more in-depth study will be performed in future.

3.3.3.5 Rh(III) Phosphite/Phosphine Complexes

In an attempt to compare the reactivity of Rh(I) and Rh(III) stibine systems, we reacted *trans-mer*-[$Rh(Cl)_2(Ph)(SbPh_3)_3$] (**3**) with triphenylphosphite. The ^{31}P NMR results, depicted in Figure 3.11, show a range of reaction intermediates and decomposition products formed. As a result of the electronic similarity between triphenylphosphite and triphenylstibine, the reaction medium contained multiple interchangeable substitution products, none of which were isolatable.

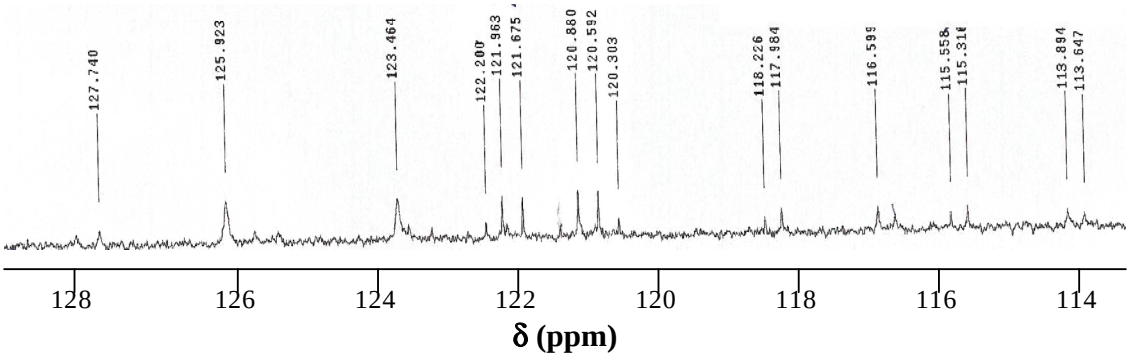

Figure 3.11: ^{31}P NMR spectrum showing reaction components resulting from addition of TPP to *trans-mer*-[$Rh(Cl)_2(Ph)(SbPh_3)_3$] in $CDCl_3$ at room temperature. [Rh] = 15.3 mM, [TPP] = 45.9 mM

As a result, we reacted (**3**) with triphenylphosphine, as per Section 3.3.2.12, to observe the substitution products. The ^{31}P NMR results showed the formation of a doublet with a $^1J_{Rh\text{-}P}$ coupling constant of 103 Hz, consistent for that of chemically equivalent phosphorous groups *trans* to a phenyl moiety. Two phosphine ligands replaced the three stibine molecules to form the five coordinate Rh(III) complex, [$Rh(Cl)_2(Ph)(PPh_3)_2$]. For a detailed description of the product formed, refer to Sec. 3.4.2.4.

3.4 CRYSTALLOGRAPHIC CHARACTERISATION OF *trans-mer*-$[Rh(Cl)_2(Ph)(SbPh_3)_3].2CH_2Cl_2$ AND $[Rh(Cl)_2(Ph)(PPh_3)_2]$

Since X-Ray crystallography forms such an integral and important part of this study, a brief description of some theoretical aspects is also included.

3.4.1 General Aspects of Crystallography

A single crystal may be defined as a solid compound in which the atoms are periodically arranged in three dimensions. They can be found in nature, in the form of ice, quartz, calcite and rock salt, or can be synthesised in the laboratory by solidification of the mother liquid, precipitation from solution or by other similar methods. The crystal structure itself is bound by plane surfaces, the interrelations of which exhibit a typical symmetry.[23]

Crystal structure analysis is based on diffraction phenomena caused by the interaction of matter with X-rays, electrons, or neutrons. Although the theory of diffraction is the same for all types of radiation, X-ray scattering attracts the most interest. Here, the interaction is between the electric field of X-rays and the electron clouds of atoms.

This interaction essentially occurs by means of two processes:

1. During diffraction some photons of the incident beam are deflected without a loss of energy. They constitute the scattered radiation and posses exactly the same wavelength as the incidental radiation. Other photons are scattered with a small loss of energy; they constitute the Compton radiation with a wavelength slightly greater than the wavelength of the incident radiation.

2. The photons can be absorbed by atoms of a target and will increase its temperature.[24]

[23] A.H. Compton, S.K. Allison, 'X-Rays in Theory and Experiment', D. van. Nostrand Company, Inc., New Jersey, 1967
[24] C. Giacovazzo, H.L. Monaco, D. Viterbo, 'Fundamentals of Crystallography', Oxford University Press, Oxford, 1992

Scattered radiation from electrons is referred to as Thomson Scattering. It occurs because the electron oscillates in the electric field of the incoming X-ray beam and an oscillating electric charge radiates electromagnetic waves. So electrons are radiated at the same frequency as the primary beam.[25]

3.4.1.1 Bragg's Law

It is important at this stage to mention Bragg's Law, which gives the geometrical conditions under which a diffracted beam can be observed:

When X-rays are diffracted by crystals, they act as though they are reflected from planes within the crystal. Unlike the reflection of light, however, X–rays are not 'reflected' continuously from a given crystal plane. Using a given wavelength, λ, a reflection takes place from a family of parallel planes only under certain conditions.

These conditions must satisfy the equation:

$$n\lambda = 2d \sin \theta \qquad (3.2)$$

Here, n is an integer, λ the wavelength, *d* the distance between successive parallel lines, and θ the angle of incidence and reflection of the X-ray beam from the given atomic plane. This equation is known as Bragg's Law.[26]

Figure 3.12 shows the difference in path length between the waves scattered at B and D is as follows:

$$AB + BC = 2d \sin \theta \qquad (3.3)$$

[25] W. Clegg, A.J. Blake, R.O. Gould, P. Main, 'Crystal Structure Analysis, Principles and Practice', International Union of Crystallography, Oxford University Press, Oxford, 2004
[26] L.S. Glasser, 'Crystallography and its Applications', Van Nostrand Reinhold. Co. LTD., UK, 1982

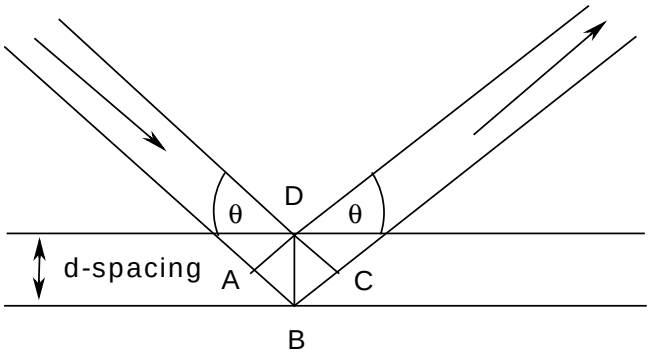

Figure 3.12: Wave scattering of θ as per Bragg's Law

3.4.1.2 X-Ray Diffraction

The systematic measurement of the geometric distribution of diffracted X-ray beams in one or more crystallographic orientation yields information about the geometry of the crystal's unit cell; specifically the lengths of the unit cell edges and the angles between them. Information about the space group is contained in the intensities of the diffracted beams, which are measured either from single crystal X-ray photographs, or more commonly, with quantum counting detectors on single crystal diffractometers.

X-rays are scattered from each atom in the unit cell to contribute to the overall scattering pattern. Since each atom acts as a source of scattered X-rays, the waves will add constructively or destructively in varying degrees depending on the direction of the diffracted beam and the atomic positions. This gives a complicated scattering pattern whose amplitude and phase vary continuously.[25]

The diffraction pattern given by the pure crystal lattice can itself be viewed as a lattice, known as the reciprocal lattice. The name comes from the reciprocal relationship between the two lattices. Large crystal lattice spacing results in small spacing in the reciprocal lattice and vise versa.

The purpose of introducing the reciprocal lattice is to produce a convenient way of visualizing and describing the diffraction pattern of the corresponding crystal.[27,28]

[27] M.F.C. Ladd, R.A. Palmer, 'Structure Determination by X-Ray Crystallography', Plenum Press, New York, 1994

[28] a = J. Hornstra, H. Vossers, 'Reciprocal Space', Philips Tech. Rundschau, **33**, 1974, 65
b = A.J.M. Duisenberg, *J. Appl. Cryst.*, **25**, 1992, 92

The combination of a single unit cell with the crystal lattice gives the complete crystal. The X-ray diffraction pattern is therefore given by the product of the scattering from the unit cell and the reciprocal lattice i.e. it is the scattering pattern of a single unit cell observed only at reciprocal lattice points.[25] The lattice that the reciprocal lattice provides is improved by assigning to each point a weight proportional to the intensity of the corresponding reflection. The resulting weighted reciprocal lattice brings out the relationship between the symmetry of the crystal and the symmetry of its pattern.[27]

3.4.1.3 Structure Factor

There are many factors affecting the intensity of X-rays in the diffraction pattern. The one which depends only upon the crystal structure is called the structure factor F(*hkl*).[25] This expresses the combined scattering of X-rays for all atoms in the unit cell compared to that for a single electron, its amplitude |F(*hkl*)| is measured in electrons.

The value of the structure factor depends upon the nature of the atom and thus the number of electrons present; the direction of the scattering or the angle θ at which the reflection occurs; the wavelength of the X-rays and the thermal vibrations of the atom.[27]

The structure factor can be expressed in terms of the contents of a single unit cell as:

$$|F(hkl)| = \sum_{j=1}^{N} f_j \exp[2\pi i(hx_j + ky_j + lz_j)] \qquad (3.4)$$

The position of the j^{th} atom, is given by the fractional coordinates (x_j, y_j, z_j), it has a scattering factor of f_j and there are N atoms in the cell. Structure factors give a mathematical description of the diffraction pattern. Each structure factor represents a diffracted beam which has an amplitude, |F(*hkl*)| and a relative phase ϕ(*hkl*).

Equation 3.4 can be rewritten in the form:

$$F(hkl) = \sum_{j=1}^{N} f_j[\cos 2\pi(hx_j + ky_j + lz_j) + i\sin 2\pi(hx_j + ky_j + lz_j)] \quad (3.5)$$

For centrosymmetric space groups this equation can be further simplified.[27] If there is a center of symmetry at the origin of the unit cell, then for every atom with coordinates x_j, y_j, z_j there is an identical atom at $-x_j$, $-y_j$, $-z_j$ and since sin(-X) = -sin(X), the imaginary part of the expression vanishes, leaving a simplified form involving only the cosine terms:

$$F(hkl) = \sum_{j=1}^{N} f_j \cos 2\pi(hx_j + ky_j + lz_j) \quad (3.6)$$

The energy associated with a cosine wave is proportional to the square of the amplitude of the wave. In an X-ray diffraction experiment, it is expressed in terms of the intensity of the scattered wave from the unit cell, $I_0(hkl)$; the subscript 0 signifies an experimentally observed quantity.

Since the amplitude of the combined wave, the structure factor, is $|F(hkl)|$, we may use the symbol $I(hkl)$ to represent $|F(hkl)|^2$, sometimes called the ideal intensity, so we get:

$$I_0(\text{hkl}) \propto |F_0(hkl)|^2 \quad (3.7)$$

This relationship forms the basis of X-ray structure analysis, where the experimentally obtained quantities for I_0(hkl) are directly related to the structure through $|F_0(hkl)|$

Using this information, an image of the crystal structure can then be calculated from the X-ray diffraction pattern. Since it is the electrons which scatter the X-rays, the image is a direct representation of these electrons. Atoms with high atomic numbers provide a greater concentration of electrons than atoms of lower atomic numbers. This concentration of electrons and its distribution around the atom is called the electron density, ρ. The units of density are number of electrons per cubic angstrom, e $Å^{-3}$.

Since it is, in general, a function of position, the electron density is specified at a point X, Y, Z as ρ(X, Y, Z).

The electron density is expressed in terms of the structure factor as:

$$\rho(xyz) = \frac{1}{V}\sum_{hkl} F(hkl)\exp[-2\pi(hx + ky + lz)] \qquad (3.8)$$

Where the summation is over all the structure factors and V is the volume of the unit cell. Since the X-rays are diffracted from the whole crystal, the calculation provides the contents of the unit cell averaged over the whole crystal.[25,27]

3.4.1.4 The 'Phase Problem' and Patterson Function

The measured X-ray intensities yield only the structure factor amplitudes and not their phases. The calculation of electron density therefore cannot be performed directly from experimental measurements and the phases must be obtained by other means. This is referred to as the 'Phase Problem'. It can be overcome by many means, the most common of which is utilizing a Patterson function or direct methods.

Direct or phase probability methods attempt to derive the structure factor phases, electron density or atomic coordinates by mathematical means from a single set of X-ray intensities. The methods are particularly effective for deriving phase information for structures containing only light atoms. The Patterson function, however, is best utilised if one atom is much heavier than the others so that the vectors involving the atom stand out clearly.[29] This method is briefly described below.

It is noticeable that the structure factor equation (eqn. 3.5) and the electron density equation (eqn. 3.8) are in fact very similar. Eqn. 3.5 transforms the electron density (in the form of atomic scattering factor, f_j) to the structure factors F(*hkl*), while eqn. 3.8 transforms the structure factors back to electron density. These are known as Fourier transforms, one equation performing the inverse transform of the other.[25]

[29] D. Mckie, C. Mckie, 'Essentials of Crystallography', Blackwell Scientific Publication, Oxford, 1986

These Fourier transforms are essential for utilizing the Patterson function to solve the phase problem.

Here, the Fourier series is calculated directly from the experimental intensity data. Phase information is not required in the Patterson series, so the results cannot be interpreted as a set of atomic positions, but rather as a collection of interatomic vectors, all taken to a common origin.

The electron density expression can be summarized as:

$$\rho(uvw) = \frac{1}{V}\sum_{hkl}\{|\,F(hkl)\,|\,2\cos[2\pi(hu+kv+lw)]\} \qquad (3.9)$$

which is centrosymmetric and can be computed directly to give $\rho(uvw)$.

The resulting function is a map of interatomic vectors, where a peak in the Patterson function at UVW implies that there are two atoms in the crystal structure at $x_1\, y_1\, z_1$ and $x_2\, y_2\, z_2$ such that $x_2 - x_1 = U$; $y_2 - y_1 = V$ and $z_2 - z_1 = W$. Also, the height of the peak in the function will be proportional to the product of the number of electrons in each of the two atoms involved.[27]

3.4.1.5 Least-Squares Refinement

Once the heavy atoms have been located, the structure factor based on these positions can be calculated.[29] The agreement between the observed and calculated factors is expressed as R, the reliability index.[30] High quality experimental data, and an accurately determined crystal structure would produce an R of no higher than 5 %.

Once an acceptable set of calculated structure factors is available, a cyclic process of refinement can be initiated. An electron density map is calculated with the magnitudes of the observed structure factors and the phases from the calculated structure factor as:

[30] M.M. Woolfson, 'An Introduction to X-Ray Crystallography', Cambridge University Press, London, 1970

$$P(r) = \frac{1}{V}\sum_{h} | F(o)h | \exp(-2\pi i h.r + i\theta) \qquad (3.10)$$

The electron density map will give an image of the structure, which is a closer approximation of the actual atomic positions.[31]

3.4.2 Crystal Structure Determination of *trans-mer*-$[Rh(Cl)_2(Ph)(SbPh_3)_3].2CH_2Cl_2$ and $[Rh(Cl)_2(Ph)(PPh_3)_2]$

3.4.2.1 Introduction

The initial aim of the crystallographic investigation was to isolate the *mono*-stibine *mono*-phosphite complex *trans*-$[Rh(Cl)(CO)(SbPh_3)(2,4\text{-TBPP})]$ (**4**), and to obtain single crystals thereof, in order to characterise this novel mixed Rh(I) system. A solution of (**4**) was produced as per Sec. 3.3.2.6, the solvent was evaporated and large orange crystals where formed after recrystallisation from CH_2Cl_2. However, it was surprising to find the crystal structure of this compound was solved as the Rh(III) complex, *trans-mer*-$[Rh(Cl)_2(Ph)(SbPh_3)_3]$. This complex formed as a combination of disproportionation of (**4**) to (**1**) and (**5**), and triphenylstibine induced oxidative addition and phenyl migration. It is also interesting to note the two chloride atoms connected to the rhodium centre, which prevents the theoretical yield exceeding 50 %.

This crystal structure has been reported previously by Cini and co-workers,[10] where the structure cocrystallised with an acetone molecule. The complex was synthesised by heating a solution of $RhCl_3.3H_2O$ in ethanol under reflux with excess $SbPh_3$, as per Sec. 3.3.2.4, Synthesis A. We followed this procedure to produce (**3**), which we subsequently reacted with a variety of phosphites and phosphines, eventually producing single crystals of $[Rh(Cl)_2(Ph)(PPh_3)_2]$ (**8**).

The X-ray crystallographic results for each of these crystal structures are presented below.

[31] H.S. Lipson, 'Crystal and X-Rays', Wykenham, London, 1959

3.4.2.2 Experimental

The X-ray data sets were collected on a Bruker SMART CCD 1K area detector diffractometer (University of the Witwatersrand), using graphite monochromated Mo-Kα radiation (λ = 0.71073 Å) at room temperature.

The structure was solved by conventional Patterson and Fourier methods and refined through full matrix least-squares calculations based on F^2, using the software packages WinGX[32] with SHELXL97.[33] All non-hydrogen atoms were refined anisotropically, while the phenyl hydrogen atoms were calculated as riding on the adjacent carbon (aromatic C – H = 0.96 Å). For both collections, the first 50 frames were recollected at the end of the data collection to check for any decomposition, both crystals remained stable throughout the collection. Absorption corrections were completed using SADABS Multi – Scan on the Bruker CCD. The program Diamond[34] was used for graphical representation of the crystal structures.

A summary of the general crystal data and refinement parameters for both Rh(III) complexes is provided in Table 3.5. Supplementary data for the bond distances and angles, atomic coordinates and anisotropic displacement parameters are given in Appendix B.1 to B.4 and Appendix C.1 to C4, for *trans-mer*-$[Rh(Cl)_2(Ph)(SbPh_3)_3].2CH_2Cl_2$ and $[Rh(Cl)_2(Ph)(PPh_3)_2]$ respectively.

[32] L.J. Farrugia, *J. Appl. Cryst.*, **32**, 1999, 837
[33] G.M. Sheldrick, SHELXL97, Program for the refinement of crystal structures, University of Göttingen, Germany, 1997
[34] K. Bradenburg, Diamond (Ver. 2.1e), Crystal Impact GbR, Bonn, Germany, 2001

Table 3.5: Crystallographic data and structure refinement details for *trans-mer*-$[Rh(Cl)_2(Ph)(SbPh_3)_3].2CH_2Cl_2$ and $[Rh(Cl)_2(Ph)(PPh_3)_2]$

	$[Rh(Cl)_2(Ph)(SbPh_3)_3].2CH_2Cl_2$	$[Rh(Cl)_2(Ph)(PPh_3)_2]$
Empirical Formula	$C_{62}H_{54}Cl_6Sb_3Rh$	$C_{42}H_{35}Cl_2P_2Rh$
Formula Weight	1480	775
Crystal System	Triclinic	Monoclinic
Space Group	P $\bar{1}$	C2/c
Cell Dimensions		
a (Å)	13.512(3)	12.889(3)
b (Å)	15.547(3)	13.850(4)
c (Å)	15.888(3)	20.099(4)
α (º)	92.73(3)	90
β (º)	109.32(3)	93.91(3)
γ (º)	108.10(3)	90
Volume ($Å^3$)	2951.4(10)	3579.6(12)
Z	2	4
$Density_{cal}$ (g. cm^{-3})	1.665	1.439
Crystal Colour	Orange	Red
Crystal Morphology	Plates	Plates
Crystal Size (mm)	0.18 x 0.12 x 0.08	0.10 x 0.10 x 0.05
Theta Range (˚)	1.38 - 28.32	2.03 - 28.29
R_{int}	0.0437	0.0708
Index Ranges	h = -17 to 18	h = -17 to 16
	k = -20 to 20	k = -18 to 9
	l = -21 to 21	l = -26 to 24
Reflections Collected	24212	12427
Independent Reflections	14535	4429
Reflection with >2σ (I)		
R1	0.0456	0.0469
wR2	0.0866	0.0835
Data / restraints / parameters	14535 / 116 / 705	4429 / 0 / 214
Goodness-of-fit on F^2	0.987	0.967
$R(F)^2$	0.0456	0.0473
$wR(F)^2$	0.0866	0.076
ρ_{max} and ρ_{min} (e. $Å^{-3}$)	0.609 and -0.650	0.504 and -0.865
μ (mm^{-1})	1.942	0.745
Completeness to θ	θ = 28.29 gives 99.5%	θ = 28.32 gives 98.9 %

3.4.2.3 Crystal Structure of *trans-mer*-$[Rh(Cl)_2(Ph)(SbPh_3)_3].2CH_2Cl_2$ (3)

(A) Introduction

Cini and co-workers[10] discovered that the reaction of $RhCl_3.3H_2O$ with $SbPh_3$ in ethanol, heated under reflux, induced the insertion of a phenyl group into the coordination sphere of Rh(III). This complex has also been synthesised by adding excess $SbPh_3$ to $[Rh(Cl)(CO)(SbPh_3)_2]$ (**1**), in the presence of nitromethane.[35] Here, we discovered that a solution of (**1**) in chloroform, with added phosphite, induced oxidative addition and phenyl migration to form (**3**). Recrystallisation from CH_2Cl_2 incorporated four CH_2Cl_2 solvent molecules into the crystal unit cell, forming a new polymorph for this rhodium complex.

(B) Results

trans-mer-$[Rh(Cl)_2(Ph)(SbPh_3)_3].2CH_2Cl_2$ crystallised from dichloromethane in the triclinic space group, $P\bar{1}$ with Z = 2. The molecular structure of (**3**) is represented in Figure 3.13 along with the atom numbering system. The CH_2Cl_2 molecules have been omitted for clarity, but are included in Figure 3.14, which shows the unit cell packing. Positional and thermal parameters of atoms for (**3**) are given in Table B.1 of the Appendix.

[35] S. Otto, A. Roodt, unpublished results

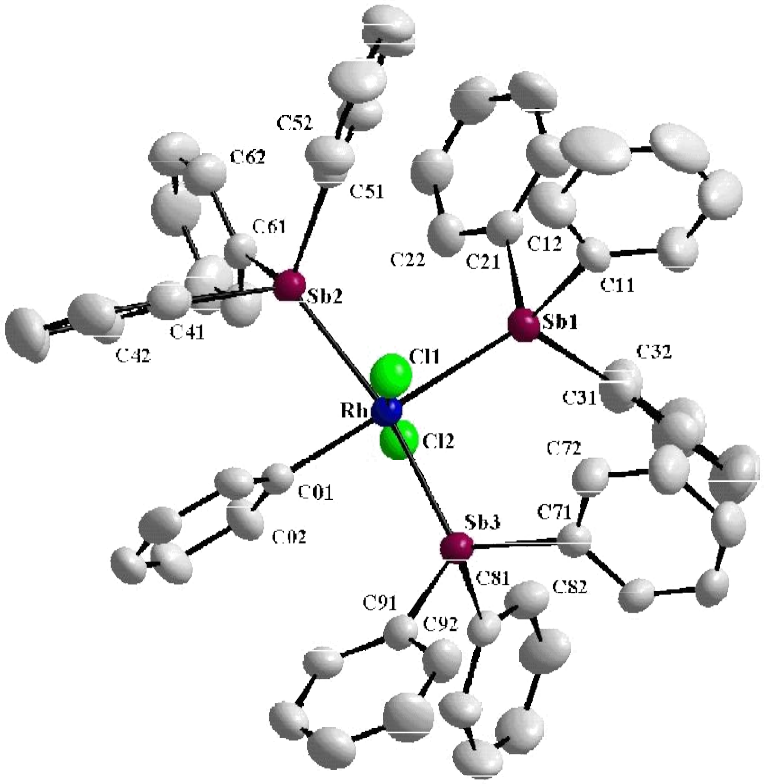

Figure 3.13: Molecular structure of *trans-mer*-$[Rh(Cl)_2(Ph)(SbPh_3)_3].2CH_2Cl_2$ showing atom numbering system. For the phenyl rings, the first digit refers to ring number, while the second digit refers to the C-atom in the ring. CH_2Cl_2 and H atoms have been omitted for clarity. Thermal ellipsoids are drawn at 50% probability level

The molecular structure of (**3**) consists of a Rh(III) metal centre connected to three $SbPh_3$ molecules and two *trans*-chloride ions. The octahedral coordination sphere is completed by the carbon atom of the phenyl moiety. There are two molecules of (**3**) per unit cell, each associated with two CH_2Cl_2 molecules. The thermal ellipsoids of the phenyl carbons of Figure 3.13 show that there is limited rotational movement of the rings.

Table 3.6 presents selected interatomic bond distances and angles. As was mentioned previously in Sec. 2.3.2.1, the large *trans* influence of the phenyl group has been used to selectively substitute $SbPh_3$ ligands *trans* to the phenyl ligand. An example of this substitution is found in Reference 36, where Cini and Giorgi refluxed (**3**) in

acetonitrile and produced crystals of $[Rh(Cl)_2(Ph)(MeCN)(SbPh_3)_2]$,[36] with the acetonitrile group *trans* to the phenyl. This large *trans* influence can be illustrated by the lengthened Rh – Sb(1) bond *trans* to the phenyl. The Rh – Sb(2) and Rh – Sb(3) bond lengths are 2.5877(10) and 2.6082(9) Å respectively, while the *trans* Rh – Sb(1) bond distance is 2.7185(8) Å. The metal atom does not deviate significantly (0.0511(5) Å) from the plane defined by the Sb(2)/Cl(1)/Sb(3)/Cl(2).

Table 3.6: Selected bond lengths and angles for *trans-mer*-$[Rh(Cl)_2(Ph)(SbPh_3)_3]$

Bond	Distance (Å)	Bond	Distance (Å)
Rh-C(01)	2.115(5)	Sb(2)-C(41)	2.139(5)
Rh-Cl(1)	2.3731(18)	Sb(2)-C(51)	2.143(5)
Rh-Cl(2)	2.3720(18)	Sb(2)-C(61)	2.147(5)
Rh-Sb(1)	2.7185(8)	Sb(3)-C(91)	2.135(5)
Rh-Sb(2)	2.6082(9)	Sb(3)-C(71)	2.139(6)
Rh-Sb(3)	2.5877(10)	Sb(3)-C(81)	2.143(5)
Sb(1)-C(11)	2.144(6)	C(01)-C(06)	1.397(7)
Sb(1)-C(31)	2.148(5)	C(01)-C(02)	1.402(8)
Sb(1)-C(21)	2.161(5)		
Angle	**Bond Angle (˚)**	**Angle**	**Bond Angle (˚)**
C(01)-Rh-Cl(2)	92.85(16)	Cl(1)-Rh-Sb(1)	93.18(5)
C(01)-Rh-Cl(1)	94.20(16)	Sb(3)-Rh-Sb(1)	97.16(2)
Cl(2)-Rh-Cl(1)	172.84(5)	Sb(2)-Rh-Sb(1)	94.55(2)
C(01)-Rh-Sb(3)	84.55(13)	C(11)-Sb(1)-Rh	125.76(16)
Cl(2)-Rh-Sb(3)	90.11(5)	C(21)-Sb(1)-Rh	113.83(15)
Cl(1)-Rh-Sb(3)	89.28(5)	C(31)-Sb(1)-Rh	117.37(15)
C(01)-Rh-Sb(2)	84.54(13)	C(41)-Sb(2)-Rh	113.34(14)
Cl(2)-Rh-Sb(2)	97.28(5)	C(51)-Sb(2)-Rh	117.92(14)
Cl(1)-Rh-Sb(2)	84.68(5)	C(61)-Sb(2)-Rh	120.84(15)
Sb(3)-Rh-Sb(2)	167.11(2)	C(71)-Sb(3)-Rh	116.54(14)
C(01)-Rh-Sb(1)	172.45(15)	C(81)-Sb(3)-Rh	117.48(14)
Cl(2)-Rh-Sb(1)	79.82(4)	C(91)-Sb(3)-Rh	120.12(14)

[36] R. Cini, G. Giorgi, *Acta Cryst.*, **C47**, 1991, 716

It is interesting to note that in similar Rh(III) complexes, with the *trans* $SbPh_3$ group substituted by nitrogen donor groups, such as 4-methylpyrimidine,[37] pyrazine,[38] purine-6-thione[39] and 1,3-thiazole,[38] the Rh – C(phenyl) bond is relatively short, i.e.: 2.017(5), 2.042(3), 2.033(9) and 2.037(6) Å for each of these complexes respectively. This is in comparison to the Rh – C (phenyl *trans* to Sb) bond of 2.115(5) Å (reported here), and 2.118(6) Å for $[Rh(Cl)_2(Ph)(SbPh_3)_3].CH_3CO_2CH_2CH_3$.[37] This difference is in agreement with the much larger *trans* influence of $SbPh_3$ when compared to that of $N(sp^2)$, which can be attributed to the high competition for back donation from the metal to the ligand in the case of $SbPh_3$.

All the $SbPh_3$ groups have approximate tetrahedral geometry, with Sb – C bond distances averaging 2.15(9), 2.14(9) and 2.14(9) Å for Sb(1), Sb(2) and Sb(3) respectively. These values are in good agreement with those obtained for $[Rh(Cl)_2(Ph)(C_5H_4N_4S)(SbPh_3)].0.5MeOH$,[39] $[Rh(Cl)_2(Ph)(MeCN)(SbPh_3)_2]$[36] and $[Rh(DPD)(SbPh_3)_2(Ph)_2].2C_6H_6$[40] (DPD = 1,3-diphenyl-1,3-propandione), which are 2.14(8), 2.13(7) and 2.13(1) respectively.

The C–Sb–C angles average 98.22(4)°, 100.46(4)° and 99.68(4)° for Sb(1), Sb(2) and Sb(3) respectively, similarly in agreement with the above mentioned complexes.

The angles between Sb(3)–Rh–C(01) and Sb(2)–Rh–C(01) are 84.55(13)˚ and 84.54(13)˚ respectively, showing that these two $SbPh_3$ molecules are pushed away from the *cis* $SbPh_3$, towards the less bulky phenyl group.

The Cl(1)–Rh–C(01)–C(06) torsion angle is 4.15(4)˚ (4.4(2)˚ and 13.8(5)˚ for (**3**) cocrystallised with ethyl acetate[37] and acetone[10] respectively), with the phenyl and Cl^- groups in an almost eclipsed conformation. It is reasonable to conclude that this eclipsed conformation is forced by the conformation of the bulky $SbPh_3$ groups introducing the *mer*-arrangement. The distances between the *ortho* carbons on the phenyl ring and the corresponding Cl^- ligands are 3.161(41) and 3.243(26) Å, for C(02)…Cl and C(06)…Cl(1) respectively. This results in the two Cl^- ligands pointing

[37] R. Cini, A. Cavaglioni, *Polyhedron*, **18**, 1999, 669
[38] A. Cavaglioni, R. Cini, *Polyhedron*, **16**, 1997, 4045
[39] A. Cavaglioni, R. Cini, *J. Chem. Soc., Dalton Trans.*, 1997, 1149
[40] G.J. Lamprecht, J.G. Leipoldt, *Inorg. Chim. Acta*, **88**, 1984, 55

away from the phenyl moiety with the Cl(1)–Rh–Cl(2) angle less than 180˚, i.e: 172.84(5)˚.

The unit cell of $[Rh(Cl)_2(Ph)(SbPh_3)_3].2CH_2Cl_2$ is presented in Figure 3.14. Large thermal elliopsoids of the carbon and chloride atoms of the CH_2Cl_2 molecules show the disorder associated with the weakly bound solvent packing. The solvent molecules were refined in two disordered positions with a free variable coupled to the occupancy factor. Two of the four molecules were generated as symmetry equivalents, with each unique molecule having an occupancy ratio of 47 % to 53 % and 42 % to 58 % respectively. Low temperature data collection would reduce the molecular vibration and provide accurate atomic positions and is to be conducted in future.

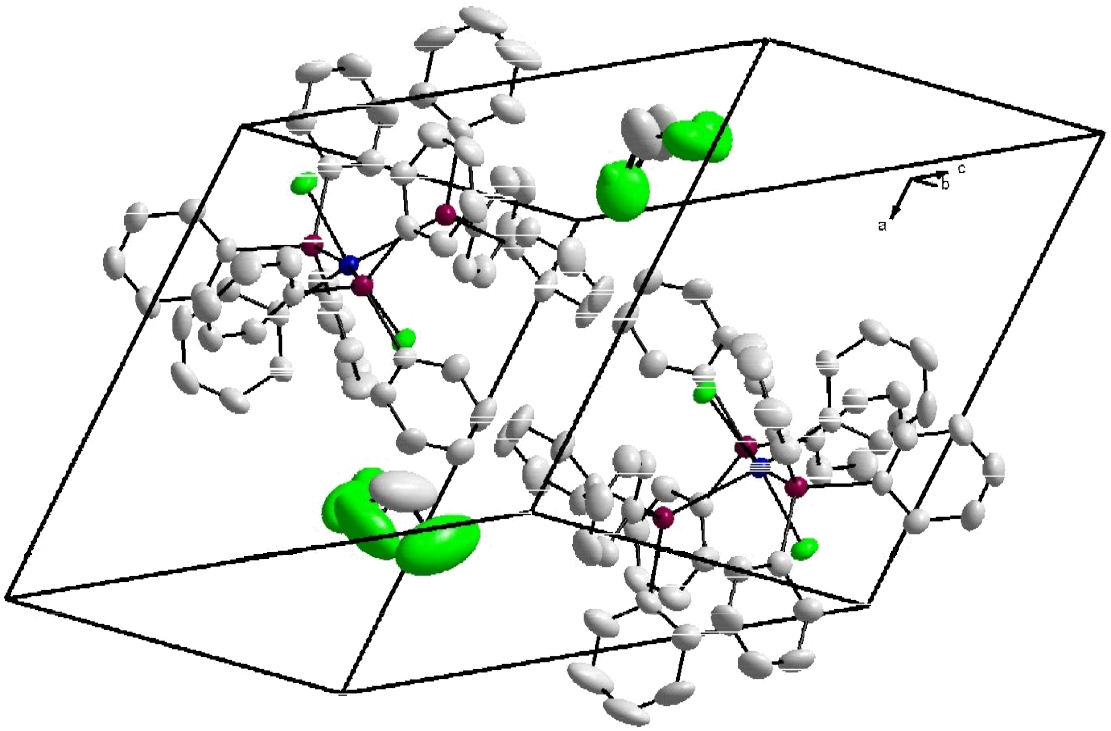

Figure 3.14: Diamond structure of the unit cell of $[Rh(Cl)_2(Ph)(Sbh_3)_3].2CH_2Cl_2$ Hydrogen atoms and two remaining symmetrically equivalent CH_2Cl_2 molecules have been omitted for clarity. Thermal ellipsoids are drawn at 50% probability level.

There is no indication of any intermolecular π–stacking, and no interaction between the solvent molecules and atoms of the metal complex. There are short intermolecular contacts between Cl(2) and the proton of C(33) measuring 2.767(75) Å.

The intramolecular stacking interaction between the phenyl donor and the C(41) – C(46) ring system is comparable to that for the same structure cocrystallised with ethyl acetate[37] as well as for the acetone polymorph.[10] Our complex exhibits a C…C distance of 3.298(66) Å for C(06)…C(46), while the other complexes exhibit intermolecular distances of 3.303 and 3.34 Å for ethyl acetate and acetone respectively (no esds reported). The Rh–Sb(2)–C(46) bond angle is 105.64(1)˚ (114.1(2)˚ for the ethyl acetate analogue), whereas the other Rh–Sb(2)–C(56/66) angles are 119.72(2)˚ and 120.84(2)˚, respectively. This indicates significant π–stacking interactions pushing the stibine phenyl ring slightly towards the rhodium bound phenyl.

Figure 3.15 shows the intramolecular contacts of (**3**). There exist numerous H – bonds between the Cl^- atoms and the protons of the stibine and rhodium bound phenyl rings. The contacts between Cl^- and the *trans* phenyl are in the range of 2.60(2) and 2.50(2) Å for H(06) – Cl(1) and H(02) – Cl(2) respectively. These interactions explain the two sets of doublets in the ^{1}H NMR spectrum of (**3**) at δ (ppm) 6.691 and 7.446. The signals correspond to the non-equivalent *ortho* protons of the phenyl ring.

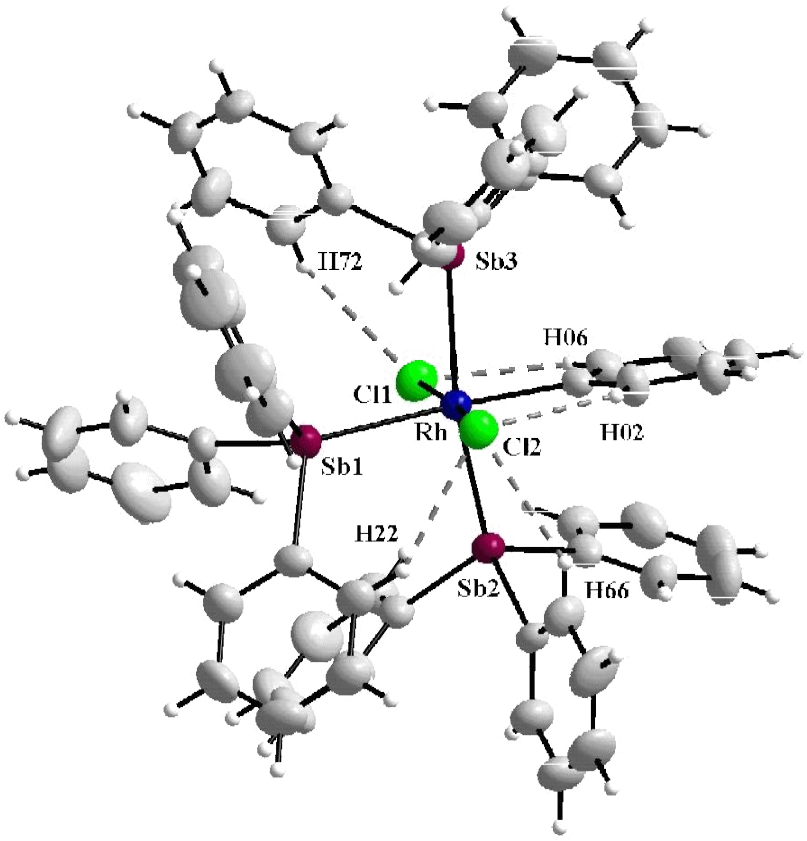

Figure 3.15: Diamond structure showing the intramolecular contacts of *trans-mer*-$[Rh(Cl)_2(Ph)(SbPh_3)_3].2CH_2Cl_2$. Thermal ellipsoids are drawn at 50% probability level.

There are also short contacts between Cl^- and the *ortho* protons on phenyl rings two, six and seven, measuring 2.69(3), 2.69(3) and 2.84(2) Å for H(22)–Cl(2), H(66)–Cl(2) and H(72)–Cl(1) respectively. These interactions result in slightly smaller Rh–Sb–C angles on the rings containing H(22) and H(72), at 113.83(2)° for Rh–Sb(1)–C(21) and 116.54(2)° for Rh–Sb(3)–C(71), while the whole of phenyl ring six is twisted, bringing C(66) towards the Cl^- atom.

3.4.2.4 Crystal Structure of $[Rh(Cl)_2(Ph)(PPh_3)_2]$

(A) Introduction

As described previously in section 3.3.2.12, this complex was obtained from the reaction of (**3**) with triphenylphosphine. The structure has been published previously by Cini *et al*.,[41] where they obtained the complex by refluxing (**3**) with PPh_3 in MeOH for 2 hours, followed by recrystallisation from CH_2Cl_2. The complex has also been synthesised by reacting $[RhH(Cl)_2(PPh_3)_3]$ with $HgPh_2$.[42] The former can be synthesised from $RhCl_3.H_2O$, via a $[Rh(Cl)(PPh_3)_3]$, Wilkinson catalyst intermediate.[43,44]

(B) Results

$[Rh(Cl)_2(Ph)(PPh_3)_2]$, (**8**) crystallised from acetone in the monoclinic space group, C2/c, with four molecules per unit cell. The molecular structure of (**8**) is represented in Figure 3.16, along with the atom numbering system. The positional and thermal parameters are given in Table C.1 of Appendix.

[41] R. Cini, A. Cavaglioni, *Inorg. Chem*., **38**, 1999, 3751
[42] J. Fawcett, J.H. Holloway, G.C. Saunders, *Inorg. Chim. Acta*, **202**, 1992, 111
[43] J.A. Osborn, G. Wilkinson, *Inorg. Synth*., **28**, 1990, 77
[44] A. Sacco, R. Ugo, A. Moles, *J. Chem. Soc. A*, 1996, 1670

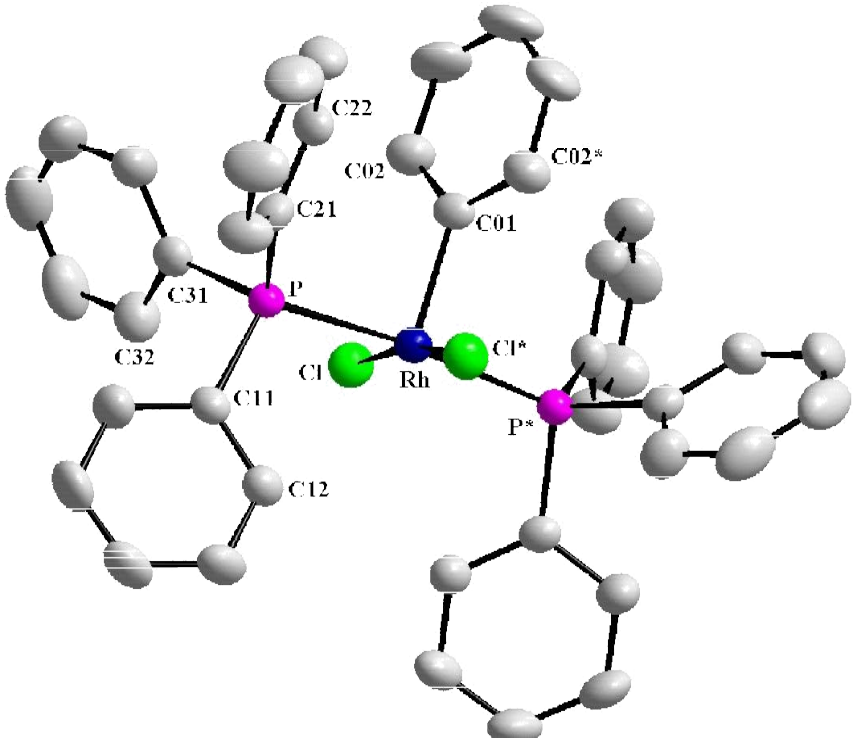

Figure 3.16 Diamond structure of $[Rh(Cl)_2(Ph)(PPh_3)_2]$ showing the atom numbering system. For the phenyl rings, the first digit refers to ring number, while the second digit refers to the C-atom in the ring. H atoms have been omitted for clarity. Thermal ellipsoids are drawn at 50% probability level. Primed atoms denote those generated by the two-fold rotation axes.

The molecular structure of (**8**) consists of a pentacoordinate Rh(III) centre. The metal coordination sphere is completed by two *trans* chloride atoms, two *trans* phosphorus atoms of PPh_3, and the carbon atom of the phenyl ring. The two chloride atoms are symmetrically equivalent, as are the two triphenylphosphine groups. The symmetry equivalents are generated by the crystallographic 2-fold rotation axis along atoms Rh–C(01)–C(04)–H(04).

Selected interatomic bond distances and angles are presented in Table 3.7.

Table 3.7: Selected bond lengths and angles for $[Rh(Cl)_2(Ph)(PPh_3)_2]$

Bond	Distance (Å)	Bond	Distance (Å)
Rh-C(01)	1.994(5)	P-C(21)	1.830(3)
Rh-Cl	2.3419(10)	C(01)-C(02)	1.393(4)
Rh-P	2.3601(11)	C(02)-C(03)	1.384(5)
P-C(31)	1.827(4)	C(03)-C(04)	1.368(5)
P-C(11)	1.828(3)		
Angle	**Bond Angle (˚)**	**Angle**	**Bond Angle (˚)**
C(01)-Rh-Cl	95.65(2)	C(31)-P-C(11)	102.13(16)
Cl-Rh-Cl*	168.71(5)	C(31)-P-C(21)	104.90(16)
C(01)-Rh-P	93.05(2)	C(11)-P-C(21)	105.97(16)
Cl*-Rh-P*	85.12(4)	C(31)-P-Rh	118.78(11)
Cl-Rh-P*	94.28(4)	C(11)-P-Rh	108.83(12)
P-Rh-P*	173.91(5)	C(21)-P-Rh	114.85(12)
C(02)-C(01)-Rh	120.8(2)		

*: Atoms generated as symmetrically equivalent through –x + 1, y, -z + ½

All phenyl rings, including the metal bound ring, are planar, within experimental error. The average C – C bond distances (1.378 Å) and bond angles (120.0°) are within the expected range for phenyl rings.[40]

The Rh atom is displaced from the plane defined by Cl/P/Cl*/P* by 0.1780(1) Å towards the phenyl ring. This is indicative of the strong *trans* influence of the phenyl group, strengthening the Rh – C(01) bond significantly.

The C–P–C bond angles average 104.33(16)°, comparable with the values previously published for this structure.[41] Similarly, the Rh–P–C angles were comparable at 114.15(12)°. This value is slightly lower than the accepted M–P–C angle for PPh_3

groups, of 115.6°.[45] This is most likely a result of the Cl-…H bond interactions, described later in the text.

The C(01)–Rh–Cl and C(01)–Rh–P angles are 95.65(2)° and 93.05(2)° respectively. Both ligand systems are pushed away from the phenyl group towards the vacant site.

Figure 3.17 and 3.18 present the unit cell and packing system of (**8**). The crystal packing does not have any appreciable stacking interaction involving the π-system of the phenyl moieties. Figure 3.17 clearly shows the slightly eclipsed conformation of the *trans* phenyl and chloride atoms. The torsion angle Cl–Rh–C(01)–C(02) measures 24.27(1)°.

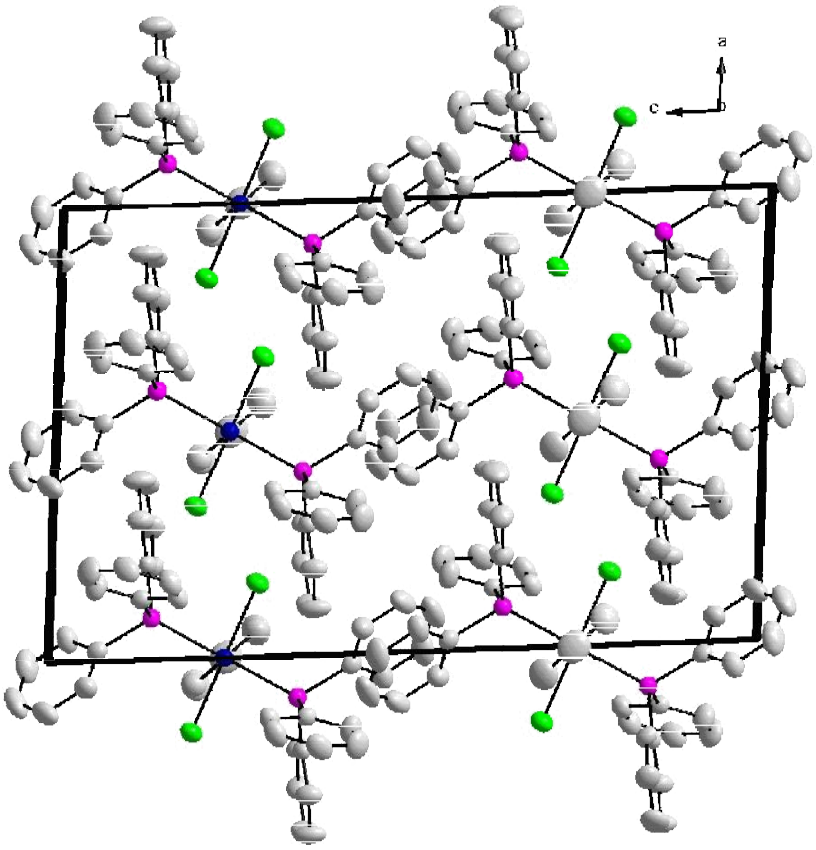

Figure 3.17 Diamond structure of [Rh(Cl)$_2$(Ph)(PPh$_3$)$_2$] unit cell packing viewed along the b axis. H atoms have been omitted for clarity. Thermal ellipsoids are drawn at 50% probability level

[45] N.R. Champness, W. Levason, *Coord. Chem. Rev.*, **113**, 1994, 115

The complexes are packed in a 'head to tail' fashion along the b axis, with each *trans*-phenyl ring pointing to the vacant site between the two phosphine groups of the adjacent molecule. There does not appear to be significant intermolecular repulsion between the phenyl groups of PPh_3.

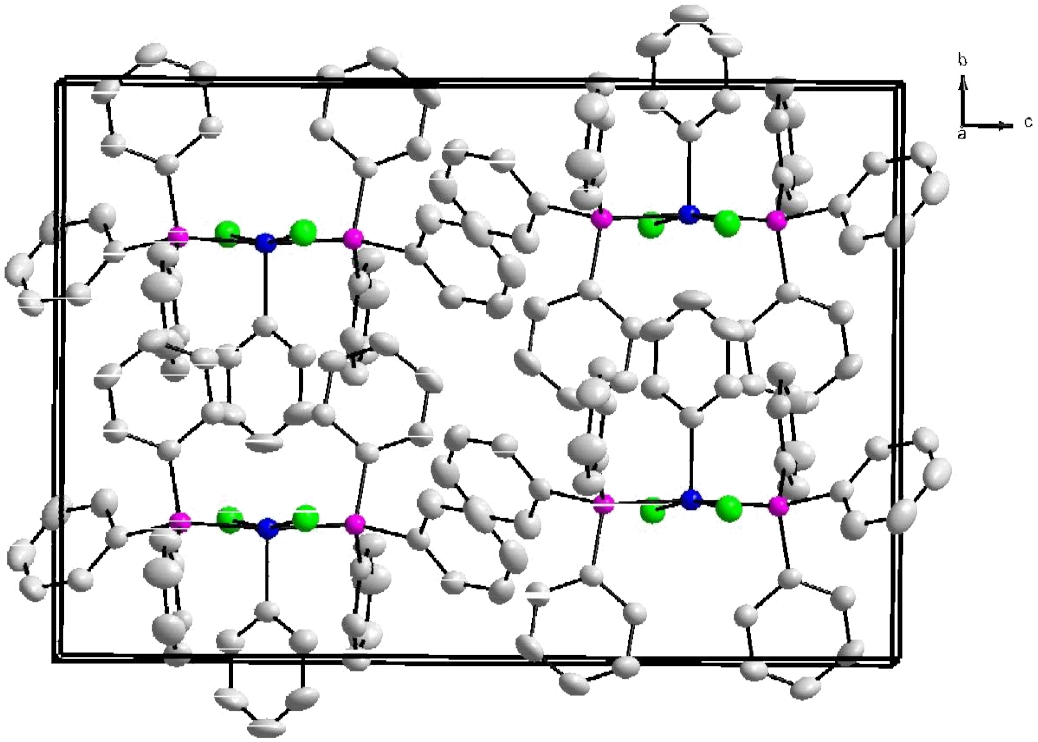

Figure 3.18 Diamond structure of $[Rh(Cl)_2(Ph)(PPh_3)_2]$ unit cell showing packing along a axis, viewed along a axis. H atoms have been omitted for clarity. Thermal ellipsoids are drawn at 50% probability level

The short intramolecular contacts of (**8**) are illustrated in Figure 3.19. There are numerous short contact, H – bond interactions between the two Cl^- atoms and the protons of both metal and phosphine bound phenyl groups. The short contact of Cl–H(02), Cl–H(12) and Cl–H(32) measure 2.671(5), 2.728(9) and 2.847(29) Å respectively.

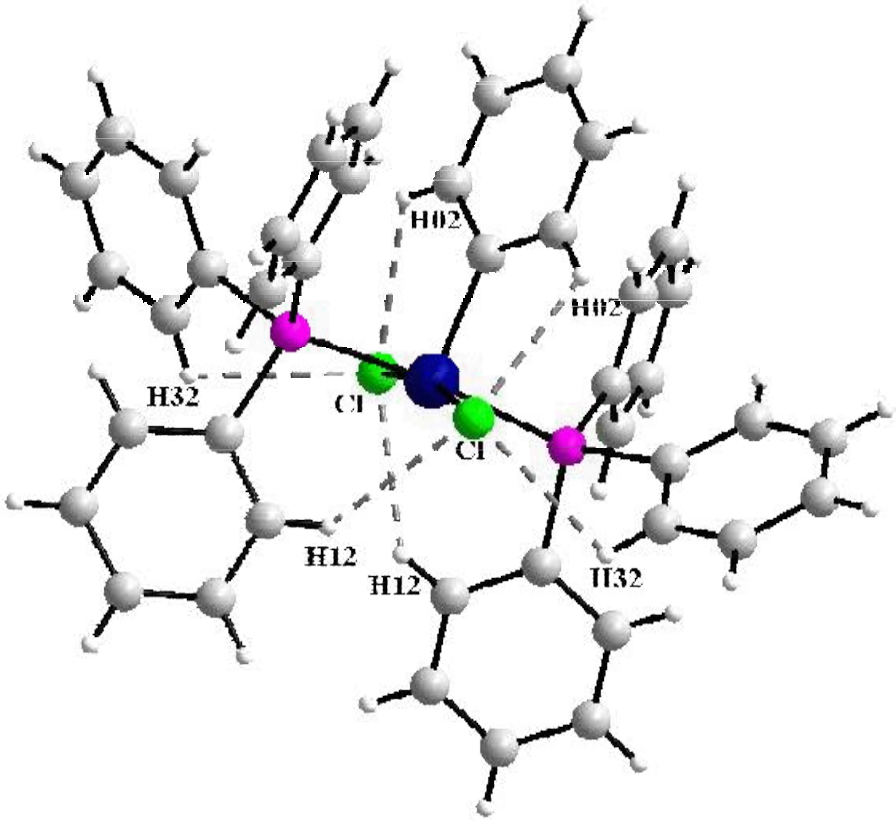

Figure 3.19 Diamond structure of $[Rh(Cl)_2(Ph)(PPh_3)_2]$ showing short intramolecular contacts. Thermal ellipsoids are drawn at 50% probability level

The angle Rh – P – C(11) of 108.83(12)° is significantly shorter than the remaining Rh – P – C(21) and Rh – P – C(31) angles measuring 114.85(12) and 118.78(11)° respectively. This is most likely a result of the H – bond pulling the phenyl ring toward the Cl^- atom.

3.4.2.5 Crystal structure comparison of *trans-mer*-$[Rh(Cl)_2(Ph)(SbPh_3)_3]$ and $[Rh(Cl)_2(Ph)(PPh_3)_2]$

Table 3.8 presents a summary of the crystal structure of (**3**) as well as the crystal data for the previously published acetone[10] and ethyl acetate[37] polymorphs of (**3**). Table 3.8 also contains a summary of the crystal data for (**8**) as well as the original crystal structure published for (**8**) by Cini and co-workers.[41] The table gives the unit cell contents and interatomic bond distances and angles for comparison between the structures.

From the table it can be seen that the interatomic bond distances and angles of *trans-mer*-$[Rh(Cl)_2(Ph)(SbPh_3)_3]$ correlate reasonably well between the three polymorphs. The unit cell parameters differ according to the size and number of solvent molecules present. The DCM polymorph investigated in this study has the largest unit cell volume as would be expected for a structure containing four DCM molecules per unit cell. Similarly, the acetone polymorph has the smallest volume,[10] with only a single acetone molecule present in the unit cell.

The crystal structure of $[Rh(Cl)_2(Ph)(PPh_3)_2]$ presented for this M.Sc. study correlates very well with that previously published by Cini and co-workers.[41] The two can be considered the same polymorph of this Rh(III) complex.

Table 3.8: Summary of crystallographic data for the three polymorphs of $[Rh(Cl)_2(Ph)(SbPh_3)_3]$ as well as $[Rh(Cl)_2(Ph)(PPh_3)_2]$ from both sources.

	***trans-mer*-$[Rh(Cl)_2(Ph)(SbPh_3)_3]$**			**$[Rh(Cl)_2(Ph)(PPh_3)_2]$**	
	DCM This M.Sc. Study	Acetone Cini *et.al*	Ethyl acetate Cini *et.al*	This M.Sc. Study	Cini *et.al*
Crystal system	Triclinic	Triclinic	Triclinic	Monoclinic	Monoclinic
Space group	P $\bar{1}$	P $\bar{1}$	P $\bar{1}$	C2/c	C2/c
Z	2	2	2	4	4
Solvent molecules per unit cell	4	1	2	None	None
a (Å)	13.512(3)	12.686(2)	13.426(2)	12.889(3)	12.9060(10)
b (Å)	15.547(3)	14.906(2)	15.352(2)	13.850(4)	13.861(2)
c (Å)	15.888(3)	15.523(3)	15.811(2)	20.099(4)	20.106(3)
α (º)	92.73(3)	107.73(2)	92.450(10)	90	90
β (º)	109.32(3)	95.10(2)	109.320(10)	93.91(3)	93.860(10)
γ (º)	108.10(3)	93.62(2)	107.970(10)	90	90
Volume($Å^3$)	2951.4(10)	2772(1)	2887.0(7)	3579.6(12)	3588.6(8)
Rh-Cl(1)	2.373(1)	2.362(5)	2.363(2)	2.341(1)	2.3458(9)
Rh-Cl(2)	2.372(1)	2.360(5)	2.367(2)	2.341(1)	2.3458(9)
Rh-C(01)	2.115(5)	2.090(22)	2.118(6)	1.994(5)	2.014(5)
$Rh\text{-}Sb(1)_{trans\ to\ Ph}$	2.7185(8)	2.706(2)	2.7056(7)	-	-
Rh-Sb(2)	2.6082(9)	2.594(2)	2.5859(7)	-	-
Rh-Sb(3)	2.5877(10)	2.582(2)	2.6077(7)	-	-
Rh-P	-	-	-	2.3601(11)	2.3635(9)
Cl(1)-Rh-Cl(2)/*	172.84(5)	173.8(2)	173.01(6)	168.71(5)	168.70(5)
C(01)-Rh-Cl(1)	94.20(16)	93.2(6)	92.8(2)	95.65(2)	95.65(2)
C(01)-Rh-Cl(2)/*	92.85(16)	92.8(6)	94.0(2)	95.65(2)	95.65(2)
C(01)-Rh-Sb(1)	172.45(15)	173.0(6)	172.2(2)	-	-
C(01)-Rh-Sb(2)	84.54(13)	86.3(6)	84.7(2)	-	-
C(01)-Rh-Sb(3)	84.55(13)	80.9(6)	84.5(2)	-	-
C(01)-Rh-P	-	-	-	93.05(2)	93.03(2)
P-Rh-P*	-	-	-	173.91(5)	173.94(5)

*: Atoms generated as symmetrically equivalent through –x + 1, y, -z + ½

The higher coordination number of (**3**) relative to (**8**) can be attributed to the ability of stibine systems to stabilise electron dense metal centres. Stibines have significantly less σ-donating ability than phosphines, as well as a better ability to accept charge from the metal (better π-accepting ability). As a result of these factors, stibines readily form 5 coordinate Rh(I) ground state complexes and stabilise highly coordinated transition states.[40,46] Strong σ-donation from the phosphine results in an electron dense metal centre and the comparable lack of any significant M → P π back donation prevents the coordination of a third triphenylphosphine molecule.

Steric factors also contribute to the higher coordination of (**3**). The Tolman cone angle of $SbPh_3$ is 137˚,[47] compared to 145˚ for PPh_3.[48] Thus, the six coordinate rhodium(III) complex is more readily attained with the triphenylstibine ligand system, compared to the analogous sterically crowded six coordinate triphenylphosphine complex.

Although complexes (**3**) and (**8**) cannot be accurately be compared due to their different coordination numbers, a few comparable points can be noted:

The Rh–Cl bond distances compare well between structures (**3**) and (**8**). However the Rh–C(01) and Rh–L (L = Sb for (**3**), L = P for (**8**)) bonds differ significantly, illustrating the respective *trans* influence and bond strength of stibine versus phosphine systems. Both Rh–C(01) and Rh–L bonds are smaller in $[Rh(Cl)_2(Ph)(PPh_3)_2]$ (**8**) than in $[Rh(Cl)_2(Ph)(SbPh_3)_3].2CH_2Cl_2$ (**3**). The Rh–C(01) bonds for (**8**) and (**3**) are 1.994(5) and 2.115(5) respectively, while Rh–P for (**8**) is 2.3601(11) and the average Rh–Sb for (**3**) is 2.6389(16).

The difference in length between the Rh–P and Rh-Sb bonds can be attributed to a combination of factors. The Rh–Sb bonds are longer as the ligands are effectively 'pushed' away from the metal centre as a result of the steric crowding. The increase is also in accordance with the increase in covalent radii of the ligands when descending periodically from PPh_3 to $AsPh_3$ to Sbh_3. The radii increases from 1.10 (P) to 1.21 (As) to 1.41 (Sb) Å.[49]

[46] S. Otto, A. Roodt, *Inorg. Chim. Acta*, **331**, 2002, 199
[47] S. Otto, A. Roodt, *Acta Cryst. C*, **C58**, 2002, m565
[48] P.B. Dias, M.E. Minas de Piedale, J.A. Martinho Simoes, *Coord. Chem. Rev.*, **125**, 1994, 737
[49] A.N. Sobolev, I.P. Romm, V.K. Belsky, E.N. Guryanova, *J. Organomet. Chem.*, **179**, 1979, 153

The Rh–C(01) bond distances of (**3**) and (**8**) differ as a result of the nature and orientation of the groups *trans* to the phenyl. The Rh-C(01) bond of (**8**) is shorter as it is *trans* to a vacant position, and is thus not influenced by *trans* groups as with the tripehnylstibine ligands of (**3**).

Phosphine-, arsine- and stibine-platinum systems have been intensively studied by Wendt et al.[50,51,52] They have proposed a *trans* effect and *trans* influence series for these ligand systems based on the platinum complexes, $[Pt(I)_3(LR_3)]^-$ (L = P, As, Sb, R = Ph).

trans Effect can be divided into σ donating and π accepting components for each atom type, and can be considered a transition state influence. Strong σ-donation from a ligand weakens the *trans* bond, while a strong π-accepting component acts to stabilise electron rich transition state intermediates formed. The *trans* effect series has been unambiguously determined as $Ph_3Sb > Ph_3P > Ph_3As$, based on a balance between σ- and π-contributions.[52]

trans Influence, however, is based on a measure of the σ component, and is a ground state effect. A *trans* influence series of P > As > Sb for numerous trialkyl complexes has been confirmed by different sources,[45,50,48] while the triaryl ligand systems have given less consistent results. The same *trans* influence series has been tentatively proposed, based on Pt – I bond distances *trans* to PPh_3, $AsPh_3$ and $SbPh_3$ in the previously mentioned Pt complex. However, further analysis by Salcedo *et. al.*[53] have concluded that the *trans* influence of stibine is comparable to that of phosphine, based on similar crystallographic investigations. So further research is needed to clear this ambiguity.

[50] O.F. Wendt, L.I. Elding, *J. Chem. Soc., Dalton Trans.*, 1997, 4725
[51] O. Wendt, A. Scodinu, L.I. Elding, *Inorg. Chim. Acta*, **277**, 1998, 237
[52] N. Kuznik, O.F. Wendt, *J. Chem. Soc., Dalton Trans*., 2002, 3074
[53] R. Salcedo, P. Sharma, A. Cabrera, S. Fomine, *J. of Mol. Struct. (Theochem),* **579**, 2002, 151

4. KINETIC INVESTIGATION OF STIBINE – PHOSPHITE SUBSTITUTION REACTIONS

4.1 INTRODUCTION

Investigating the kinetics of a chemical reactions involves determining the rate of the reaction and all factors influencing the rate, as well as explaining the rate in terms of the reaction mechanism. The kinetic data can be used to contrast and compare various chemical systems, with regards to their stability, reactivity and selectivity.

4.1.1 History of Kinetics

The first kinetic study of a chemical reaction was carried out in 1850 by Wilhelmy[1] who measured the rate of conversion of an acidic solution of sucrose into glucose and fructose. This reaction was especially suitable for kinetic study as the extent of the reaction could be determined at any time by measuring the optical rotation of the solution in a polarimeter. Wilhelmy found that at a given concentration of acid, the rate of the reaction at any instant was proportional to the amount of sucrose remaining in the solution.[2]

4.1.2 Reaction Rates and Rate Laws

The rate of a chemical reaction can be expressed in terms of the rate of formation of any product, or the rate of consumption of any reactant.

For a general reaction with stoichiometric equation of:

[1] L. Wilhelmy, *Ann. Physik. Chemie,* **81**, 413, 1850, 499
[2] J.L. Lantham, 'Elementary Reaction Kinetics', Butterworths, London, 1964

$$aA + bB \rightarrow gG + hH \quad (4.1)$$

The rate may be expressed by:

$$\text{rate} = -d[A]/dt; -d[B]/dt; +d[G]/dt; \text{ or } +d[H]/dt \quad (4.2)$$

Here t is time, and brackets indicate species concentration. A derivative is used because the rate almost always changes as time goes on.

If the concentration of a product affects the rate, this effect is called either auto-inhibition or autocatalysis. If a substance, neither a reactant nor a product, affects the rate it is called an inhibitor, retarder, sensitizer, or catalyst, depending on the nature of the effect.

The functional relation between rate and concentration is called a rate expression or rate law.[3,4]

For the reaction:

$$H_2 + I_2 \rightarrow 2HI \quad (4.3)$$

The corresponding rate law can be written as:

$$r = d[HI]/dt = k[H_2][I_2] \quad (4.4)$$

While for the reaction:

$$OCl^- + I^- \rightarrow OI^- + Cl^- \quad (4.5)$$

The rate law was calculated as:

$$r = d[Cl^-]/dt = k[OCl^-][I^-]/[OI^-] \quad (4.6)$$

[3] A. Frost, R. Pearson, 'Kinetics and Mechanism', 2nd Edition, John Wiley and Sons, New York, 1961
[4] L. Meites, 'An Introduction to Chemical Equilibrium and Kinetics', Permagon Press, Oxford, 1981

Several important points can be noted from these expressions regarding the nature of rate laws. Firstly, the rate law bears no simple relationship to the stoichiometric equation. Secondly, the rate law may not depend on the concentration of every reactant or product, and the rate law may depend on the concentration of species (eg. catalysts or inhibitors) which do not appear in the equation for the overall reaction. In general, it is not possible to predict the rate expression for a given reaction by just knowing the stoichiometric equation, therefore the rate equation must be determined experimentally.[5]

The constant of proportionality, k, is called the rate constant and has dimensions of $[conc]^{-1}[time]^{-1}$. Commonly used concentration units are moles/liter, moles/cc, etc. The unit of time may be seconds, minutes and so forth. Although rate constants are independent of concentration and time they usually show a marked temperature dependence.[4,5]

4.1.3 Reaction Order

For rate laws that consist of a product of powers of concentration, such as:

$$-d[A]/dt = k[A]^{n_1}[B]^{n_2}[C]^{n_3} \qquad (4.7)$$

The sum of the exponents of all the concentrations on the right-hand side correspond to the order of the reaction. Also, each individual exponent is termed the order with respect to that component. For example, the hydrogen-iodine reaction (equation 4.3), is a second order reaction and first order with respect to both hydrogen and iodide.

If conditions for a given reaction are such that one or more of the concentration factors are constant or nearly constant during a 'run', these factors may be included in the rate constant. In this case the reaction is said to be of pseudo-nth order, where n is the sum of the exponents of those concentration factors which change during the run.

[5] F. Wilkinson, 'Chemical Kinetics and Reaction Mechanisms', Van Nostrand Reinhold Company, New York, 1980

This occurs for catalytic reactions, with the catalyst remaining constant during the run, or if one reactant is in large excess over another so that during the run there is only a small percentage change in the concentration of the former.[3]

4.1.4 Reaction Rates in Practice

The determination of a reaction rate by conventional methods basically involves studying the change in concentration of a species, as a function of time. Many analytical procedures have been devised that can be used to measure quantities that are proportional to concentration. Which quantity is chosen for any particular reaction depends on the properties of the reactants and products. It is necessary that the property being measured differs appreciably from reactants to products, and the property must vary in some simple manner with concentration of reactants and products.

In general, the analytical procedures may be divided into 2 broad categories: chemical and physical. Chemical analysis implies a direct determination of one of the reactants or products by gravimetric or volumetric processes. These methods have the advantage of giving an absolute value of the concentration. However, physical methods are usually much more convenient. Common physical methods include pressure measurements in gaseous reactions, dilatometry, or measurement of volume change. Optical methods such as polarimetry, refractometry, colorimetry and spectrophotometry, as well as electrical methods such as conductivity, potentiometry, polarography and mass spectrometry are frequently utilised. Whatever the measured quantity, its value can be plotted at each of a number of instants after the solutions have been mixed, to produce a plot of species concentration change with time.

A typical result for such a run would be as shown in Figure 4.1, where the concentration, C, of a reactant starts at zero time at some initial value, C_0, and decreases more and more slowly, approaching zero or some equilibrium value, C_∞. The rate at any time would be the negative of the slope of the curve expressed in the appropriate units. However, since it is the concentration that is usually observed, the integrated form of the rate expression is more convenient to work with.[3]

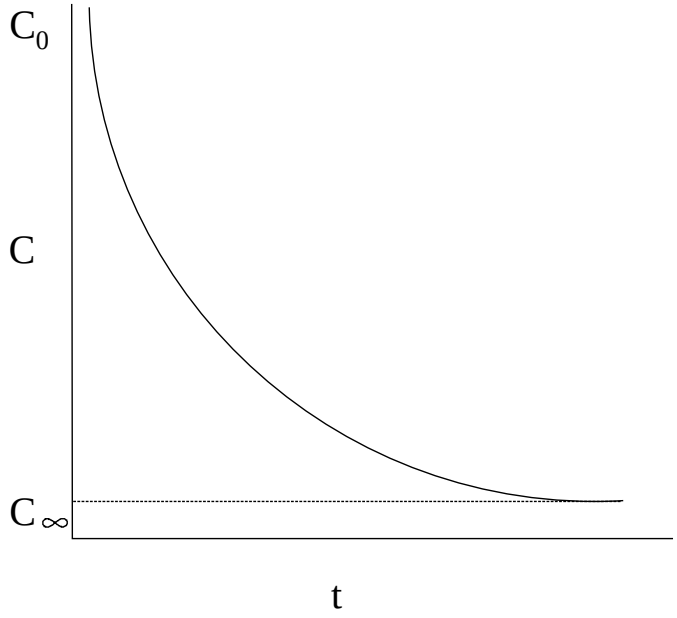

Figure 4.1: Concentration versus time for a typical first order reaction

For a single component rate expression there are several possible reaction orders, namely zero, first and less frequently encountered, second order, as per equations 4.8 to 4.10:

$$d[A]/dt = -k([B]\ldots) \quad (4.8)$$

$$d[A]/dt = -k[A]([B]\ldots) \quad (4.9)$$

$$d[A]/dt = -k[A]^2([B]\ldots) \quad (4.10)$$

These expressions show the species A is a reactant whose concentration decreases as the reaction proceeds. The other reaction components have been grouped together as ([B]…) to focus attention on the changing concentration of species A. For simplification, this term will be expressed as k'. The integrated form of the common rate expressions for zero and first order reactions are as follows:[4]

For zero order in A:

$$d[A]/dt = -k' \quad (4.11)$$

Integration yields:

$$[A] = -k't + C \quad (4.12)$$

The constant of integration, C, is equal to the value of [A] at t = 0, or the initial concentration of A, and may be expressed as the symbol $[A_0]$. So the expression becomes:

$$[A] = [A_0] - k't \quad (4.13)$$

For first order in A:

$$d[A]/dt = -k'[A] \quad (4.14)$$

Integration with limits taken as $[A] = [A_0]$ at t = 0 and [A] at t = t respectively gives:

$$\ln[A] = -k't + C \quad (4.15)$$

Again, C represents [A] at t = 0 or $\ln[A_0]$ and:

$$\ln[A] = \ln[A_0] - k't \quad (4.16)$$

This can be rewritten as:

$$[A] = [A_0]\exp -k't \quad (4.17)$$

The system of integration may be used to determine the order of a reaction being investigated. The method involves plotting the experimental data according to each of the integrated expressions in turn, i.e., the expressions on the left-hand side of the

integrated equations are plotted against time. A linear plot is obtained only when the integrated form of the correct rate law is used.[5] The rate can be calculated from the linear plots by determining the slope and rearranging the slope term of the integrated expression to get k.

For the purpose of this investigation, the absorbance of a solution containing the reaction components is plotted as a function of time after the components are mixed together and the reaction commences. The plot obtained can be viewed as an increase or decrease in absorbance representing the changing concentration of one of the reaction components. The observed rate constants for these reactions can then be determined from equation 4.18:

$$A_{obs} = A_f - (A_f - A_i)\exp(-k_{obs}T) \qquad (4.18)$$

Here A_i is the initial absorbance and A_f is the final absorbance.

4.1.5 Reaction Half-Life

In a first order or pseudo-first order reaction the time in which half of the reactant disappears is independent of the concentration of the reactant. This can be proved by solving the integrated law for t and setting [A] equal to $[A_0]/2$:

$$t = \ln[A_0] - \ln[A]/k' = \{\ln([A_0]/[A_0]/2)/k'\} = \ln 2/k' = 0.693/k' \qquad (4.19)$$

The time described by this equation is called the half-life for the reaction, and is given the symbol $t_{1/2}$. Half of the initial concentration of reactant disappears during the half-life, half of the remaining half during another and so on. If the reactant is zero order in A, all of the A will be gone at $2t_{1/2}$. If it is second order in A, a third of the initial amount will still be left after $2t_{1/2}$, a quarter after $3t_{1/2}$ and a fifth after $4t_{1/2}$ and so on. All these things are true regardless of the values of k' or $[A_0]$ and can often be used to find the order in a particular reactant by simply inspecting the data obtained under the

pseudo-nth-order conditions, then constructing a linear plot of the data to obtain the value of k' from its slope.

The pseudo-nth-order rate constant is the product of the actual rate constant k, and a quantity ([B]…), that might include the concentrations of various other substances. To derive the complete rate law we need to determine which substances are involved and their exponents.

This involves changing the concentration of a second species, ([B]) and observing the effect this has on k'. If there is no change in the slope, this indicates the reaction is zero order in B, while various concentrations of B producing proportional changes in k' will show the reaction to be first order with respect to B, and so forth.

It is essential that all other reaction concentrations and conditions are held constant during these runs to ensure accurate interpretation of the results.[4]

At this stage we have the value of k' (k' = k[B]) and the value of k can be calculated by dividing the slope of the linear plot by [B] and the results obtained from all of the different experiments can be averaged to obtain the final result.

4.1.6 Reaction Thermodynamics

In 1889, Arrhenius postulated that normal chemical molecules do not, in fact, take part in chemical reactions.[6] Only those molecules which posses more than a certain critical energy, called the energy of activation, are able to react. The activated molecules are extremely few in number and arise as a result of random collisions between molecules. These collisions occasionally give a molecule many times its average energy.[1]

Increasing the temperature increases the kinetic energy of the reacting particles, causing them to move through the solution more rapidly and thus collide more

[6] S. Arrhenius, *Z. Physik. Chem.*, **1**, 1887, 110

frequently. Increasing the viscosity of the solution has the opposite effect, it slows their motions and makes collisions less frequent. The signs and magnitudes of charges on the reacting particles are also very important and account for the attractive and repulsive forces between the ions.[4]

Figure 4.2, shows a plot of potential energy versus the reaction coordinate for any general elementary reaction. In the transition state theory, also referred to as the activated complex theory, attention is focussed on the species existing at the maximum point on this curve at the point where the reactants are just about to transform into products. This species is called the activated complex, $X^{\dagger}$, or transition state.[5]

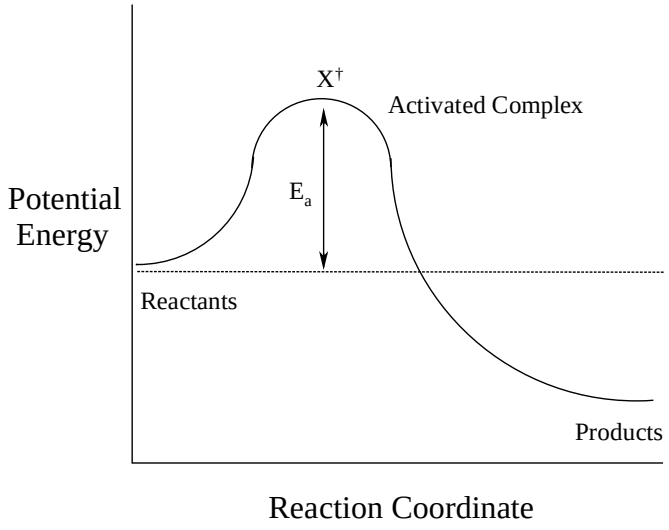

Figure 4.2: Variation in potential energy along the reaction coordinate for a spontaneous elementary reaction

In forming the activated complex, the kinetic energies of the colliding molecules are transformed into chemical energy. Initially the reacting ions have a certain amount of chemical energy between them. As they approach each other they also have a certain amount of kinetic energy between them. Kinetic energy is transformed into chemical energy when they collide, and if enough kinetic energy is available, the resulting increase in chemical energy of the system will cause the activated complex to form.

Then the activated complex may reorganise to yield the products, liberating energy as it does so.[4]

Using the idea of activation, Arrhenius derived an equation to describe the variation of rate constant with temperature:

$$k = A\exp(-E_a/RT) \qquad (4.20)$$

Here R is the gas constant, A is known as the Arrhenium pre-exponential or frequency factor (for first order reactions), and E_a is the term for the activation energy. The frequency factor is equal to the total number of collisions that will occur during 1 second in a solution having a volume of 1 dm^3 and containing 1 mole of each reactant.[4] A has the same dimension as the rate constant, while E_a has dimensions of energy per amount of substance. Both E_a and A can be determined experimentally by measuring k at a series of different temperatures.

In logarithmic form the equation becomes:

$$\ln k = -E_a/RT + \ln A \qquad (4.21)$$

And thus a plot of lnk versus 1/T will have a slope equal to $-E_a/R$ and an intercept of lnA.[7]

An additional fact to consider is the extent to which rate constants are affected by increasing temperature. Because different reactions have different energies of activation, their rates are affected to different extents by changes of temperature. Heating a reaction mixture from 298 K to 308 K increases the value of the rate constant only 14 percent if the energy of activation is 10 $kJ.mol^{-1}$, but almost quadruples if the energy of activation is 100 $kJ.mol^{-1}$. Similarly, it increases it by a factor of 50 if the energy of activation is 300 $kJ.mol^{-1}$. When the energy of activation is large, the rate constant is small and increases rapidly as the temperature increases. When the energy of activation is small the rate constant is large and only slightly

[7] A.E. Merbach, P. Moore, O.W. Howarth, C.H. McAteer, *Inorg. Chim. Acta*, **39**, 1980, 129

dependant on the temperature. Small rate constants therefore increase more rapidly with increasing temperature than large ones do.[4]

4.1.7 Transition State Theory

The Transition State Theory is used almost exclusively in considering, and understanding the kinetics of reactions in solution.[5] The basic assumption of the theory is that the activated complex, $X^{\dagger}$, can be treated as a thermodynamic entity in equilibrium with the reactants. The general reaction may be written as:

$$\text{Reactants} \overset{K_c^{\dagger}}{\rightleftharpoons} X^{\dagger} \xrightarrow{vt} \text{Products}$$

Scheme 4.1

The rate of reaction per unit volume, r, is given by the concentration of the activated complex multiplied by the frequency, ν_t, with which this activated complex is transformed into products,[8] i.e:

$$r = \nu_t[X^{\dagger}] \tag{4.22}$$

The frequency can be shown to be equal to $k_B T/h$ where k_B is Boltzmann's constant and h is Planck's constant. So for the reaction:

$$A + B \overset{K_c^{\dagger}}{\rightleftharpoons} X^{\dagger} \xrightarrow{vt} \text{Products}$$

Scheme 4.2

The rate can be expressed as:

$$r = k_B T[X^{\dagger}]/h = k_B T[A][B]/h \tag{4.23}$$

[8] D.A. House, H.K.J. Powell, *Inorg. Chem.*, **10**, 1971, 1583

So the second order rate constant is given by:

$$k = k_B T K_c^{\dagger}/h \qquad (4.24)$$

As a result of the reaction equilibrium, the free energy of activation $\Delta G^{\dagger}$ can be defined as in normal thermodynamics:

$$\Delta G^{\dagger} = -RT\ln K_c^{\dagger} = \Delta H^{\dagger} - T\Delta S^{\dagger} \qquad (4.25)$$

Leading to:

$$k = (k_B T/h)\exp(-\Delta G^{\dagger}/RT) = (k_B T/h)\exp(-\Delta H^{\dagger}/RT)\exp(\Delta S^{\dagger}/R) \qquad (4.26)$$

Where $\Delta H^{\dagger}$ and $\Delta S^{\dagger}$ are the enthalpy and entropy of activation. This equation strictly applies to non-electrolytes in dilute solution and must be modified for ionic reactions in electrolyte solutions.

Equation 4.26 can be rewritten in the exponential form as:

$$\ln(k/T) = -\Delta H^{\dagger}/RT + (\ln k_B/h + \Delta S^{\dagger}/R) \qquad (4.27)$$

A plot of ln(k/T) against 1/T is linear with a slope, $-\Delta H^{\dagger}/R$ and an intercept $(\ln k_B/h + \Delta S^{\dagger}/R) = (23.8 + \Delta S^{\dagger}/R)$. This is often referred to as the Eyring relationship.[9] Non-linear Arrhenius or Eyring plots are unusual and indicate reactions involving equilibria, parallel or consecutive processes.[10]

Once an Eyring plot has been established, it can be used to calculate the rate constant at varying temperatures.

[9] C.H. McAteer, P. Moore, *J. Chem. Soc., Dalton Trans.*, 1983, 353
[10] R.G. Wilkins, 'Kinetics and Mechanism of Reaction of Transition Metal Complexes', Wiley, New York, 2002

4.2 KINETIC INVESTIGATION FOR THE REACTION OF 2,4-TBPP WITH *trans*-[Rh(Cl)(CO)($SbPh_3$)$_2$] (1)

4.2.1 Introduction

The aim of the investigation was to determine the kinetic data for the stibine substitution reaction described in Section 3.3.3.3, and to obtain the reaction mechanism. For the purpose of the investigation, *trans*-[Rh(Cl)(CO)($SbPh_3$)$_2$] (**1**) was reacted with tris(2,4-di-^{t}butylphenyl)phosphite in order to follow the step-wise substitution of stibine to form *trans*-[Rh(Cl)(CO)($SbPh_3$){P(O-2,4-^{t}Bu$_2$C$_6$H$_3$)$_3$}] followed by *trans*-[Rh(Cl)(CO){P(O-2,4-^{t}Bu$_2$C$_6$H$_3$)$_3$}$_2$]. From here forward tris(2,4-di-^{t}butylphenyl)phosphite shall be referred to as 2,4-TBPP.

4.2.2 Experimental

trans-[Rh(Cl)(CO)($SbPh_3$)$_2$] was prepared as per Section 3.3.2.2; the remaining chemicals were commercially available. The solvents used for the kinetic study were all pre-dried over alumina.

Stopped-flow kinetic measurements were performed on an Applied Photophysics Bio Sequential SX-17 MX stopped-flow spectrophotometer in CH_2Cl_2. The reactions were observed as a decrease in absorbance with time at 310 nm. Equal volumes of the Rh(I) complex and ligand solution were mixed directly in the stopped-flow instrument. The reactions were carried out under pseudo first-order conditions with phosphite concentrations exceeding rhodium complex concentrations in excess of at least ten fold. The variable temperature experiments were conducted between 268 and 313 K. The kinetic traces were plotted as single exponentials using the software supplied by Applied Photophysics.[11] The rate constants were calculated from an average of at

[11] Bio Sequential SX-17MV Stopped Flow ASVD Spectrophotometer, software manual, Applied Photophysics, Leatherhead, 1994

least five kinetic runs. The software calculates the kinetic values using the first order absorbance changes as follows:

$$A_{obs} = A_1 - (A_1 - A_0)\exp(-k_{obs}T) \quad (4.28)$$

A_1 and A_0 are the final and initial absorbances, respectively. This equation was used throughout for the determination of the observed rate constants.

4.2.3 Mechanistic Investigation

In order to construct a complete reaction mechanism, the following arguments were utilized as obtained from preliminary measurements, characterisation studies and literature:

- The starting material, *trans*-[Rh(Cl)(CO)($SbPh_3$)$_2$] (**1**), has been characterised by IR and UV-Vis. The data is the same as that quoted in the original synthesis paper,[12] where the complex has been characterised crystallographically.

- The final *bis*-phosphite product, *trans*-[Rh(Cl)(CO)(2,4-TBPP)$_2$] (**5**), has been characterised by IR and ^{31}P NMR. The data obtained is the same as that for the same complex synthesised directly from the rhodium dimer.[13]

- The reaction of (**1**) with tris(2,4-di-^{t}butylphenyl)phosphite was monitored by IR and ^{31}P NMR. The IR spectrum can be found in Section 3.3.3.3 (A) as Figure 3.3. The spectrum shows three carbonyl absorption peaks, two of which correspond to the known peaks, attributed to the frequencies for complexes (**1**) and (**5**). The reaction proceeds through the intermediate species as identified by the peak at 1994 cm^{-1}, from (**1**) to form (**5**). The ^{31}P NMR spectra, Sec. 3.3.3.3 (B), Figure 3.5, shows the formation of an NMR active species at similar phosphite concentrations to conditions where this third IR carbonyl

[12] S. Otto, A. Roodt, *Inorg. Chim. Acta*, **331**, 2002, 199
[13] L. Kirsten, M.Sc. Thesis, University of Johannesburg, 2005

absorption peak was observed. The NMR integrals show the complex is a single phosphite containing species.

- Although five-coordinate stibine complexes readily form, it seems highly unlikely that [Rh(Cl)(CO)($SbPh_3$)$_2$(2,4-TBPP)] is the reaction intermediate as this would be very sterically hindered. The kinetic results show a slow second reaction step (order of a minute) to form the *bis*-phosphite complex. If a sterically unstable intermediate species formed one would expect a faster reaction to form the stable *bis*-phosphite.

As a result of the above, a general reaction mechanism was postulated as follows:

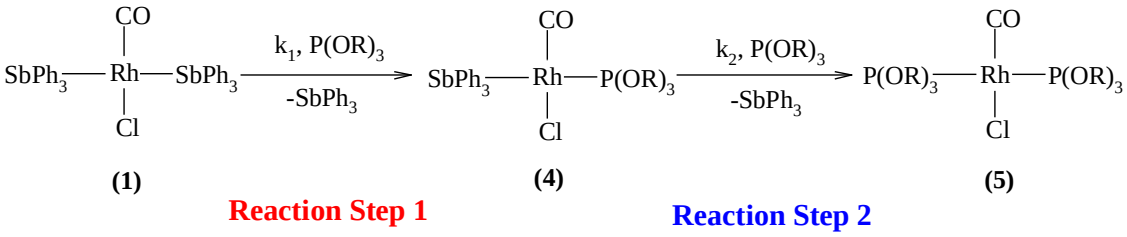

$P(OR)_3$ = 2,4-TBPP

Scheme 4.1: General mechanism for the reaction of *trans*-[Rh(Cl)(CO)($SbPh_3$)$_2$] (1) with 2,4-TBPP. Reaction steps 1 and 2 indicate the substitution of the two $SbPh_3$ ligands respectively.

The ^{31}P NMR and IR studies revealed irreversible reaction steps forming (**4**) and (**5**). Addition of stibine to the system did not affect the NMR doublets or IR carbonyl peaks for either (**4**) or (**5**).

4.2.4 Results

4.2.4.1 General

The reaction of *trans*-[Rh(Cl)(CO)($SbPh_3$)$_2$] with tris(2,4-di-^{t}butylphenyl)phosphite was studied in two solvents having significantly different polarity and donicities, i.e. CH_2Cl_2 and ethyl acetate, to evaluate the solvent influence, if any.

A variable temperature study was also conducted to determine the activation parameters. The first reaction was investigated at 298 K in CH_2Cl_2 and at 268 K in ethyl acetate, while the second reaction was followed in each solvent over a temperature range of 35 K; i.e., at 278, 293 and 313 K.

Preliminary kinetic results confirmed the mechanism proposed in Scheme 4.1, and it was possible to observe two reactions at 310 nm: a first, very fast reaction ($t_{1/2}$ < *ca*. 2 ms) followed by a slower second reaction ($t_{1/2}$ < *ca*. 17 s). These reactions were observed at rhodium and phosphite concentrations of 0.25 and 2.5 mM respectively. Figure 4.3 and 4.4 give representative plots showing the change in absorbance over time for each reaction step.

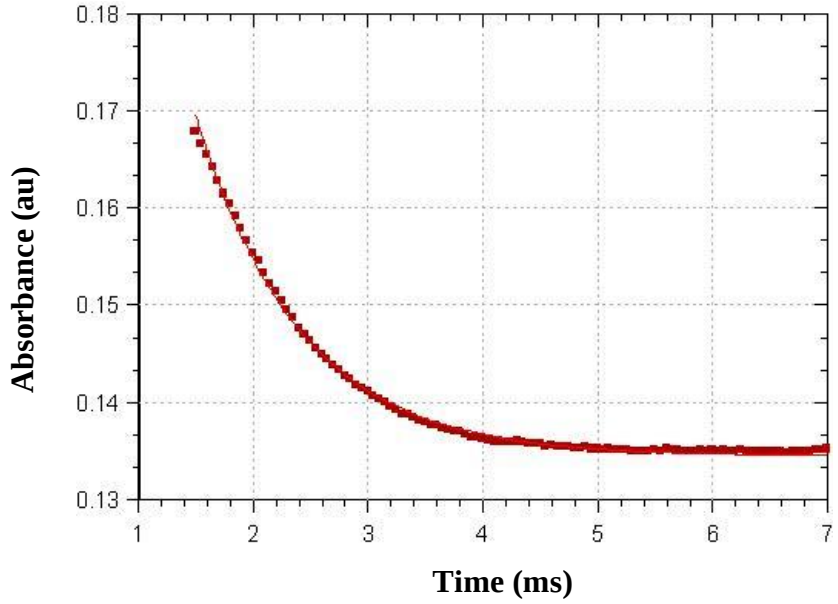

Figure 4.3: **UV-Vis absorbance change for the first reaction at 310 nm for the addition of 2,4-TBPP to *trans*-[Rh(Cl)(CO)($SbPh_3$)$_2$] to form *trans*-[Rh(Cl)(CO)($SbPh_3$)(2,4-TBPP)] in CH_2Cl_2 at T = 25 ˚C. [Rh] = 0.25 mM, [2,4-TBPP] = 2.5 mM**

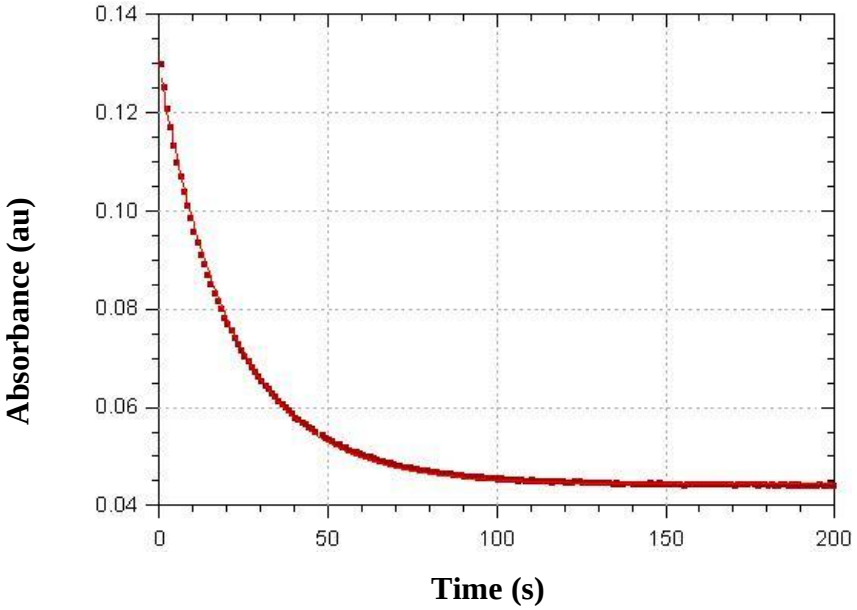

Figure 4.4: UV-Vis absorbance change for the second reaction at 310 nm for the addition of 2,4-TBPP to *trans*-[Rh(Cl)(CO)(SbPh$_3$)(2,4-TBPP)] to form *trans*-[Rh(Cl)(CO)(2,4-TBPP)$_2$] in CH_2Cl_2 at T = 25 ˚C. [Rh] = 0.25 mM, [2,4-TBPP] = 2.5 mM

4.2.4.2 Formation kinetics of *trans*-[Rh(Cl)(CO)(SbPh$_3$)(2,4-TBPP)] (4)

It soon became evident that the first reaction step is too fast to follow under standard pseudo-first order conditions and the observed rate constants that were calculated for higher phosphite concentrations were beyond the limits of the stopped flow instrument. Room temperature observed rate constants for the addition of a ten fold excess of phosphite (2.5×10^{-3} M) to (**1**) were in the range of 508(11) s^{-1}. A low temperature (278 K) investigation gave a more accurate observed rate constant of 500(5) s^{-1}, not a significant decrease, but more reliably determined. In order to complete a full kinetic investigation of the first reaction step, the reaction conditions in both solvents were modified and the reaction in ethyl acetate was studied at low temperatures.

It is known from literature that the addition of excess stibine to a solution of (**1**) would introduce the *tris*-stibine complex, *trans*-[Rh(Cl)(CO)($SbPh_3$)$_3$], in equilibrium with with the *bis*-stibine *trans*-[Rh(Cl)(CO)($SbPh_3$)$_2$].[12] It was postulated that this new five coordinate stibine species has the ability to slow the reaction by acting as a sink for the *bis*-stibine complex, as well as introducing a substantially more crowded Rh(I) center for reacting with the phosphite.

The addition of excess stibine did, in fact, slow down the first reaction step. Figures 4.5 and 4.6 show the plots of k_{obs} versus stibine concentration for the reaction in CH_2Cl_2 and ethyl acetate respectively. Data points for these plots are tabulated in Appendix C.1 and C.2, respectively. In the discussion below, k^1_{obs} indicates the observed rate constant (defined in eqn. 4.35) for the first step in Scheme 4.1.

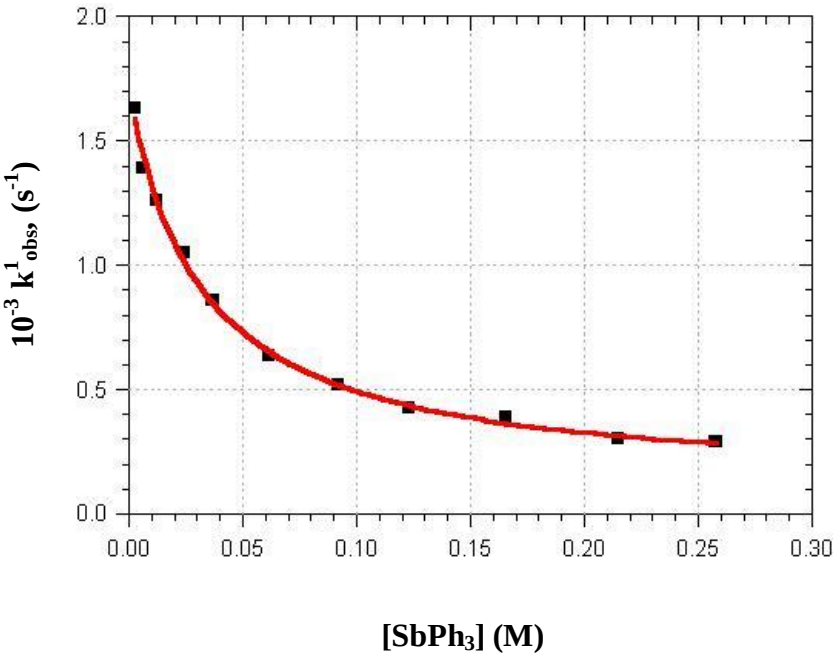

Figure 4.5: k^1_{obs} versus [$SbPh_3$] for the reaction of *trans*-[Rh(Cl)(CO)($SbPh_3$)$_2$] with 2,4-TBPP to form *trans*-[Rh(Cl)(CO)($SbPh_3$)(2,4-TBPP)] in CH_2Cl_2 at 25 ˚C. [Rh] = 0.25 mM, [2,4-TBPP] = 6.5 mM

The data points on the plot at the lower triphenylstibine concentrations correspond to observed rate constants that are so high they are barely within the limits of the stopped flow. Even though the reactions have been slowed down by the addition of triphenylstibine, they are still extremely fast and only just detectable on the stopped flow instrument.

As a result of the increased reactivity of the system in ethyl acetate, the reaction was too fast to follow at room temperature and was studied at –5 ˚C.

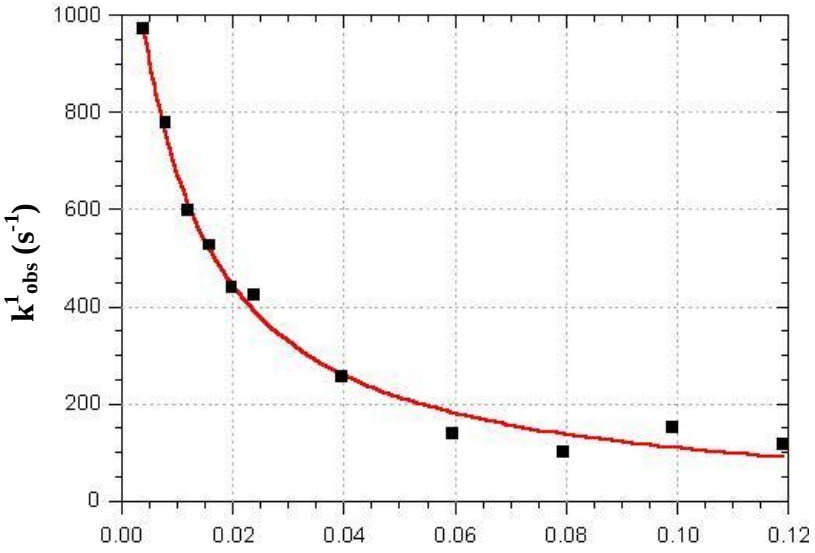

Figure 4.6: k^1_{obs} versus [$SbPh_3$] for the reaction of [Rh(Cl)(CO)($SbPh_3$)$_2$] with 2,4-TBPP to form [Rh(Cl)(CO)($SbPh_3$)(2,4-TBPP)] in ethyl acetate at -5˚ C. [Rh] = 0.25 mM, [2,4-TBPP] = 6.5 mM

It is evident from Figure 4.6 that there is significant data point scattering at the higher triphenylstibine concentrations. This is a result of the limited solubility of triphenylstibine in ethyl acetate at these high concentrations and low temperatures. Triphenylstibine is far more soluble in DCM so the plot of Figure 4.5 could be extended to higher concentrations without any significant scattering occurring. Unfortunately, this data scatter introduced significant errors to the rate constant

calculated for the contribution from the *tris*-stibine complex, k_{13}, in ethyl acetate, as described below. However the basic curve confirms the results observed for DCM as presented in Figure 4.5.

It is also important to note at this point, that the addition of excess stibine did not affect the k_{obs} values calculated for the second step. This confirms a second reaction step that is independent of stibine concentration.

As a result of the above factors, a modified reaction mechanism to that given in Scheme 4.1 was postulated to incorporate the *tris*-stibine complex:

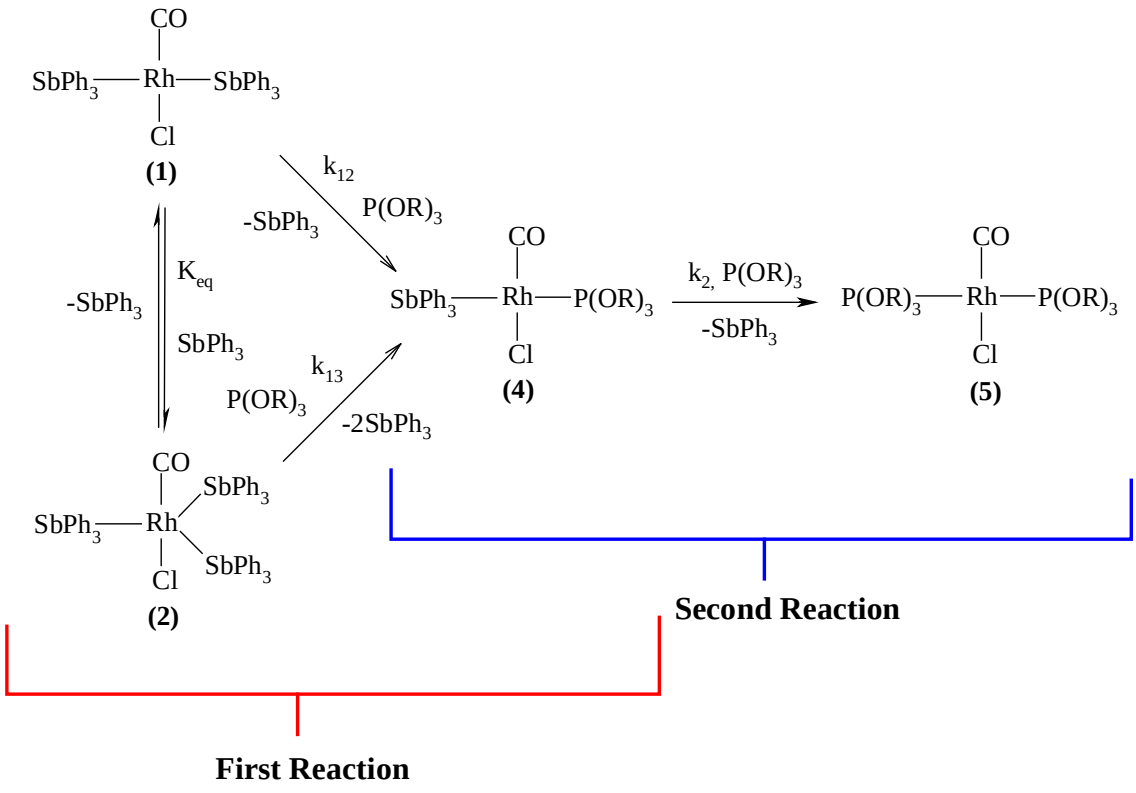

$P(OR)_3$ = 2,4-TBPP

Scheme 4.2: Modified mechanism for the reaction of *trans*-$[Rh(Cl)(CO)(SbPh_3)_2]$ (1) with 2,4-TBPP. k_{12} and k_{13} correspond to the rate constants for the formation of (4) from (1) and (2) respectively, while k_2 is the rate constant for the formation of (5) from (4).

A rate law for this mechanism was derived as follows:

For the formation of *trans*-[Rh(Cl)(CO)($SbPh_3$)(2,4-TBPP)] (**4**), the rate is given by eq. 4.29, with the equilibrium and total rhodium concentration given by eq. 4.30 and 4.31 respectively:

$$\text{Rate} = k_{12}[\mathbf{1}][L] + k_{13}[\mathbf{2}][L] \quad (4.29)$$

$$K_{eq} = [\mathbf{2}]/[\mathbf{1}][SbPh_3] \quad (4.30)$$

$$Rh_{tot} = [\mathbf{1}] + [\mathbf{2}] \quad (4.31)$$

[L] = Tris(2,4-di-^{t}butylphenyl)phosphite, [**1**] = *trans*-[Rh(Cl)(CO)($SbPh_3$)$_2$] and [**2**] = [Rh(Cl)(CO)($SbPh_3$)$_3$]. Combining reactions 4.30 and 4.31 gives:

$$[\mathbf{1}] = Rh_{tot}/\{1 + K_{eq}[SbPh_3]\} \quad (4.32)$$

$$[\mathbf{2}] = Rh_{tot}K_{eq}[SbPh_3]/\{1 + K_{eq}[SbPh_3]\} \quad (4.33)$$

Substituting these equations for [**1**] and [**2**] in equation 4.29 gives:

$$\text{Rate} = ((k_{12} + k_{13}\, K_{eq}[SbPh_3])/(1 + K_{eq}[SbPh_3]))[L]Rh_{tot} \quad (4.34)$$

If $[Rh_{tot}] << [SbPh_3]$ and [L], rearrangement following integration gives:

$$k^1_{obs} = (k_{12} + k_{13}K_{eq}[SbPh_3])/(1 + K_{eq}[SbPh_3])[L] \quad (4.35)$$

Here, k^1_{obs} denotes the observed rate constant for step 1.

This rate law was applied to the plots of Figures 4.5 and 4.6, in order to calculate k_{12}, k_{13} and K_{eq} for the reactions in the two solvents used. The results are reported in Table 4.1.

Table 4.1: Summary of kinetic results for for the formation of *trans*-[Rh(Cl)(CO)($SbPh_3$)(2,4-TBPP)]. [Rh] = 0.25 mM

Constant	CH_2Cl_2, 25° C	EtOAc, -5° C
K_{eq} (M^{-1})	62(6)	200(40)
10^{-5} k_{12} ($M^{-1}.s^{-1}$)	5.01(5)	4.2(2)
10^{-4} k_{13} ($M^{-1}.s^{-1}$)	2.4(7)	5(8)

Next, the second reaction (Scheme 4.2) was studied.

4.2.4.3 Formation kinetics of *trans*- [Rh(Cl)(CO)(2,4-TBPP)$_2$] (5)

In the discussion below, k^2_{obs} indicates the observed rate constant for the second reaction in Scheme 4.2. For the reaction to form *trans*-[Rh(Cl)(CO)(2,4-TBPP)$_2$] (**5**) from *trans*-[Rh(Cl)(CO)($SbPh_3$)(2,4-TBPP)] (**4**), the rate equation is given by eqn. 4.36.

$$\text{Rate} = k_2[\mathbf{4}][L] + k_{-2}[\mathbf{5}][SbPh_3] \qquad (4.36)$$

Here L = Tris(2,4-di-^{t}butylphenyl)phosphite. The reverse reaction path can be omitted from the rate equation as IR and ^{31}P NMR experimental results indicate there is no reverse reaction (Sec. 3.3.3.3 (B)) and this reaction step is independent of added stibine concentration. The rate equation can therefore be simplified to:

$$\text{Rate} = k_2[\mathbf{4}][L] \qquad (4.37)$$

If [Rh] << [L], integration gives:

$$k^2_{obs} = k_2[L] \qquad (4.38)$$

In order to calculate k_2 for each solvent, the second reaction was followed at 310 nm and the corresponding k^2_{obs} values obtained were plotted against the various phosphite concentrations used. The reaction was followed at three temperatures over a 35 ˚C range. The resulting plots for CH_2Cl_2 and ethyl acetate are represented in Figures 4.7 and 4.8 respectively. The phosphite concentrations and calculated k^2_{obs} values for each reaction can be found in Tables 4.2 and 4.3 for CH_2Cl_2 and ethyl acetate respectively.

Table 4.2: Tabulated k^2_{obs} values and corresponding phosphite concentrations for reaction of [Rh(Cl)(CO)($SbPh_3$)(2,4-TBPP)] (4) with 2,4-TBPP to form *trans*-[Rh(Cl)(CO)(2,4-TBPP)$_2$] (5) in CH_2Cl_2. [Rh] = 0.25 mM, no $SbPh_3$ added.

10^3 [2,4-TBPP], (M)	$10^2 k^2_{obs}$, (s^{-1})		
	5˚ C	25˚ C	40˚ C
2.5	2.554(3)	4.581(1)	7.164(2)
6.3	4.717(4)	7.704(1)	16.65(3)
12.5	8.377(4)	19.14(3)	32.93(8)
18.8	14.07(1)	28.80(5)	51.53(10)
25.0	18.94(3)	38.48(7)	71.35(10)
37.5	29.55(7)	60.85(14)	101.8(2)
50.0	41.29(10)	84.46(20)	140.0(5)

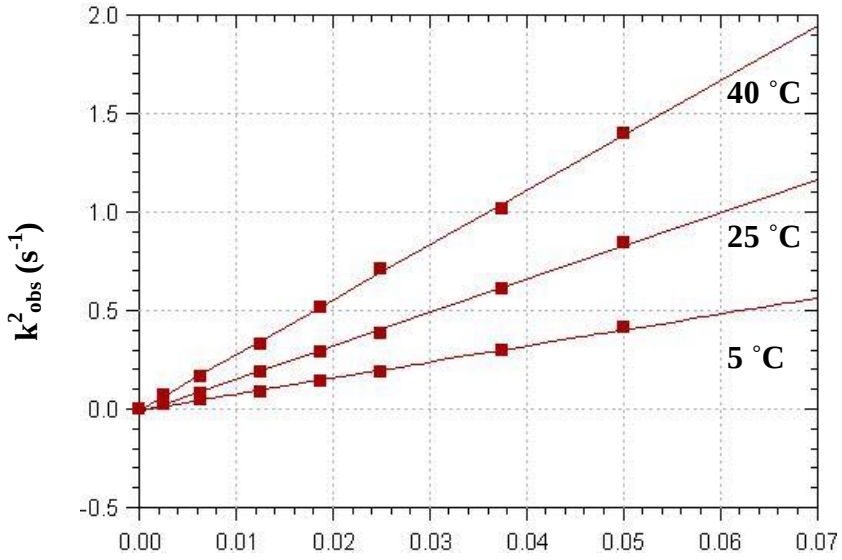

Figure 4.7: **Temperature variation for k^2_{obs} *vs* [2,4-TBPP] for the second reaction in CH_2Cl_2. [Rh] = 0.25 mM**

Table 4.3: **Tabulated k^2_{obs} values and corresponding phosphite concentrations for reaction of [Rh(Cl)(CO)($SbPh_3$)(2,4-TBPP)] (4) with 2,4-TBPP to form *trans*-[Rh(Cl)(CO)(2,4-TBPP)$_2$] (5) in ethyl acetate. [Rh] = 0.25 mM, no $SbPh_3$ added.**

10^3 [2,4-TBPP], (M)	$10^2 k^2_{obs}$, (s^{-1})		
	5˚ C	25˚ C	40˚ C
2.5	30.64(4)	72.82(14)	114.4(4)
6.3	81.50(10)	183.2(4)	315.0(12)
12.5	170.1(2)	377.1(15)	687.3(25)
18.8	263.6(4)	586.0(31)	1103(35)
25.0	354.7(7)	853.3(33)	1519(4)
37.5	535.5(15)	1304(4)	2346(6)

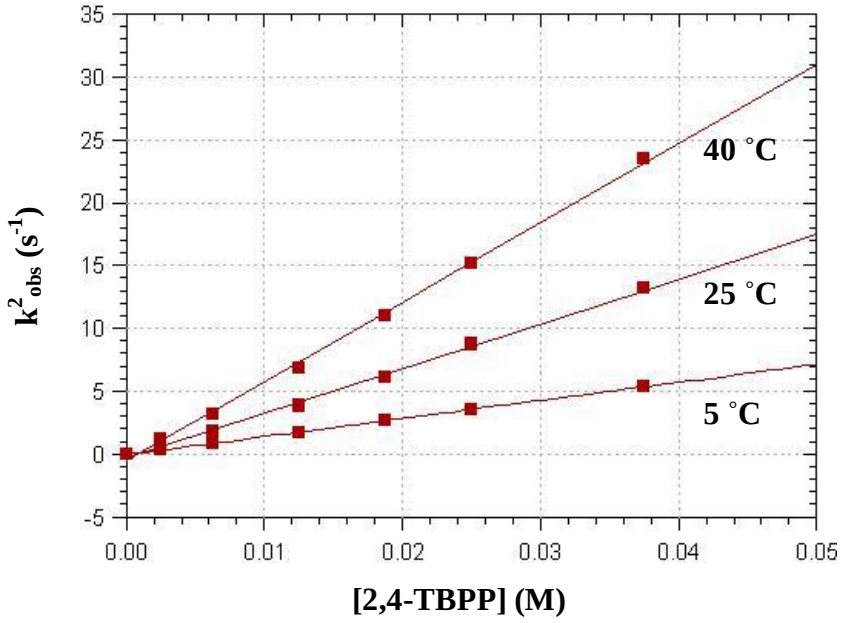

Figure 4.8: Temperature variation for k^2_{obs} *vs* [2,4-TBPP] for the second reaction in ethyl acetate. [Rh] = 0.25 mM

Figures 4.7 and 4.8 confirm there is no intercept and thus no detectable reverse reaction, in either solvent. This is to be expected if one considers the steric bulk surrounding the Rh(I) center when two bulky phosphites are bonded to the metal. Thus, there is little space for an incoming stibine ligand to attack the metal center. Furthermore, the $SbPh_3$ ligand is a weaker entering moiety than the phosphite.

The rate constant, k_2, as well as the thermodynamic data calculated for the second reaction in both solvents can be found in Table 4.4. The activation entropy, ($\Delta S^{\dagger}$) and activation enthalpy, ($\Delta H^{\dagger}$) can be determined from an Eyring plot containing $\ln(k_2/T)$ versus 1/T (eqn. 4.27, esd's determined using 4.26). These plots are presented in Figures 4.9 and 4.10 for CH_2Cl_2 and ethyl acetate respectively.

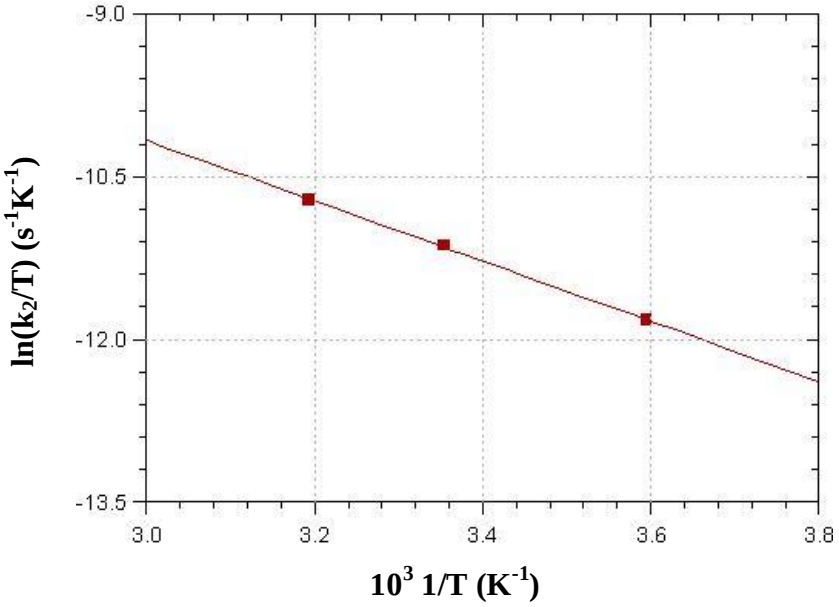

Figure 4.9: **Eyring plot for the reaction of *trans*-[Rh(Cl)(CO)($SbPh_3$)(2,4-TBPP)] (4) with 2,4-TBPP to form *trans*-[Rh(Cl)(CO)(2,4-TBPP)$_2$] (5) in CH_2Cl_2. [Rh] = 0.25 mM**

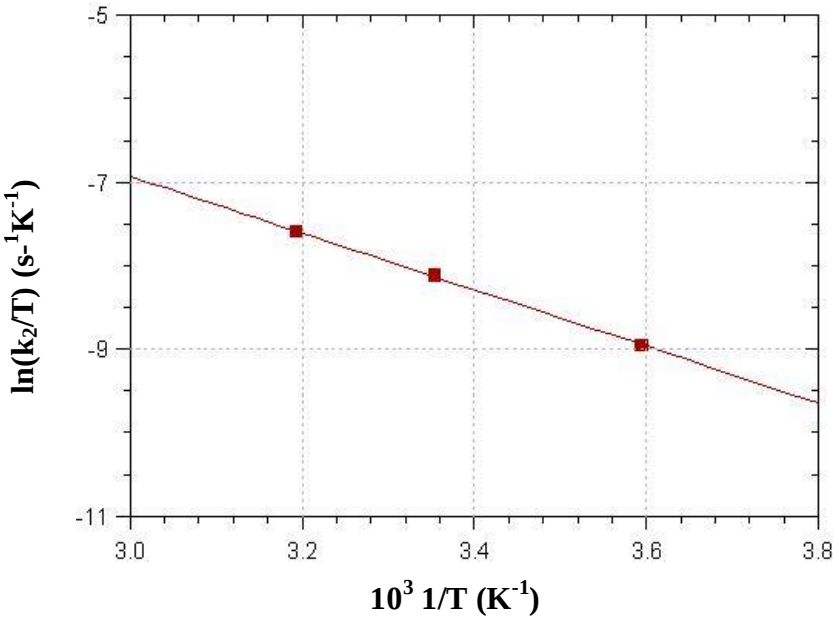

Figure 4.10: **Eyring plot for the reaction of *trans*-[Rh(Cl)(CO)($SbPh_3$)$_2$(2,4-TBPP)] (4) with 2,4-TBPP to form *trans*-[Rh(Cl)(CO)(2,4-TBPP)$_2$] (5) in ethyl acetate. [Rh] = 0.25 mM**

The Gibbs free energy for the second reaction in each solvent can be calculated as follows:

$$\Delta G^{\dagger} = \Delta H^{\dagger} - T\Delta S^{\dagger} \quad (4.39)$$

From the $\Delta G^{\dagger}$ calculated, the relative percentage contribution from $\Delta H^{\dagger}$ and $\Delta S^{\dagger}$ can therefore be obtained. These values are presented in Table 4.4.

Table 4.4: Summary of kinetic and thermodynamic data for the reaction of *trans*-[Rh(Cl)(CO)(SbPh$_3$)$_2$] (1) with 2,4-TBPP to form *trans*-[Rh(Cl)(CO)(SbPh$_3$)(2,4-TBPP)] (4) followed by *trans*-[Rh(Cl)(CO)(2,4-TBPP)$_2$] (5). [Rh] = 0.25 mM

Kinetic and Thermodynamic Data		CH_2Cl_2	EtOAc
K_{eq} (M^{-1})		62(6)	200(40)
10^{-5}, k_{12} ($M^{-1}.s^{-1}$) *		5.01(5)	4.2(2)
10^{-4}, k_{13} ($M^{-1}.s^{-1}$) *		2.4(7)	5(8)
k_2 ($M^{-1}.s^{-1}$)	5° C	20.4(5)	359(2)
	25° C	43.4(8)	885(19)
	40° C	69.6(8)	1577(29)
$\Delta H^{\dagger}$ (kJ.mol^{-1})		22.6(6)	27.8(5)
$\Delta S^{\dagger}$ (J.mol^{-1}.K^{-1})		-214(2)	-171(2)
$\Delta G^{\dagger}$ (kJ.mol^{-1})		86.3(3)	78.8(3)
% Contribution of $\Delta H^{\dagger}$ term to $\Delta G^{\dagger}$		26%	35%
% Contribution of $\Delta S^{\dagger}$ term to $\Delta G^{\dagger}$		74%	65%

*: Rate constant in DCM calculated at 25 °C

Rate constant in ethyl acetate calculated at -5 °C

4.2.5 Discussion

The results presented in Table 4.4 reveal additional information regarding the mechanism proposed in Scheme 4.2. Reaction paths k_{12} and k_{13} forming *trans*-[Rh(Cl)(CO)($SbPh_3$)(2,4-TBPP)] (**4**) are significantly faster than the following reaction path, k_2, to form *trans*-[Rh(Cl)(CO)(2,4-TBPP)$_2$] (**5**); between four and five orders of magnitude difference. This is assumed to be in part due to the large *trans* effect of stibine compared to that exhibited by phosphorus ligands.[14] Strong σ-donation from the stibine atom weakens the *trans* Rh-P bond and activates the complex for substitution reactions. However, the strong π-accepting ability of stibine acts to stabilise the electron rich transition state that forms, to be discussed further below. Tertiary stibines are known to have inferior coordinating abilities when compared to phosphines,[15] and thus increased reaction rates.

Another contributing factor is the significantly different steric environments of *trans*-[Rh(Cl)(CO)($SbPh_3$)$_2$] (**1**) and *trans*-[Rh(Cl)(CO)($SbPh_3$)$_3$] (**2**) versus *trans*-[Rh(Cl)(CO)($SbPh_3$)(2,4-TBPP)] (**4**). The phosphite ligand in the latter complex introduces significant steric bulk to the system. This, combined with the large steric contribution of the second incoming phosphite group results in a significant decrease of the reaction rate for the second step.

Rh – Sb bonds in these Vaska-type complexes[16] are known to be longer than the corresponding Rh – P bonds.[17] This introduces larger cavities in the *trans*-stibine complexes for the attack of incoming ligands. However this also inhibits nucleophilic attack at the Rh-center in (**2**). This reasoning can also be applied to the irreversibility of the second step, where the two bulky phosphite groups inhibit the attack of stibine on the metal center.

The first reaction step (Scheme 4.2) could unfortunately not be studied in detail due to the high reactivity of the stibine system (**1**). However, since the *bis*-stibine complex

[14] N. Kuznik, O.F. Wendt, *J. Chem. Soc., Dalton Trans*., 2002, 3074
[15] S.M. Godfrey, C.A. McAuliffe, R.G. Pritchard, *J. Chem. Soc., Chem. Commun*., 1994, 45
[16] L. Vaska, J.W. DiLuzio, *J. Am. Chem. Soc*., **83**, 1961, 2784
[17] 'Modern Coordination Chemistry: The Legacy of Joseph Chatt', Ed G.J. Leigh, N. Winterton, Royal Society of Chemistry, 2002. Paper submitted by S. Otto, S.N. Mzamane, A. Roodt, page 328

(**1**) is clearly more reactive than the *tris*-stibine complex (**2**), increased nucleophilic attack by an entering phosphite ligand is expected in an associative process, typical of the current system studied. Similarly, the second reaction step is expected to exhibit classic square-planar substitution behaviour, i.e., associative activation. This is clearly observed by the large negative values for the entropy of activation, see Table 4.4. Pure associative intimate mechanisms are therefore concluded for both the reaction steps.

There is an order of magnitude difference between the calculated k_{12} and k_{13} values given in Table 4.4. These rate constants correspond to the reactions forming (**4**) from (**1**) and (**2**) respectively. This difference in magnitude is to be expected as a result of steric influences in the pure associative intimate mechanism for the two reaction steps. The *tris*-stibine system presents a more crowded metal coordination sphere and thus inhibited attack of the incoming ligand and correspondingly slower substitution rates.

The error on the value of k_{13} for the reaction in ethyl acetate introduces significant doubt as to the accuracy of the value, and it was decided that this rate constant would be considered as zero. This shows the reaction path forming (**4**) from (**2**) in ethyl acetate is insignificant and the formation of (**4**) can be attributed solely to the pathway from (**1**). However, it can be clearly seen from Figure 4.6 (the plot of k_{obs} versus stibine concentration in ethyl acetate), that the data points deviate from the plotted trend at higher stibine concentrations. Thus significant error is introduced at these temperatures and concentrations where the stibine solubility becomes limited. It is at these concentrations that the k_{13} reaction pathway from (**2**) becomes significant. As a result, further investigation is needed in order to confirm the contribution of the k_{13} path to the formation of (**4**).

Tables 4.1 and 4.4 also show significant differences in the rate constants calculated in the two solvents. The rate constants k_{12} and k_{13} in each solvent cannot be directly compared as they were calculated at different temperatures, but we can assume at least an order of magnitude difference in the values. The ethyl acetate reaction rates were too rapid to follow at 25 ˚C, where the CH_2Cl_2 reactions gave observable rates. Unfortunately, due to time constraints it was not possible to obtain k_{12} and k_{13} values

for the reaction in CH_2Cl_2 at –5˚ C, for direct comparison with those of ethyl acetate and thus a more detailed study of the first step. This was however considered beyond the scope of this M.Sc. project and is to be pursued in future. Fortunately, the reaction rates for the k_2 pathway sufficiently demonstrate the solvent trend. Here the rate constants calculated for ethyl acetate exceed those for CH_2Cl_2 by between one and two orders of magnitude.

The equilibrium between (**1**) and (**2**) has been previously investigated by Otto and Roodt.[12] They described the stability of the two complexes in a number of solvents and found the formation of (**2**) was favored in ethyl acetate over CH_2Cl_2. The results obtained here show similar trends with calculated K_{eq} values of 62(6) M^{-1} and 200(40) M^{-1} for CH_2Cl_2 and ethyl acetate respectively. The equilibrium constants obtained in this study are in reasonable agreement with those from Otto and Roodt,[12] further supporting the proposed mechanism and reaction scheme.

The two solvents have similar polarities, with dielectric constants of 6.0 and 8.9 for ethyl acetate and CH_2Cl_2 respectively.[17] However, ethyl acetate has a significantly larger coordinating ability, 17.1 as opposed to 4.0 for CH_2Cl_2.[18] As a result, it seems the enhanced reaction rates in ethyl acetate may be attributed to the coordinating ability of the solvent.

This phenomenon has been observed in similar systems studied by Otto *et al.*[17] Here they investigated the oxidative addition of CH_3I to similar systems, such as $[Rh(Cl)(CO)(YPh_3)_2]$ (Y = P, As). They found that in the instance of the As complex, there was a 4 fold increase in the oxidative addition rate constant (k_{oa}) compared to that for the P complex when the reaction was followed in ethyl acetate. The same reactions studied in CH_2Cl_2 showed the opposite trend. Here the k_{oa} for the oxidative addition on the P complex is larger than that for the As complex. It seems there is an increase in the rate of reactions which form sterically bulky metal environments (4-coordinate Rh(I) to 6-coordinate Rh(III), or introduction of bulky phosphite for our systems), when the metal substrate contains ligand systems which introduce larger cavities around the metal center.

[18] A. Roodt, S. Otto, G. Steyl, *Coord. Chem. Rev.*, **245**, 2003, 121

A possible explanation for this is that the coordination of solvents to the complex results in the Rh – Sb (As) bonds lengthening (ligand being pushed away from the metal center) which weakens the bonds and opens up larger cavities around the metal for the entering phosphite/CH_3I ligand. This concept would also apply to the equilibrium reaction between (**1**) and (**2**), where the coordinating ethyl acetate solvent enhances the reaction to form predominantly the *tris*-stibine species. This effect would not be as extensive with CH_2Cl_2 as a result of the solvents lower donicity, thus the large difference in rate constants for the reactions in the two solvents. However, this definitely needs to be investigated further in future in a more detailed and extensive study.

As mentioned above, activation parameters for the second reaction (Table 4.4) are typical of an associatively activated process. They are characterised by low, positive enthalpies and largely negative entropies. The Gibbs free energy, $\Delta G^{\dagger}$, for the reaction in each solvent has been calculated in order to determine the percentage contribution of $\Delta H^{\dagger}$ and $\Delta S^{\dagger}$ to $\Delta G^{\dagger}$. For both solvents there is a large contribution from the enthalpy relative to the entropy change. For general substitution reactions this enthalpy component is often significantly higher. However for systems where there is substantial π-acceptor interaction, such as with stibine ligands, this acts to lower the enthalpy change for the reaction.

The activation parameters indicate very little bond breaking has occurred in the transition state. The large *trans*-effect exhibited by stibine aids in π-stabilisation of the transition state.[19] This stabilistaion is also responsible for the ability of stibine systems to form five coordinate ground state complexes, and thus to readily stabilize five coordinate transition states and react via associative pathways. The smaller contribution of the enthalpy term to the $\Delta G^{\dagger}$ has also been observed in Pt(II) systems.[20,21] This also explains the relatively small effect of temperature on the observed rate constants since the dominating term to $\Delta G^{\dagger}$ is the activation entropy.

[19] M.R. Plutino, S. Otto, A. Roodt, L.I. Elding, *Inorg. Chem.*, **38**, 1999,1233
[20] S. Otto, L.I. Elding, *J. Chem. Soc., Dalton Trans.*, 2002, 2354
[21] S. Otto, A. Roodt, L.I. Elding, *J. Chem. Soc., Dalton Trans.*, 2003, 2519

The calculated enthalpy is slightly lower for the reaction in CH_2Cl_2. While the corresponding entropies show the reaction is less associatively activated in ethyl acetate. The same drop in entropy was found by Otto *et al.*[17] for the oxidative addition reaction in ethyl acetate for $[(Rh(Cl)(CO)(AsPh_3)_2]$. It seems possible solvent coordination results in weaker metal - ligand bonds in the transition state in ethyl acetate, relative to that in CH_2Cl_2.

The kinetic investigation and mechanism elucidation provided valuable insight into the reaction of stibine complexes. It effectively showed the tendency to form five coordinate complexes particularly in strong coordinating solvents as well as their extreme lability and significant *trans* effect.

5. STUDY EVALUATION

5.1 INTRODUCTION

This chapter includes a summary of the results obtained in the M.Sc. study, as well as a discussion of future projects related to this work.

5.2 SCIENTIFIC RELEVANCE OF THE STUDY

One of the original motivations of the M.Sc study was to gain further insight into the chemistry and reactivity of stibine ligand systems and to investigate their reactivity relative to phosphite ligands. Both stibine and phosphite ligand complexes have recently received attention for their potential role in catalyst complexes. Phosphite ligand systems have received particular interest for their application in hydroformylation catalyst ligand systems.

It was possible to react the *bis*-stibine complex, *trans*-[Rh(Cl)(CO)($SbPh_3$)$_2$] (**1**), with a range of phosphite ligands of varying steric bulk. Analysis of the results revealed the stibine complex reacted via two different mechanisms depending on the steric bulk of the incoming phosphite ligand. Mechanisms for the two modes of reaction were proposed according to results obtained from IR and ^{31}P NMR analysis.

Solution state IR and ^{31}P NMR characterisation was obtained for each of the species formed for the reaction of (**1**) with the various phosphites, as well as UV-Vis, ^{1}H and ^{13}C NMR, where possible. *trans*-[Rh(Cl)(CO)($SbPh_3$)$_2$] in DCM with various phosphites reacted to form *trans-mer*-[Rh(Cl)$_2$(Ph)($SbPh_3$)$_3$] (**3**) by triphenylstibine oxidative addition and phenyl migration. Single crystals of (**3**) were obtained and the crystal

structure was solved for this complex as a new polymorph co-crystalised with a DCM solvate molecule. This was subsequently reacted with triphenylphosphine and single crystals of the product were obtained and the crystal structure of the product, $[Rh(Cl)_2(Ph)(PPh_3)_2]$ (**8**), was solved.

Kinetic investigation confirmed the mechanism proposed for the reaction of *trans*-$[Rh(Cl)(CO)(SbPh_3)_2]$ with the bulky phosphite, tris(2,4-di-^{t}butylphenyl)phosphite (2,4-TBPP). The mechanism revealed two consecutive substitution reactions that involved the formation of *trans*-$[Rh(Cl)(CO)(SbPh_3)$(2,4-TBPP)] (**4**) as stable intermediate and *trans*-$[Rh(Cl)(CO)$(2,4-$TBPP)_2]$ (**5**) as final product, respectively. The reaction forming *trans*-$[Rh(Cl)(CO)(SbPh_3)$(2,4-TBPP)] was in fact too fast to be observed using the Stopped-Flow Spectrophotometer under standard first order conditions. As a result of this, excess stibine was added to the reaction medium to introduce the *tris*-stibine species, *trans*-$[Rh(Cl)(CO)(SbPh_3)_3]$ and thus slow the reaction down. Following this a new mechanism was proposed to include this species. The kinetic results indicated both (**4**) and (**5**) were formed via an associative reaction mechanism and a five-coordinate transition state.

The two consecutive reactions were investigated in two different solvents, namely DCM and ethyl acetate, with the latter giving significantly enhanced reaction rates compared to those obtained in DCM..

5.3 FUTURE RESEARCH

Following is a few step-wise aims for future research on these stibine and phosphite systems:

- Synthesis and isolation of the mixed stibine and phosphite Rh(I) complexes, *trans*-$[Rh(Cl)(CO)(SbPh_3)\{P(OR)_3\}]$, where $P(OR)_3$ = tris(2,4-di-^{t}butylphenyl)-phosphite and tris(2,6-dimethylphenyl)phosphite, with the purpose of obtaining single crystals.

CHAPTER 5 STUDY EVALUATION

- An investigation to determine the mechanism by which *trans*-[Rh(Cl)(CO)($SbPh_3$)$_2$] reacts in the presence of phosphites to form *trans-mer*-[Rh(Cl)$_2$(Ph)($SbPh_3$)$_3$].

- Synthesis of the five coordinate Rh(III) complex with various phosphines and isolation of single crystals thereof for further crystallographic investigation. An extended project would include reacting *trans-mer*-[Rh(Cl)$_2$(Ph)($SbPh_3$)$_3$] with various bases to selectively substitute the stibine ligand *trans* to the phenyl moiety, and to obtain single crystals of the products formed.

- To modify the reaction conditions and phosphites used for reaction with *trans-mer*-[Rh(Cl)$_2$(Ph)($SbPh_3$)$_3$] in order to isolate the reaction products formed.

- An extended kinetic investigation to study the first and second reaction steps for the reaction of (**1**) with 2,4-TBPP in different solvents to gain further insight into the solvent effect on these reaction steps.

- To repeat the reaction of *trans*-[Rh(Cl)(CO)($SbPh_3$)$_2$] and excess stibine with tris(2,4-di-^{t}butylphenyl)phosphite in DCM at low temperatures for a direct comparison of the rate constants calculated for the first step, with those determined for the same reaction in ethyl acetate.

- Determination of the kinetic data for the reaction of *trans*-[Rh(Cl)(CO)($SbPh_3$)$_2$] with tris(2,6-dimethylphenyl)phosphite to determine the effect of changing the steric bulk of the incoming phosphite ligand system on the substitution rates.

- Evaluate the catalytic activity of these systems in hydroformylation reactions.

APPENDIX

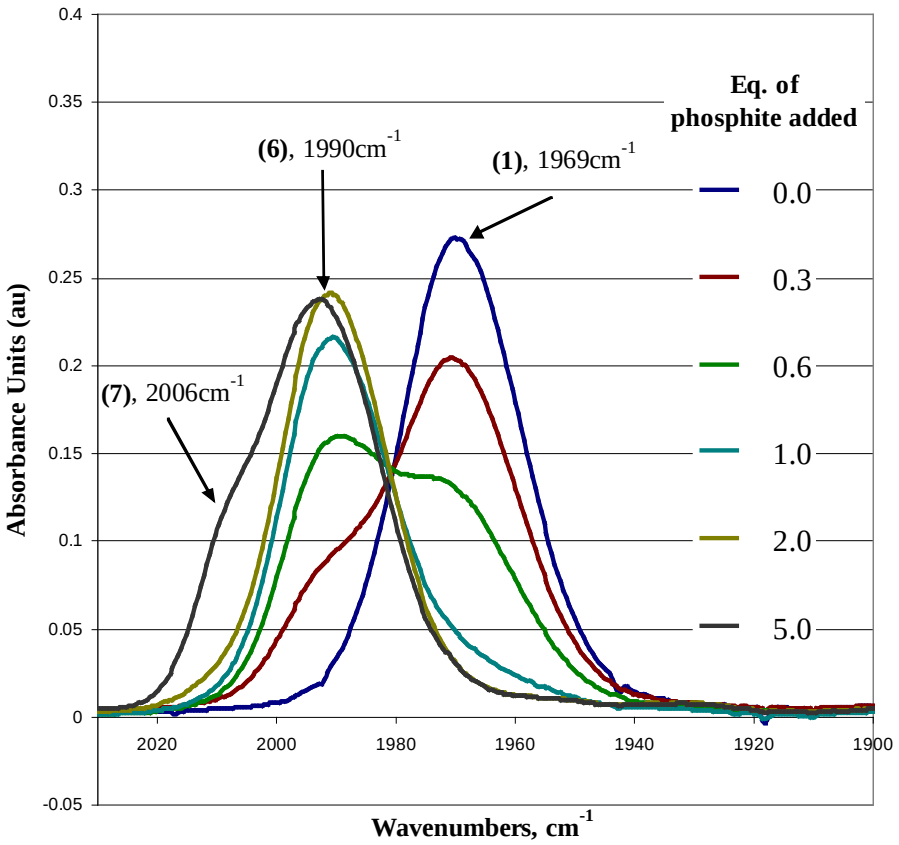

Figure A.1: Spectral change in the IR spectrum for the addition of 2,6-MPP to *trans*-[Rh(Cl)(CO)($SbPh_3$)$_2$] (1) in $CHCl_3$ at T = 25 ˚C. [Rh] = 5 mM, [2,6-MPP] correspond to = 0, 1.5, 3, 5, 10 and 25 mM for 0, 0.3, 0.6, 1.0, 2.0 and 5.0 equivalents respectively

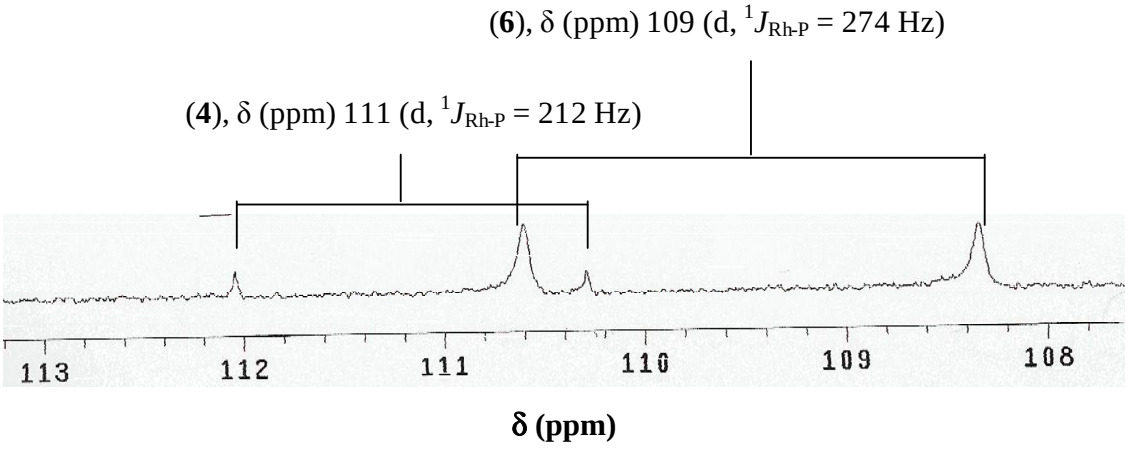

Figure A.2: **^{31}P NMR showing *trans*-[Rh(Cl)(CO)($SbPh_3$)(2,6-MPP)] (6) and *trans*-[Rh(Cl)(CO)(2,6-MPP)$_2$] (7) formed from the addition of 2,6-MPP to *trans*-[Rh(Cl)(CO)($SbPh_3$)$_2$] (1) in $CDCl_3$ at 25 ˚C. [Rh] = 11.5 mM, [2,6-MPP] = 34.5 mM.**

APPENDIX

Table B.1: Atomic coordinates (x 10^4) and equivalent isotropic displacement parameters (Å x 10^3) for *trans-mer*-[$Rh(Cl)_2(Ph)(SbPh_3)_3$].2CH_2Cl_2. U(eq) is defined as one third of the trace of the orthogonalized Uij tensor

	x	y	z	U(eq)
Rh	2883(1)	2100(1)	1999(1)	28(1)
Sb(1)	1857(1)	2788(1)	2932(1)	33(1)
Sb(2)	2071(1)	2736(1)	534(1)	32(1)
Sb(3)	3719(1)	1201(1)	3204(1)	32(1)
Cl(1)	1297(1)	752(1)	1301(1)	45(1)
Cl(2)	4354(1)	3481(1)	2818(1)	40(1)
C(01)	3845(5)	1739(4)	1325(3)	35(1)
C(02)	4953(5)	2304(4)	1512(4)	48(2)
C(03)	5576(6)	2073(5)	1044(5)	57(2)
C(04)	5138(6)	1318(5)	394(4)	60(2)
C(05)	4045(6)	760(5)	207(4)	58(2)
C(06)	3396(5)	950(4)	670(3)	42(1)
C(11)	173(5)	2151(4)	2864(4)	42(1)
C(12)	-647(5)	1788(5)	2024(5)	64(2)
C(13)	-1772(6)	1472(6)	1942(6)	91(3)
C(14)	-2034(7)	1526(6)	2705(8)	94(3)
C(15)	-1249(7)	1887(8)	3510(6)	103(3)
C(16)	-135(6)	2200(6)	3602(5)	75(2)
C(21)	1708(5)	4088(4)	2611(4)	41(1)
C(22)	2496(5)	4705(4)	2358(4)	48(2)
C(23)	2361(6)	5509(4)	2109(4)	58(2)
C(24)	1457(7)	5712(5)	2100(4)	66(2)
C(25)	657(7)	5103(5)	2356(5)	71(2)
C(26)	775(6)	4298(4)	2614(4)	58(2)
C(31)	2718(5)	3214(4)	4367(3)	40(1)
C(32)	3425(6)	4106(4)	4703(4)	60(2)
C(33)	4035(7)	4382(6)	5617(5)	86(3)
C(34)	3952(7)	3771(7)	6200(5)	89(3)
C(35)	3269(7)	2894(6)	5891(4)	76(2)
C(36)	2640(5)	2603(4)	4967(4)	53(2)
C(41)	2093(5)	2040(4)	-650(3)	37(1)
C(42)	2913(5)	2467(4)	-991(4)	51(2)
C(43)	2998(6)	2041(5)	-1731(4)	68(2)
C(44)	2265(6)	1166(5)	-2137(4)	67(2)
C(45)	1449(6)	728(5)	-1816(4)	58(2)
C(46)	1363(5)	1162(4)	-1063(4)	46(2)
C(51)	369(5)	2675(4)	129(3)	40(1)
C(53)	-1618(5)	1845(6)	-536(5)	72(2)
C(54)	-1832(6)	2615(6)	-343(5)	70(2)
C(55)	-963(6)	3426(6)	62(5)	69(2)
C(56)	140(5)	3462(4)	306(4)	50(2)
C(61)	2896(5)	4106(4)	376(4)	38(1)
C(62)	2358(6)	4534(4)	-282(4)	56(2)
C(63)	2920(7)	5427(5)	-362(5)	68(2)
C(64)	4000(7)	5870(5)	183(5)	71(2)

Table B.1 Cont.: Atomic coordinates (x 10^4) and equivalent isotropic displacement parameters (Å x 10^3) for *trans-mer*-$[Rh(Cl)_2(Ph)(SbPh_3)_3].2CH_2Cl_2$.

	x	y	z	U(eq)
C(65)	4546(6)	5450(5)	820(5)	73(2)
C(66)	3993(5)	4580(4)	918(4)	51(2)
C(71)	2756(5)	625(4)	4002(4)	39(1)
C(72)	1595(5)	293(4)	3614(4)	48(2)
C(73)	966(6)	-49(5)	4136(5)	65(2)
C(74)	1478(6)	-61(5)	5035(4)	60(2)
C(75)	2633(6)	264(5)	5420(4)	55(2)
C(76)	3272(5)	606(4)	4924(4)	47(2)
C(81)	5298(4)	1938(4)	4255(3)	34(1)
C(82)	5448(5)	2750(4)	4762(4)	51(2)
C(83)	6457(6)	3222(5)	5438(4)	63(2)
C(84)	7331(6)	2895(5)	5614(4)	65(2)
C(85)	7184(5)	2094(5)	5126(4)	66(2)
C(86)	6176(5)	1602(4)	4449(4)	49(2)
C(91)	4047(4)	19(4)	2805(3)	37(1)
C(92)	3597(5)	-824(4)	3052(4)	52(2)
C(93)	3837(6)	-1588(4)	2833(5)	66(2)
C(94)	4550(6)	-1520(5)	2367(4)	62(2)
C(95)	5002(5)	-699(5)	2108(4)	53(2)
C(96)	4757(5)	69(4)	2325(4)	44(1)
Cl(3A)	337(14)	7547(14)	2471(8)	133(6)
Cl(4A)	-542(14)	7463(14)	3897(8)	157(6)
C(1A)	-690(30)	6910(20)	2870(18)	158(11)
Cl(3B)	331(17)	7587(14)	2548(12)	181(6)
Cl(4B)	-338(8)	6889(19)	3960(7)	168(6)
C(1B)	-770(20)	7290(20)	2956(18)	166(9)
Cl(5A)	7701(13)	4293(13)	2783(8)	335(11)
Cl(6A)	8750(9)	4766(10)	4613(8)	335(9)
C(3A)	7569(18)	4240(30)	3765(10)	211(11)
Cl(5B)	7099(8)	4867(8)	2543(6)	137(4)
Cl(6B)	8338(16)	3955(12)	3611(14)	251(9)
C(3B)	7480(20)	4520(20)	3507(17)	149(8)

Table B.2: Bond lengths (Å) for *trans-mer*-$[Rh(Cl)_2(Ph)(SbPh_3)_3].2CH_2Cl_2$

Bond	Distance	Bond	Distance	Bond	Distance
Rh-C(01)	2.115(5)	C(34)-H(34)	0.930	C(82)-C(83)	1.373(8)
Rh-Cl(2)	2.3720(18)	C(35)-C(36)	1.399(8)	C(32)-C(33)	1.379(9)
Rh-Cl(1)	2.3731(18)	C(35)-H(35)	0.930	C(32)-H(32)	0.930
Rh-Sb(3)	2.5877(10)	C(36)-H(36)	0.930	C(33)-C(34)	1.364(11)
Rh-Sb(2)	2.6082(9)	C(41)-C(46)	1.384(8)	C(33)-H(33)	0.930
Rh-Sb(1)	2.7185(8)	C(41)-C(42)	1.391(8)	C(34)-C(35)	1.343(11)
Sb(1)-C(11)	2.144(6)	C(42)-C(43)	1.377(8)	C(82)-H(82)	0.930
Sb(1)-C(31)	2.148(5)	C(42)-H(42)	0.930	C(83)-C(84)	1.378(9)
Sb(1)-C(21)	2.161(5)	C(43)-C(44)	1.380(9)	C(83)-H(83)	0.930
Sb(2)-C(41)	2.139(5)	C(43)-H(43)	0.930	C(84)-C(85)	1.359(9)
Sb(2)-C(51)	2.143(5)	C(44)-C(45)	1.370(9)	C(84)-H(84)	0.930
Sb(2)-C(61)	2.147(5)	C(44)-H(44)	0.930	C(85)-C(86)	1.379(8)
Sb(3)-C(91)	2.135(5)	C(45)-C(46)	1.402(8)	C(85)-H(85)	0.930
Sb(3)-C(71)	2.139(6)	C(45)-H(45)	0.930	C(86)-H(86)	0.930
Sb(3)-C(81)	2.143(5)	C(46)-H(46)	0.930	C(91)-C(96)	1.397(7)
C(01)-C(06)	1.397(7)	C(51)-C(52)	1.386(8)	C(91)-C(92)	1.398(8)
C(01)-C(02)	1.402(8)	C(51)-C(56)	1.389(7)	C(92)-C(93)	1.383(8)
C(02)-C(03)	1.402(8)	C(52)-C(53)	1.408(8)	C(92)-H(92)	0.930
C(02)-H(02)	0.930	C(52)-H(52)	0.930	C(93)-C(94)	1.379(9)
C(03)-C(04)	1.357(9)	C(53)-C(54)	1.360(9)	C(93)-H(93)	0.930
C(03)-H(03)	0.930	C(53)-H(53)	0.930	C(94)-C(95)	1.380(9)
C(04)-C(05)	1.383(9)	C(54)-C(55)	1.373(10)	C(94)-H(94)	0.930
C(04)-H(04)	0.930	C(54)-H(54)	0.930	C(95)-C(96)	1.392(8)
C(05)-C(06)	1.402(8)	C(55)-C(56)	1.393(8)	C(95)-H(95)	0.930
C(05)-H(05)	0.930	C(55)-H(55)	0.930	C(96)-H(96)	0.930
C(06)-H(06)	0.930	C(56)-H(56)	0.930	Cl(3A)-C(1A)	1.758(17)
C(11)-C(12)	1.373(8)	C(61)-C(66)	1.378(8)	Cl(4A)-C(1A)	1.725(16)
C(11)-C(16)	1.375(8)	C(61)-C(62)	1.388(8)	C(1A)-H(1A1)	0.970
C(12)-C(13)	1.402(10)	C(62)-C(63)	1.395(9)	C(1A)-H(1A2)	0.970
C(12)-H(12)	0.930	C(62)-H(62)	0.930	Cl(3B)-C(1B)	1.759(15)
C(13)-C(14)	1.378(11)	C(63)-C(64)	1.355(9)	Cl(4B)-C(1B)	1.725(15)
C(13)-H(13)	0.930	C(63)-H(63)	0.930	C(1B)-H(1B1)	0.970
C(14)-C(15)	1.318(1)	C(64)-C(65)	1.366(9)	C(1B)-H(1B2)	0.970
C(14)-H(14)	0.930	C(64)-H(64)	0.930	Cl(5A)-C(3A)	1.632(15)
C(15)-C(16)	1.385(10)	C(65)-C(66)	1.372(8)	Cl(6A)-C(3A)	1.640(17)
C(15)-H(15)	0.930	C(65)-H(65)	0.930	C(3A)-H(3A1)	0.970
C(16)-H(16)	0.930	C(66)-H(66)	0.930	C(3A)-H(3A2)	0.970
C(21)-C(22)	1.379(8)	C(71)-C(72)	1.391(8)	Cl(5B)-C(3B)	1.624(15)
C(21)-C(26)	1.398(8)	C(71)-C(76)	1.405(7)	Cl(6B)-C(3B)	1.629(15)
C(22)-C(23)	1.376(8)	C(72)-C(73)	1.386(8)	C(3B)-H(3B1)	0.970
C(22)-H(22)	0.930	C(72)-H(72)	0.930	C(3B)-H(3B2)	0.970
C(23)-C(24)	1.349(9)	C(73)-C(74)	1.369(8)		
C(23)-H(23)	0.930	C(73)-H(73)	0.930		
C(24)-C(25)	1.386(10)	C(74)-C(75)	1.384(8)		
C(24)-H(24)	0.9300	C(74)-H(74)	0.930		
C(25)-C(26)	1.376(8)	C(75)-H(75)	0.930		
C(25)-H(25)	0.9300	C(76)-H(76)	0.930		
C(26)-H(26)	0.9300	C(81)-C(82)	1.385(7)		
C(31)-C(32)	1.375(8)	C(81)-C(86)	1.391(7)		

Table B.3: Bond angles (°) for *trans-mer*-$[Rh(Cl)_2(Ph)(SbPh_3)_3].2CH_2Cl_2$

Bond	Angle	Bond	Angle
C(01)-Rh-Cl(2)	92.85(16)	C(01)-C(06)-H(06)	120.1
C(01)-Rh-Cl(1)	94.20(16)	C(05)-C(06)-H(06)	120.1
Cl(2)-Rh-Cl(1)	172.84(5)	C(12)-C(11)-C(16)	118.9(6)
C(01)-Rh-Sb(3)	84.55(13)	C(12)-C(11)-Sb(1)	117.8(4)
Cl(2)-Rh-Sb(3)	90.11(5)	C(16)-C(11)-Sb(1)	122.7(5)
Cl(1)-Rh-Sb(3)	89.28(5)	C(11)-C(12)-C(13)	119.4(7)
C(01)-Rh-Sb(2)	84.54(13)	C(11)-C(12)-H(12)	120.3
Cl(2)-Rh-Sb(2)	97.28(5)	C(13)-C(12)-H(12)	120.3
Cl(1)-Rh-Sb(2)	84.68(5)	C(14)-C(13)-C(12)	119.3(8)
Sb(3)-Rh-Sb(2)	167.11(2)	C(14)-C(13)-H(13)	120.3
C(01)-Rh-Sb(1)	172.45(15)	C(12)-C(13)-H(13)	120.3
Cl(2)-Rh-Sb(1)	79.82(4)	C(15)-C(14)-C(13)	121.3(8)
Cl(1)-Rh-Sb(1)	93.18(5)	C(15)-C(14)-H(14)	119.3
Sb(3)-Rh-Sb(1)	97.16(2)	C(13)-C(14)-H(14)	119.3
Sb(2)-Rh-Sb(1)	94.55(2)	C(14)-C(15)-C(16)	120.0(8)
C(11)-Sb(1)-C(31)	100.7(2)	C(14)-C(15)-H(15)	120.0
C(11)-Sb(1)-C(21)	96.5(2)	C(16)-C(15)-H(15)	120.0
C(31)-Sb(1)-C(21)	97.5(2)	C(11)-C(16)-C(15)	121.0(7)
C(11)-Sb(1)-Rh	125.76(16)	C(11)-C(16)-H(16)	119.5
C(31)-Sb(1)-Rh	117.37(15)	C(15)-C(16)-H(16)	119.5
C(21)-Sb(1)-Rh	113.83(15)	C(22)-C(21)-C(26)	118.7(5)
C(41)-Sb(2)-C(51)	102.5(2)	C(22)-C(21)-Sb(1)	121.0(4)
C(41)-Sb(2)-C(61)	97.1(2)	C(26)-C(21)-Sb(1)	120.2(5)
C(51)-Sb(2)-C(61)	101.7(2)	C(23)-C(22)-C(21)	120.5(6)
C(41)-Sb(2)-Rh	113.34(14)	C(23)-C(22)-H(22)	119.7
C(51)-Sb(2)-Rh	117.92(14)	C(21)-C(22)-H(22)	119.7
C(61)-Sb(2)-Rh	120.84(15)	C(24)-C(23)-C(22)	121.1(7)
C(91)-Sb(3)-C(71)	99.2(2)	C(24)-C(23)-H(23)	119.4
C(91)-Sb(3)-C(81)	99.8(2)	C(22)-C(23)-H(23)	119.4
C(71)-Sb(3)-C(81)	100.1(2)	C(23)-C(24)-C(25)	119.4(6)
C(91)-Sb(3)-Rh	120.12(14)	C(23)-C(24)-H(24)	120.3
C(71)-Sb(3)-Rh	116.54(14)	C(25)-C(24)-H(24)	120.3
C(81)-Sb(3)-Rh	117.48(14)	C(26)-C(25)-C(24)	120.7(7)
C(06)-C(01)-C(02)	118.1(5)	C(26)-C(25)-H(25)	119.7
C(06)-C(01)-Rh	121.6(4)	C(24)-C(25)-H(25)	119.7
C(02)-C(01)-Rh	120.3(4)	C(25)-C(26)-C(21)	119.6(6)
C(01)-C(02)-C(03)	120.0(6)	C(25)-C(26)-H(26)	120.2
C(01)-C(02)-H(02)	120.0	C(21)-C(26)-H(26)	120.2
C(03)-C(02)-H(02)	120.0	C(32)-C(31)-C(36)	118.4(5)
C(04)-C(03)-C(02)	122.2(6)	C(32)-C(31)-Sb(1)	119.6(5)
C(04)-C(03)-H(03)	118.9	C(36)-C(31)-Sb(1)	122.0(4)
C(02)-C(03)-H(03)	118.9	C(31)-C(32)-C(33)	120.6(7)
C(03)-C(04)-C(05)	117.9(6)	C(31)-C(32)-H(32)	119.7
C(03)-C(04)-H(04)	121.0	C(33)-C(32)-H(32)	119.7
C(05)-C(04)-H(04)	121.0	C(34)-C(33)-C(32)	120.4(7)
C(04)-C(05)-C(06)	122.0(6)	C(34)-C(33)-H(33)	119.8
C(04)-C(05)-H(05)	119.0	C(32)-C(33)-H(33)	119.8
C(06)-C(05)-H(05)	119.0	C(35)-C(34)-C(33)	120.3(7)
C(01)-C(06)-C(05)	119.7(6)	C(35)-C(34)-H(34)	119.8

Table B.3 Cont.: Bond angles (º) for *trans-mer*-[$Rh(Cl)_2(Ph)(SbPh_3)_3$].$2CH_2Cl_2$

Bond	Angle	Bond	Angle
C(33)-C(34)-H(34)	119.8	C(63)-C(62)-H(62)	120.0
C(34)-C(35)-C(36)	120.1(7)	C(64)-C(63)-C(62)	120.3(6)
C(34)-C(35)-H(35)	120.0	C(64)-C(63)-H(63)	119.8
C(36)-C(35)-H(35)	120.0	C(62)-C(63)-H(63)	119.8
C(31)-C(36)-C(35)	120.3(6)	C(63)-C(64)-C(65)	120.3(6)
C(31)-C(36)-H(36)	119.9	C(63)-C(64)-H(64)	119.8
C(35)-C(36)-H(36)	119.9	C(65)-C(64)-H(64)	119.8
C(46)-C(41)-C(42)	118.6(5)	C(64)-C(65)-C(66)	119.8(7)
C(46)-C(41)-Sb(2)	122.7(4)	C(64)-C(65)-H(65)	120.1
C(42)-C(41)-Sb(2)	118.6(4)	C(66)-C(65)-H(65)	120.1
C(43)-C(42)-C(41)	121.4(6)	C(65)-C(66)-C(61)	121.5(6)
C(43)-C(42)-H(42)	119.3	C(65)-C(66)-H(66)	119.2
C(41)-C(42)-H(42)	119.3	C(61)-C(66)-H(66)	119.2
C(42)-C(43)-C(44)	119.4(7)	C(72)-C(71)-C(76)	118.9(5)
C(42)-C(43)-H(43)	120.3	C(72)-C(71)-Sb(3)	119.7(4)
C(44)-C(43)-H(43)	120.3	C(76)-C(71)-Sb(3)	121.3(4)
C(45)-C(44)-C(43)	120.5(6)	C(73)-C(72)-C(71)	120.0(5)
C(45)-C(44)-H(44)	119.8	C(73)-C(72)-H(72)	120.0
C(43)-C(44)-H(44)	119.8	C(71)-C(72)-H(72)	120.0
C(44)-C(45)-C(46)	120.1(6)	C(74)-C(73)-C(72)	120.5(6)
C(44)-C(45)-H(45)	119.9	C(74)-C(73)-H(73)	119.7
C(46)-C(45)-H(45)	119.9	C(72)-C(73)-H(73)	119.7
C(41)-C(46)-C(45)	120.0(6)	C(73)-C(74)-C(75)	119.5(6)
C(41)-C(46)-H(46)	120.0	C(73)-C(74)-H(74)	120.2
C(45)-C(46)-H(46)	120.0	C(75)-C(74)-H(74)	120.2
C(52)-C(51)-C(56)	119.3(5)	C(76)-C(75)-C(74)	121.2(6)
C(52)-C(51)-Sb(2)	121.2(4)	C(76)-C(75)-H(75)	119.4
C(56)-C(51)-Sb(2)	119.5(4)	C(74)-C(75)-H(75)	119.4
C(51)-C(52)-C(53)	119.6(6)	C(75)-C(76)-C(71)	119.8(6)
C(51)-C(52)-H(52)	120.2	C(75)-C(76)-H(76)	120.1
C(53)-C(52)-H(52)	120.2	C(71)-C(76)-H(76)	120.1
C(54)-C(53)-C(52)	120.6(7)	C(82)-C(81)-C(86)	119.1(5)
C(54)-C(53)-H(53)	119.7	C(82)-C(81)-Sb(3)	120.1(4)
C(52)-C(53)-H(53)	119.7	C(86)-C(81)-Sb(3)	120.7(4)
C(53)-C(54)-C(55)	119.9(6)	C(83)-C(82)-C(81)	120.3(6)
C(53)-C(54)-H(54)	120.0	C(83)-C(82)-H(82)	119.9
C(55)-C(54)-H(54)	120.0	C(81)-C(82)-H(82)	119.9
C(54)-C(55)-C(56)	120.6(7)	C(82)-C(83)-C(84)	120.3(6)
C(54)-C(55)-H(55)	119.7	C(82)-C(83)-H(83)	119.9
C(56)-C(55)-H(55)	119.7	C(84)-C(83)-H(83)	119.9
C(51)-C(56)-C(55)	120.0(6)	C(85)-C(84)-C(83)	119.7(6)
C(51)-C(56)-H(56)	120.0	C(85)-C(84)-H(84)	120.2
C(55)-C(56)-H(56)	120.0	C(83)-C(84)-H(84)	120.2
C(66)-C(61)-C(62)	118.1(5)	C(84)-C(85)-C(86)	121.1(6)
C(66)-C(61)-Sb(2)	120.3(4)	C(84)-C(85)-H(85)	119.4
C(62)-C(61)-Sb(2)	121.6(5)	C(86)-C(85)-H(85)	119.4
C(61)-C(62)-C(63)	119.9(6)	C(85)-C(86)-C(81)	119.5(6)
C(61)-C(62)-H(62)	120.0	C(85)-C(86)-H(86)	120.3

Table B.3 Cont.: Bond angles (º) for *trans-mer*-[$Rh(Cl)_2(Ph)(SbPh_3)_3$].$2CH_2Cl_2$

Bond	Angle	Bond	Angle
C(81)-C(86)-H(86)	120.3	Cl(4A)-C(1A)-H(1A2)	109.4
C(96)-C(91)-C(92)	117.7(5)	Cl(3A)-C(1A)-H(1A2)	109.4
C(96)-C(91)-Sb(3)	121.4(4)	H(1A1)-C(1A)-H(1A2)	108.0
C(92)-C(91)-Sb(3)	120.9(4)	Cl(4B)-C(1B)-Cl(3B)	108.4(12)
C(93)-C(92)-C(91)	121.8(6)	Cl(4B)-C(1B)-H(1B1)	110.0
C(93)-C(92)-H(92)	119.1	Cl(3B)-C(1B)-H(1B1)	110.0
C(91)-C(92)-H(92)	119.1	Cl(4B)-C(1B)-H(1B2)	110.0
C(94)-C(93)-C(92)	119.6(6)	Cl(3B)-C(1B)-H(1B2)	110.0
C(94)-C(93)-H(93)	120.2	H(1B1)-C(1B)-H(1B2)	108.4
C(92)-C(93)-H(93)	120.2	Cl(5A)-C(3A)-Cl(6A)	112.8(15)
C(93)-C(94)-C(95)	120.1(6)	Cl(5A)-C(3A)-H(3A1)	109.0
C(93)-C(94)-H(94)	120.0	Cl(6A)-C(3A)-H(3A1)	109.0
C(95)-C(94)-H(94)	120.0	Cl(5A)-C(3A)-H(3A2)	109.0
C(94)-C(95)-C(96)	120.4(6)	Cl(6A)-C(3A)-H(3A2)	109.0
C(94)-C(95)-H(95)	119.8	H(3A1)-C(3A)-H(3A2)	107.8
C(96)-C(95)-H(95)	119.8	Cl(5B)-C(3B)-Cl(6B)	114.8(14)
C(95)-C(96)-C(91)	120.5(6)	Cl(5B)-C(3B)-H(3B1)	108.6
C(95)-C(96)-H(96)	119.7	Cl(6B)-C(3B)-H(3B1)	108.6
C(91)-C(96)-H(96)	119.7	Cl(5B)-C(3B)-H(3B2)	108.6
Cl(4A)-C(1A)-Cl(3A)	111.3(14)	Cl(6B)-C(3B)-H(3B2)	108.6
Cl(4A)-C(1A)-H(1A1)	109.4	H(3B1)-C(3B)-H(3B2)	107.5
Cl(3A)-C(1A)-H(1A1)	109.4		

Table B.4: Anisotropic displacement parameters (Å x 10^3) for *trans-mer*-$[Rh(Cl)_2(Ph)(SbPh_3)_3].2CH_2Cl_2$

	U11	U22	U33	U23	U13	U12
Rh	27(1)	26(1)	27(1)	2(1)	8(1)	7(1)
Sb(1)	33(1)	33(1)	33(1)	3(1)	13(1)	11(1)
Sb(2)	33(1)	31(1)	30(1)	6(1)	10(1)	10(1)
Sb(3)	31(1)	33(1)	30(1)	6(1)	9(1)	12(1)
Cl(1)	38(1)	35(1)	45(1)	-1(1)	10(1)	-2(1)
Cl(2)	36(1)	32(1)	39(1)	-2(1)	9(1)	3(1)
C(01)	42(3)	39(3)	31(3)	12(3)	15(3)	22(3)
C(02)	50(4)	46(4)	55(4)	3(3)	28(3)	18(3)
C(03)	51(4)	59(4)	78(5)	20(4)	41(4)	24(4)
C(04)	69(5)	89(6)	56(4)	26(4)	37(4)	54(5)
C(05)	78(5)	68(5)	32(3)	-6(3)	6(3)	49(4)
C(06)	39(3)	47(4)	39(3)	4(3)	8(3)	22(3)
C(11)	42(4)	50(4)	49(4)	17(3)	26(3)	23(3)
C(12)	45(4)	71(5)	67(5)	-5(4)	15(4)	15(4)
C(13)	34(4)	80(6)	118(7)	-17(5)	-6(5)	6(4)
C(14)	59(6)	100(7)	155(9)	58(7)	69(7)	33(5)
C(15)	66(6)	183(11)	93(7)	73(7)	53(5)	55(7)
C(16)	57(5)	121(7)	65(5)	34(5)	33(4)	40(5)
C(21)	52(4)	38(3)	36(3)	7(3)	14(3)	21(3)
C(22)	61(4)	38(3)	49(4)	8(3)	26(3)	18(3)
C(23)	79(5)	45(4)	60(4)	16(3)	32(4)	25(4)
C(24)	101(6)	48(4)	59(4)	16(4)	30(4)	38(4)
C(25)	90(6)	72(5)	83(5)	19(4)	44(5)	57(5)
C(26)	67(5)	51(4)	74(5)	20(4)	38(4)	28(4)
C(31)	45(4)	43(3)	32(3)	-2(3)	15(3)	15(3)
C(32)	75(5)	46(4)	45(4)	-10(3)	18(4)	7(4)
C(33)	97(7)	68(5)	56(5)	-26(4)	9(5)	5(5)
C(34)	96(7)	102(7)	34(4)	-27(5)	-2(4)	19(6)
C(35)	102(7)	100(7)	40(4)	22(4)	25(4)	52(6)
C(36)	61(4)	46(4)	47(4)	-1(3)	15(3)	19(3)
C(41)	40(3)	43(3)	25(3)	2(2)	7(2)	18(3)
C(42)	55(4)	53(4)	47(4)	4(3)	25(3)	14(3)
C(43)	73(5)	81(6)	60(4)	1(4)	40(4)	25(5)
C(44)	75(5)	84(6)	46(4)	-8(4)	23(4)	33(5)
C(45)	60(5)	57(4)	49(4)	-12(3)	7(3)	24(4)
C(46)	43(4)	42(4)	45(3)	5(3)	11(3)	11(3)
C(51)	40(3)	48(4)	33(3)	11(3)	12(3)	19(3)
C(52)	44(4)	55(4)	63(4)	5(3)	13(3)	18(3)
C(53)	33(4)	80(6)	74(5)	3(4)	-2(3)	6(4)
C(54)	43(4)	93(6)	78(5)	15(5)	17(4)	35(5)
C(55)	55(5)	85(6)	78(5)	9(4)	18(4)	46(5)
C(56)	44(4)	52(4)	50(4)	6(3)	10(3)	21(3)
C(61)	50(4)	36(3)	40(3)	17(3)	24(3)	20(3)
C(62)	64(5)	51(4)	62(4)	24(3)	28(4)	24(4)

Table B.4 Cont.: Anisotropic displacement parameters (Å x 10^3) for *trans-mer*-$[Rh(Cl)_2(Ph)(SbPh_3)_3].2CH_2Cl_2$.

	U11	U22	U33	U23	U13	U12
C(63)	73(5)	61(5)	86(5)	42(4)	38(5)	30(4)
C(64)	89(6)	39(4)	95(6)	31(4)	52(5)	15(4)
C(65)	67(5)	57(5)	79(5)	20(4)	34(4)	-9(4)
C(66)	48(4)	48(4)	53(4)	13(3)	21(3)	6(3)
C(71)	44(4)	43(3)	38(3)	12(3)	17(3)	21(3)
C(72)	41(4)	58(4)	37(3)	8(3)	9(3)	11(3)
C(73)	52(4)	82(5)	61(5)	20(4)	30(4)	13(4)
C(74)	66(5)	78(5)	59(4)	31(4)	41(4)	30(4)
C(75)	75(5)	70(5)	42(4)	29(3)	31(4)	41(4)
C(76)	47(4)	61(4)	39(3)	20(3)	15(3)	25(3)
C(81)	32(3)	36(3)	30(3)	6(2)	8(2)	7(3)
C(82)	51(4)	50(4)	46(4)	6(3)	7(3)	19(3)
C(83)	72(5)	48(4)	47(4)	-10(3)	1(4)	17(4)
C(84)	47(4)	80(5)	46(4)	-6(4)	1(3)	12(4)
C(85)	34(4)	95(6)	55(4)	-5(4)	-2(3)	26(4)
C(86)	35(4)	63(4)	44(3)	0(3)	6(3)	19(3)
C(91)	40(3)	40(3)	28(3)	3(2)	8(3)	16(3)
C(92)	71(5)	44(4)	53(4)	17(3)	32(3)	25(3)
C(93)	87(6)	32(3)	85(5)	17(4)	39(5)	20(4)
C(94)	67(5)	60(5)	68(5)	7(4)	23(4)	35(4)
C(95)	47(4)	71(5)	46(4)	2(3)	18(3)	29(4)
C(96)	42(4)	50(4)	42(3)	10(3)	12(3)	23(3)
Cl(3A)	173(11)	222(15)	76(6)	45(7)	49(6)	156(11)
Cl(4A)	178(9)	202(12)	107(6)	32(6)	70(5)	67(9)
C(1A)	153(18)	240(30)	122(16)	11(15)	46(14)	126(18)
Cl(3B)	234(16)	168(13)	167(12)	62(10)	65(11)	108(12)
Cl(4B)	101(5)	234(16)	162(7)	36(7)	44(4)	53(6)
C(1B)	154(15)	250(30)	113(16)	-19(13)	-8(11)	165(16)
Cl(5A)	259(16)	380(20)	211(9)	-90(12)	146(11)	-134(13)
Cl(6A)	255(11)	350(16)	234(10)	101(10)	-3(8)	-24(10)
C(3A)	128(15)	310(30)	182(13)	115(18)	70(10)	35(17)
Cl(5B)	99(6)	167(8)	117(5)	-15(5)	45(5)	8(5)
Cl(6B)	302(17)	269(15)	370(20)	162(15)	242(16)	207(13)
C(3B)	105(16)	260(20)	129(14)	16(14)	86(14)	87(14)

APPENDIX

Table C.1: Atomic coordinates (x 10^4) and equivalent isotropic displacement parameters (Å x 10^3) for $[Rh(Cl)_2(Ph)(PPh_3)_2]$.
U(eq) is defined as one third of the trace of the orthogonalized Uij tensor

	x	y	z	U(eq)
Rh	0	2741(1)	7500	29(1)
P	-934(1)	2651(1)	6450(1)	29(1)
Cl(1)	-1629(1)	2575(1)	7938(1)	41(1)
C(12)	-1378(3)	753(3)	6826(2)	40(1)
C(31)	-254(3)	2909(2)	5702(2)	35(1)
C(35)	40(4)	3797(3)	4708(2)	67(1)
C(21)	-2111(3)	3393(3)	6368(2)	34(1)
C(11)	-1363(3)	1406(2)	6305(2)	33(1)
C(16)	-1671(3)	1077(3)	5667(2)	51(1)
C(14)	-2030(3)	-487(3)	6102(2)	53(1)
C(01)	0	4181(3)	7500	32(1)
C(22)	-2043(3)	4386(3)	6446(2)	39(1)
C(13)	-1714(3)	-182(3)	6722(2)	48(1)
C(36)	-522(3)	3654(3)	5270(2)	50(1)
C(32)	567(3)	2309(3)	5558(2)	50(1)
C(26)	-3090(3)	2991(3)	6250(2)	48(1)
C(23)	-2923(3)	4958(3)	6408(2)	49(1)
C(34)	848(4)	3211(4)	4575(2)	70(2)
C(02)	-594(3)	4696(3)	7932(2)	46(1)
C(25)	-3970(3)	3564(3)	6220(2)	63(1)
C(03)	-595(4)	5695(3)	7917(2)	66(1)
C(24)	-3882(3)	4542(3)	6293(2)	59(1)
C(15)	-2011(3)	136(3)	5568(2)	57(1)
C(04)	0	6202(5)	7500	73(2)
C(33)	1104(4)	2469(3)	4997(2)	64(1)

Table C.2: Bond lengths (Å) for $[Rh(Cl)_2(Ph)(PPh_3)_2]$.

Bond	Distance	Bond	Distance	Bond	Distance
Rh-C(01)	1.994(5)	C(31)-C(36)	1.378(5)	C(01)-C(02)	1.393(4)
Rh-Cl(1)#	12.3419(10)	C(31)-C(32)	1.390(5)	C(01)-C(02)#	11.393(4)
Rh-Cl(1)	2.3419(10)	C(35)-C(34)	1.362(6)	C(22)-C(23)	1.382(5)
Rh-P#	12.3601(11)	C(35)-C(36)	1.396(5)	C(32)-C(33)	1.381(6)
Rh-P	2.3601(11)	C(21)-C(26)	1.384(5)	C(26)-C(25)	1.383(5)
P-C(31)	1.827(4)	C(21)-C(22)	1.387(4)	C(23)-C(24)	1.370(6)
P-C(11)	1.828(3)	C(11)-C(16)	1.393(5)	C(34)-C(33)	1.358(6)
P-C(21)	1.830(3)	C(16)-C(15)	1.385(5)	C(02)-C(03)	1.384(5)
C(12)-C(13)	1.377(5)	C(14)-C(13)	1.353(5)	C(25)-C(24)	1.366(5)
C(12)-C(11)	1.384(5)	C(14)-C(15)	1.379(6)	C(03)-C(04)	1.368(5)

#: Atoms generated as symmetrically equivalent through –x + 1, y, -z + ½

Table C.3: Bond angles (º) for $[Rh(Cl)_2(Ph)(PPh_3)_2]$.

Bond	Angle	Bond	Angle
C(01)-Rh-Cl(1)#	195.65(2)	C(22)-C(21)-P	120.1(3)
Cl(1)#1-Rh-Cl(1)	168.71(5)	C(12)-C(11)-C(16)	117.7(3)
C(01)-Rh-P#	193.05(2)	C(12)-C(11)-P	121.0(3)
Cl(1)#1-Rh-P#	185.12(4)	C(16)-C(11)-P	121.3(3)
Cl(1)-Rh-P#	194.28(4)	C(15)-C(16)-C(11)	120.6(4)
C(01)-Rh-P	93.05(2)	C(13)-C(14)-C(15)	120.1(4)
Cl(1)#1-Rh-P	94.28(4)	C(02)-C(01)-C(02)#	118.4(5)
Cl(1)-Rh-P	85.12(4)	C(02)-C(01)-Rh	120.8(2)
P#1-Rh-P	173.91(5)	C(02)#1-C(01)-Rh	120.8(2)
C(31)-P-C(11)	102.13(16)	C(23)-C(22)-C(21)	121.1(4)
C(31)-P-C(21)	104.90(16)	C(14)-C(13)-C(12)	120.4(4)
C(11)-P-C(21)	105.97(16)	C(31)-C(36)-C(35)	119.6(4)
C(31)-P-Rh	118.78(11)	C(33)-C(32)-C(31)	120.3(4)
C(11)-P-Rh	108.83(12)	C(21)-C(26)-C(25)	120.8(4)
C(21)-P-Rh	114.85(12)	C(24)-C(23)-C(22)	119.8(4)
C(13)-C(12)-C(11)	121.3(4)	C(33)-C(34)-C(35)	119.0(4)
C(36)-C(31)-C(32)	118.5(4)	C(03)-C(02)-C(01)	119.9(4)
C(36)-C(31)-P	123.5(3)	C(24)-C(25)-C(26)	120.2(4)
C(32)-C(31)-P	118.0(3)	C(04)-C(03)-C(02)	121.8(5)
C(34)-C(35)-C(36)	121.4(4)	C(25)-C(24)-C(23)	120.2(4)
C(26)-C(21)-C(22)	117.9(3)	C(14)-C(15)-C(16)	119.9(4)
C(26)-C(21)-P	122.0(3)	C(03)#1-C(04)-C(03)	118.2(6)
C(34)-C(33)-C(32)	121.2(4)		

#: Atoms generated as symmetrically equivalent through –x + 1, y, -z + ½

Table C.4: Anisotropic displacement parameters (Å x 10^3) for $[Rh(Cl)_2(Ph)(PPh_3)_2]$

	U11	U22	U33	U23	U13	U12
Rh	29(1)	26(1)	30(1)	0	2(1)	0
P	32(1)	26(1)	29(1)	1(1)	1(1)	1(1)
Cl(1)	36(1)	45(1)	44(1)	-1(1)	8(1)	-3(1)
C(12)	48(2)	35(2)	38(2)	-2(2)	8(2)	-1(2)
C(31)	35(2)	34(2)	35(2)	-5(2)	-1(2)	-4(2)
C(35)	112(4)	46(3)	45(3)	9(2)	13(3)	-17(3)
C(21)	32(2)	38(2)	31(2)	5(2)	1(2)	4(2)
C(11)	32(2)	29(2)	38(2)	-4(2)	2(2)	2(2)
C(16)	70(3)	40(3)	41(2)	-3(2)	-4(2)	-6(2)
C(14)	63(3)	35(2)	62(3)	-12(2)	16(2)	-13(2)
C(01)	27(3)	30(3)	40(3)	0	-3(2)	0
C(22)	38(2)	39(2)	38(2)	-4(2)	-7(2)	1(2)
C(13)	64(3)	32(2)	51(3)	2(2)	19(2)	-4(2)
C(36)	69(3)	38(3)	45(3)	1(2)	13(2)	-4(2)
C(32)	45(2)	58(3)	48(3)	-5(2)	5(2)	5(2)
C(26)	36(2)	41(3)	67(3)	4(2)	3(2)	1(2)
C(23)	51(3)	42(3)	53(3)	-3(2)	-1(2)	14(2)
C(34)	90(4)	72(4)	53(3)	-12(3)	31(3)	-36(3)
C(02)	49(3)	38(2)	51(3)	-2(2)	4(2)	1(2)
C(25)	31(2)	61(3)	96(4)	4(3)	0(2)	-1(2)
C(03)	86(4)	37(3)	74(4)	-15(2)	7(3)	13(2)
C(24)	44(3)	60(3)	74(3)	6(2)	9(2)	21(2)
C(15)	75(3)	47(3)	49(3)	-19(2)	-4(2)	-8(2)
C(04)	98(6)	26(4)	94(6)	0	-5(5)	0
C(33)	51(3)	81(4)	61(3)	-24(3)	18(2)	-9(2)

APPENDIX

Table D.1: k_{obs} values and triphenylstibine concentrations for the reaction of *trans*-[Rh(Cl)(CO)($SbPh_3$)$_2$] with 2,4-TBPP in CH_2Cl_2 at 25 ºC. [Rh] = 0.25 mM, [2,4-TBPP] = 6.5 mM

k_{obs} (s^{-1})	[$SbPh_3$] mM
1630	0
1390	6.13
1260	12.3
1050	24.5
859	36.8
634	61.3
520	92.0
429	122.7
389	165.6
303	214.7
289	257.7

Table D.2: k_{obs} values and triphenylstibine concentrations for the reaction of *trans*-[Rh(Cl)(CO)($SbPh_3$)$_2$] with 2,4-TBPP in ethyl acetate at -5 ºC. [Rh]= 0.25 mM, [2,4-TBPP] = 6.5 mM

k_{obs} (s^{-1})	[$SbPh_3$] mM
973	3.97
780	7.94
598	11.9
527	15.87
439	19.84
425	23.81
255	39.68
139	59.52
100	79.37
150	99.21
116	119.05